UNIVERSITÀ DEGLI STUDI
DI MILANO

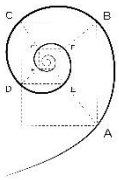

DOTTORATO DI MEDICINA MOLECOLARE E TRASLAZIONALE

CICLO XXXII

Anno Accademico 2018/2019

TESI DI DOTTORATO DI RICERCA

MED/50

Assessment of intracellular redox-balance role in TMZ-resistance-related cytoprotective pathways in GBM

Dottorando : Daniela SALVATORE

Matricola N° : R11666

TUTORE : Dott.ssa Luisa OTTOBRINI

CO-TUTORE: Dott.ssa Alessia LO DICO

COORDINATORE DEL DOTTORATO: Prof. Michele SAMAJA

INDEX

LIST OF ABBREVIATIONS

^{11}C-MET: ^{11}C-methionine

^{18}FAZA: ^{18}F-FluoroAzomycin Arabinoside

^{18}F-FDG: ^{18}F-Fluorodeoxyglucose

^{18}F-FET: ^{18}F-Fluoroethyl-L-Tyrosine

^{18}F-MISO: ^{18}F-Fluoromisonidazole

AAG: Alkyl Adenine DNA Glycosylase

AIC: 5-amino-imidazole-4-carboxamide

AKT: Protein kinase B

APE1: Apurinic/Apyrimidinic Edonuclease 1

ARF: ADP-Ribosylation Factor

ASCT2: Alanine, Serine, Cysteine Transporter 2

ATCC: American Type Culture Collection

BAD: Bcl-2 Associated Death Promoter

BAX: Bcl-2 Associated Protein X

BBB: Blood Brain Barrier

BCL-2: B-cell Lymphoma 2

BER: Base Excision Repair

BL: Bioluminescence

C145: Cysteine 145

CBP: CREB Binding Protein

CDK4/6: cyclin-dependent kinase 4/6

CDKN2A and CDKN2B: cyclin-dependent kinase inhibitors p16INK4A and p15INK4B

CMA: Chaperone-Mediated Autophagy

CNS: Central Nervous System

CpG: Cysteine-phosphate-Guanine site

CT: Computed Tomography

CTGF: connective tissue growth factor

CuZn SOD/SOD1: Copper/Zinc Superoxide Dismutase/ Superoxide Dismutase 1

D2R: Dopamine Receptor D2

DASA: *N,N*-diarylsulfonamides

DCE: Dynamic Contrast-Enhanced

DNA POLβ: DNA Polymerase B

DR: MGMT-mediated Direct Repair

DTI: Diffusion Tensor Imaging

ECM: extracellular matrix

EGFR: Epidermal Growth Factor Receptor

EMT: Epithelial-Mesenchymal Transition

ER stress: Endoplasmic Reticulum stress

ErbB: erythroblastic leukemia viral oncogene homolog

FACBC: ^{18}F-Fluciclovine, Axumin, 1r, 3r-1- amino 3-^{18}F-fluorocyclobutane-1-carboxylic acid

FDA: Food and Drug Administration

FL: Fluorescence

fMRI: Functional MRI

GBM: Glioblastoma Multiforme

GEM: Genetically Engineered Models

GFAP: Glial Fibrillary Acidic Protein

GLUT-1/3: Glucose Transporter-1/3

GPx (1): Glutathione Peroxidase (1)

GR: GSH Reductase

GSCs: Glioblastoma stem cells

GSH: Glutathione in general / reduced form

GSS: GSH synthetase

GSSG: Glutathione Oxidised Form

HIF-1α: hypoxia-inducible factor-1α

HIF-1β / ARNT: hypoxia-inducible factor-1β / Hydrocarbon Receptor Nuclear Translocator

HRE: Hypoxia Response Element

HSC70: Heat Shock Chaperone 70 kDa

IDH1: Isocitrate Dehydrogenase 1

IDH2: Isoctrate Dehydrogenase 2

IHC: Immunohistochemistry

i.c./i.v. injection: intracranial/intravein

KFERQ: Lysine-Phenylalanine-Glutamate-Arginine-Glutamine

LAMP-2A: Lysosome-Associated Membrane Protein Type-2A

LAT-1: L-Type Amino Acid Transporter-1

Lys-HSC70: Lysosomal-HSC70

MDM2/4: murine double minute 2/4

MGMT: O6-methylguanine-DNA methyltransferase enzyme

MitoT: MitoTEMPO

MLH1: Mutl Homolog 1

MMR: Mismatch Repair

MnSOD/SOD2: Manganese Superoxide Dismutase/Superoxide Dismutase 2

MPT: Mitochondrial Permeability Transition

MRI: Magnetic Resonance Imaging

MRS: Magnetic Resonance Spectroscopy

MSH2/MSH6: Melanocyte-Stimulating Hormone 2/6

MTIC: 5-(3-methyltriazol-1-yl)imidazole- 4-carboxamide

mTOR: Mammalian Target of Rapamycin

N3MA: N3 Methyl Adenine

N7MeG: N7 Methyl Guanine

NADP/NADPH: Nicotinamide Adenine Dinucleotide Phosphate Oxidised Form / Reduced Form

NF-κB: nuclear factor kappa B

NMR: Nuclear Magnetic Resonance

O6-MeG: O6 Methyl-Guanine

OXPHOS: Mitochondrial Oxidative Phosphorylation System

p300: Histone acetyltransferase p300 / E1A-associated protein p300

P402/564 and N803: Proline 402/564 and Asparagine 803

PD: Proton density

PDX: Patient-Derived Xenograft

PET: Positron Emission Tomography

PHD: Prolyl-Hydroxylase

PHLPP1: Pleckstrin Homology (PH) Domain And Leucine-Rich Repeat Protein Phosphatase 1

PI3K: Phosphatidylinositol 3-Kinase

PIK3CA: phosphatidylinositol-4,5-bisphosphate 3-kinase catalytic subunit alpha

PIK3R1: phosphoinositide-3-kinase, regulatory subunit 1 (alpha)

PIKC2B: Protein kinase C-isoform 2β

PMS2: Post-Meiotic Segregation-Increased Saccharomyces Cerevisiae 2

pO_2: oxygen partial pressure

PP2C: Phosphatase 2C

pRB: Retinoblastoma-related protein

PTEN: phosphatase and tensin homolog

pVHL: Von Hippel-Lindau protein

PX-478: S-2-amino-3-[4-N,N,-bis(2-chloroethyl)amino] phenyl propionic acid N-oxide dihydrochloride

R132/172: Arginine 132/172

RANO: Response Assessment in Neuro-Oncology

Ras: renin-angiotensin system

ROS: Reactive Oxygen Species

RT: Radiotherapy

RTK: Receptor tyrosine kinases

S/T Phosphatase: Serine/Threonine phosphatase

SMAD 2/3: Small Mother Against Decapentaplegic 2/3

SPECT: Single Photon Emission Computed Tomography

T1: longitudinal relaxation/recovery

T2/T2*: transverse relaxation

TCGA: The Cancer Genome Atlas

TERT: telomerase reverse transcriptase

TGF-β: Tumour Growth Factor-β

TMZ: Temozolomide

TrkA: Tyrosine Kinase Receptor Type A

TSPO: 18-kDa Translocator Protein

US: Ultrasound

VEGF A/C: Vascular Endothelial Growth Factor A/C

VEGF: Vascular Endothelial Growth Factor

VEGFR 1/2/3: Vascular Endothelial Growth Factor Receptor 1/2/3

WHO: World Health Organisation

XRCC1: X-ray repair cross-complementing protein 1

ZEB1: E-box binding homeobox 1

LIST OF FIGURES AND TABLES

RESEARCH INTEGRITY

All data reported in this work are compliant to the fundamental principles of research integrity, according to The European Code of Conduct for Research Integrity (ALLEA, Berlin, 2018), as follows:

- Data are **reliable** in reflecting quality research based on the appropriate design, methodology, the analysis and the use of resources

- Data are developed, undertaken, reviewed, reported and communicated in a transparent fair, full and unbiased way, reflecting research **honesty**

- Data are produced, elaborated and communicated **respecting** colleagues, research participants, society, ecosystems, cultural heritage and the environment

Data are synonymous of **accountability** for the research from idea to publication, for its management and organisation, for training, supervision and mentoring, and for its wider impacts.

SOMMARIO

Introduzione: *Il Glioblastoma (GBM) rappresenta il tumore astrocitico più aggressivo negli adulti, esibisce una prognosi infausta correlata alla resistenza alla terapia, che è principalmente focalizzata sull'uso della TMZ e della radioterapia (protocollo Stupp). Tra i fattori cruciali che sono coinvolti nella resistenza al trattamento con la TMZ emerge HIF-1α, che attiva diversi meccanismi tra cui angiogenesi ed EMT. Oltre alla sua primaria azione alchilante, la TMZ può esercitare altri effetti secondari dentro le cellule, come il rilascio delle ROS dai mitocondri mediato dallo stress del RE e l'attivazione dell'autofagia. Diversi lavori hanno riportato la degradazione di HIF-1α nei lisosomi attraverso l'autofagia chaperon-mediata (CMA). L'importanza di questo potenziale terapeutico indiretto deve ancora essere dedotta, ma la comprensione dei principali meccanismi sta conferendo una nuova luce alle strategie di resistenza al tumore. Allo stesso tempo, nuove procedure atte a migliorare i trattamenti di radioterapia potrebbero essere utili per lo sviluppo di approcci maggiormente mirati.*

Scopo del lavoro: *I principali obiettivi di questo progetto di ricerca sono stati: la comprensione dei meccanismi molecolari che sottendono alla resistenza del GBM alla TMZ, l'analisi del ruolo di HIF-1α nella resistenza e la valutazione di una nuova strategia atta a ripristinare la sensibilità al trattamento. Inoltre, data la necessità di un modello murino di GBM resistente per testare l'efficacia della nuova strategia terapeutica, un altro obiettivo di questo progetto è stato quello di utilizzare lo stesso modello ortotopico per sviluppare una procedura non invasiva per valutare il GBM tramite la PET utilizzando la ^{18}F-Fluciclovine, la cui diffusione cellulare dipende dal grado di attività dei trasportatori amminoacidici (ASCT2).*

Materiali e metodi: *Il ruolo cruciale dell'attività di HIF-1α nella risposta al trattamento con la TMZ è stato valutato caratterizzando due linee cellulari di GBM umano, le U251 sensibili alla TMZ e le T98 resistenti al farmaco, mediante saggi molecolari, biochimici, di espressione genica, mediante silenziamento genico ed inibizione farmacologica mediata dal PX-478. È stato valutato anche il coinvolgimento della CMA nella risposta alla TMZ caratterizzando, seguendo l'approccio sperimentale sopra riportato per HIF-1α e mediante analisi biochimiche e di proteine coinvolte in questo pathway. Il contributo delle ROS mitocondriali e il ruolo del macchinario di detossificazione delle ROS nel trattamento con la TMZ sono stati studiati, rispettivamente, trattando le cellule con il MitoT utilizzando tutte le tecniche menzionate sopra (includendo lo scratch test), e mediante Il profilo di espressione genica e le analisi di proteine. I trattamenti con H_2O_2, che seguono l'approccio sperimentale usato per il MitoT, sono stati utilizzati per testare il potenziale ruolo delle ROS nel ripristinare la resistenza alla TMZ. La linea cellulare di glioma murino CT-2A, dopo essere stata caratterizzata come le U251 e le T98 per valutare la responsività alla TMZ, sono state inoculate i.c. in topi C57BL/6J per sviluppare modelli ortotopici di glioma. Le acquisizioni MRI sono state fatte ai giorni 9 e 15 dopo l'impianto per monitorare la crescita del tumore. La MRI è servita anche per monitorare la crescita del tumore in seguito alla radioterapia (15Gy-hemibrain). La PET con la ^{18}F-Fluciclovine è stata fatta 16 giorni dopo l'impianto. I cervelli dei topi trattati e non trattati con la RT sono stati raccolti per successive analisi IHC riguardanti i livelli di espressione di ASCT2.*

Risultati: *Questo studio ha permesso di identificare i biomarcatori di risposta e quei meccanismi coinvolti nella resistenza del GBM al trattamento con TMZ. HIF-1α è*

stato individuato come il fattore cruciale di resistenza alla TMZ: le cellule ipossiche sono caratterizzate da una minore sensibilità al farmaco, mentre dopo trattamento, nelle cellule sensibili, è stata osservata una diminuzione sia nella vitalità che nell'attività di HIF-1α, invece nelle cellule resistenti non si è registrata alcuna modulazione né per la vitalità né per l'attività di HIF-1α. Questi risultati sono stati confermati dal profilo di espressione dei geni correlati all'apoptosi, CMA ed EMT. Ulteriori risultati hanno dimostrato il coinvolgimento della CMA nella degradazione di HIF-1α e la conseguente citotossicità dovuta al farmaco: infatti, il silenziamento di LAMP-2A ha indotto la resistenza nelle cellule precedentemente sensibili, mentre il silenziamento genico di HIF-1α ha ripristinato il fenotipo sensibile nelle T98 in precedenza resistenti. Anche l'annullamento dell'attività di HIF-1α mediata dal PX-478 ha confermato il risultato precedente. Inoltre, l'attivazione della CMA che segue il trattamento con la TMZ può essere indotta dal rilascio delle ROS dai mitocondri come dimostrato utilizzando il MitoT. Inoltre, lo studio sul sistema di detossificazione delle ROS ha mostrato una sua down-regolazione nelle cellule sensibili dopo trattamento con TMZ, coerentemente alla fluttuazione temporanea delle ROS. Per di più, un aumento esogeno nei livelli di ROS intracellulari indotto dal trattamento con H_2O_2 ha prodotto gli stessi meccanismi attivati dalla TMZ nelle cellule sensibili dopo il rilascio delle ROS, determinando un profilo sensibile sia nelle cellule responsive che resistenti. Il profilo di espressione dei geni correlati alla CMA, all'apoptosi e a EMT è stato significativamente modificato in relazione all'apparente sensibilità, delucidando il ruolo cruciale delle ROS nel citoplasma ma anche l'importanza della CMA nel mediare l'effetto tossico della TMZ. Da notare, qui riportiamo che solo il trattamento combinato con H_2O_2 e TMZ ha significativamente indotto un profilo totalmente responsivo nelle cellule resistenti, mostrando il ruolo cruciale delle ROS, CMA, della modulazione di HIF-1α e del farmaco. Il risultato finale di questo lavoro è stato lo sviluppo di un modello murino ortotopico resistente alla TMZ inoculando mediante stereotassi (i.c.) le cellule murine CT-2A. Questo modello è risultato essere responsivo alla RT, come riportato dagli studi di MRI. Il tracciante ^{18}F-Fluciclovine è stato utilizzato per monitorare la grandezza del tumore in vista di una sua implementazione nella valutazione della risposta al trattamento tramite PET. Alla fine, dati preliminari IHC di cervelli di topo non trattati e trattati con RT hanno confermato la down-regolazione dell'espressione di ASCT2 nei topi trattati rispetto a quelli non trattati.

Conclusioni: *In questo lavoro di tesi è stato dimostrato che l'attività di HIF-1α ha un ruolo chiave nella resistenza alla TMZ, che la CMA ha un ruolo cruciale nel mediare la citotossicità indotta dal farmaco e che l'induzione di questo pathway è dovuta a un incremento transitorio del livello di ROS intracellulari. Inoltre, un incremento esogeno dei livelli intracellulari di ROS ha ripristinato un profilo completamente sensibile nelle cellule resistenti, aprendo la strada per la valutazione di nuovi approcci terapeutici. I modelli ortotopici murini di CT-2A rappresentano una buona opportunità per la valutazione in vivo di questi nuovi trattamenti, in particolare utilizzando un imaging multimodale non invasivo, strategia discussa in questo lavoro.*

ABSTRACT

Background: *Glioblastoma (GBM) represents the most aggressive astrocytic brain tumour in adults and exhibits a dismal prognosis related to resistance to therapy, which is principally based on Temozolomide plus RT (Stupp protocol). Among crucial factors which are involved in resistance to TMZ treatment, HIF-1α emerges since it activates several pathways, among which angiogenesis and EMT. Beyond its primary alkylating power, TMZ can exerts other secondary effects within cells, as ER stress-mediated ROS release from mitochondria and activation of autophagy. Several works have described HIF-1α degradation in lysosomes through the chaperone mediated autophagy (CMA) pathway. Importance of this indirect therapeutic potential has to be yet fully elucidated but the comprehension of the main mechanisms is shedding new light on tumour resistance strategies. At the same time, new procedures for the improvement of radiotherapy treatments could help the development of more precise approaches.*

Aims: *The main purposes of this research project have been: to understand the molecular mechanisms underlying GBM resistance to TMZ, to investigate HIF-1α role in resistance and to assess a new strategy able to restore sensitivity to this treatment. Moreover, since the need for a murine model of resistant GBM to test the efficacy of the new therapeutic strategy, a secondary aim of this project has been the setting up of an orthotopic model of GBM, resistant to TMZ, and to characterize it as regards its radio-responsiveness. Final aim of the study has been to use the same orthotopic model to set up a non-invasive procedure to assess GBM by means of PET using ^{18}F-Fluciclovine, whose cellular uptake is dependent upon the rate of activity of amino acid transporters (ASCT2).*

Materials and methods: *HIF-1α activity crucial role in responsiveness to TMZ has been evaluated characterising two human GBM cell lines, U251-responsive cells to TMZ and T98-resistant ones, through molecular, biochemical ang gene expression analyses, by means of gene silencing and PX-478-mediated pharmacological inhibition. Moreover, CMA engagement in responsiveness to TMZ has been evaluated, following the experimental approach used for HIF-1α and through biochemical and protein studies of CMA pathway. Mitochondrial ROS contribution and the detox machinery role in TMZ treatment have been investigated, respectively, treating cells with MitoT utilising all the aforementioned techniques (including scratch test) and by means of gene expression profile and protein analyses. H_2O_2 treatments, which retrace the experimental approach used for MitoT, have been used for testing the potential ROS role in reverting resistance to TMZ. Murine glioma cell line CT-2A, after having been characterised as U251 and T98 for evaluating its responsiveness to TMZ, have been stereotaxically injected (i.c.) in C57BL/6J mice to set up orthotopic glioma models. MRI scans have been carried out at days 9 and 15 after i.c. injection for monitoring tumour growth. MRI has been exploited also for monitoring tumour growth after RT (15Gy-hemibrain). ^{18}F-Fluciclovine-PET has been performed 16 days after i.c. injection. Untreated and RT-treated mice brains have been collected for IHC analyses regarding ASCT2 expression levels.*

Results: *This study allowed the identification of response biomarkers and mechanisms involved in GBM resistance to TMZ treatment. HIF-1α has been*

identified as a crucial factor in resistance to TMZ: hypoxic cells are characterized by a lower sensitivity to the drug, while a significant decrease both in viability and HIF-1α activity has been detected after treatment in sensitive cells while no modulation in HIF-1α activity and viability was observed in T98 resistant cells. These results were confirmed by assessing also apoptosis-, CMA- and EMT-related gene expression. Further results showed the involvement of CMA in HIF-1α degradation and the consequent cytotoxicity due to the drug: in fact, LAMP-2A silencing induced resistance in previously sensitive cells, while HIF-1α gene silencing reverted T98 phenotype from a previously resistant to a sensitive one. Also, the PX-478 mediated HIF-1α activity abrogation confirmed the previous result. CMA activation following TMZ treatment can be induced by ROS release from the mitochondria as demonstrated by using the MitoT. The study of detox machinery showed a down-regulation in sensitive cells after TMZ treatment, consistently with the temporary ROS fluctuations. At the same time, an external-mediated increase in intracellular ROS level by H_2O_2 treatment resulted to be able to induce the same mechanisms activated by TMZ in sensitive cells after ROS release, determining a responsive profile both in sensitive and resistant cells. Of note, here we report that, only the concurrent treatment with H_2O_2 and TMZ induced a completely significant responsive profile in resistant cells, confirming the crucial role of ROS, CMA, HIF-1α modulation and the drug. The final result of this work is the development of a TMZ-resistant murine orthotopic model by i.c. injection of CT-2A cells. This model resulted to be responsive to RT, as reported by MRI studies. ^{18}F-Fluciclovine tracer was used to monitor tumour extent in view of its implementation on the evaluation of response to treatment by PET. Finally, preliminary IHC data of untreated and RT-treated mice brains have confirmed a down-regulation of ASCT2 expression after RT compared to the untreated ones.

Conclusions: *In this thesis work, it has been demonstrated that HIF-1α activity is a key player in resistance to TMZ, that CMA has a crucial role in mediating TMZ-induced cytotoxicity and that the induction of this pathway was due to a transitory increase in intracellular ROS level. Moreover, an exogenous increase in ROS levels has been able to restore a completely responsive profile in resistant cells opening the way for the evaluation of new therapeutic approaches. CT-2A orthotopic murine models represent a good opportunity for the in vivo assessment of these new treatments, especially using the non-invasive multimodal imaging, strategy described herein.*

INTRODUCTION

1. GLIOMA

Glioma represents the most frequent Central Nervous System (CNS) tumours in adults [1], in fact it accounts for 75 percent of all the primary brain cancers. Among gliomas, glioblastoma multiforme (GBM), belonging to the high-grade gliomas, is the most diffused one [2]. Gliomas are generally categorised in:

- **Diffuse gliomas**, defined by a high infiltrative growth within the neighbouring parenchyma
- **Non diffused/circumscribed gliomas**, as pilocytic astrocytoma and ependymomas
- **Rare histological categories** [1,2].

For what concerns the first category, since diffuse glioma takes origin from individual glial or glial precursors cells, it has an infiltrating power to occupy brain or spinal cord parenchyma in an uncontrolled manner, increasing intracranial pressure, rousing symptoms as headaches, emesis, convulsions and brain nerve disfunctions [2,3]. By cellular side, these individual cancer cells provoke morphological and functional disorders on surrounding neurons and vessels, entrapping them and forming with them structures which characterise diffuse gliomas. These latter have been classified based on histopathological analyses and according to the fifth edition of the World Health Organization (WHO) of CNS published in 2016 [1], as follows:

- **Diffuse astrocytomas**, whose glioblastoma is the most recurrent and aggressive one
- **Oligodendrogliomas**

- **Oligoastrocytomas**, with mixed astrocytic and oligodendroglial cell populations.

Another classification that could be taken into account is based on the level of mitotic activity, necrosis and vascular proliferation that allows assigning a growing malignancy grade (from **I** to **IV**) [2].

1.1 Genetic Background

For what concerns the genetic background, a discriminating component among diffuse gliomas is represented by the high presence of frequent point **mutation in isocitrate dehydrogenase enzyme**, both isoforms 1 and 2, (**IDH1** and **IDH2**) at arginine 132 (R132) or the analogous residue arginine 172 in IDH2 (R172) in WHO grades II and III astrocytomas, oligodendrogliomas, oligoastrocytomas and glioblastomas derived by lower grade cancers (defined secondary glioblastomas). Strictly related to this IDH mutation, a total **1p/19q co-deletion** has been included as defining gliomas grading [4].
An intersection between the aforementioned parameters and the presence/absence of already described histological features needs to be made in order to further compartmentalise diffuse gliomas (which are WHO grade II, III and IV, the WHO grade I contains none of the aforementioned histologic features) **(Figure 1)** [5,6] defined as:

- **WHO grade II,** as low grade, that can be distinguished in astrocytic and oligodendroglial gliomas. As molecular genetic signature, this grade presents IDH1/IDH2 mutation and 1p/19q

non-codeleted for astrocytomas and 1p/19q-codeleted for oligodendrogliomas

- **WHO grade III**, defined anaplastic as well and, as for the grade II, it is categorised in astrocytic and oligondendroglial gliomas, which are different, respectively, for being IDH1/IDH2 mutant, 1p/19q non-codeleted and IDH1/IDH2 mutant, 1p/19q-codeleted. Anaplastic glioma is featured by a significant cell proliferation, atypical cytological aspect, high vascular proliferation, necrosis, and mitotic activity.
- **WHO grade IV**, defined also glioblastoma (GBM): this grade presents neither mutations in IDH1/IDH2 nor 1p/19q-codeletion. Moreover, it is characterised by an elevated vascular proliferation and necrosis.

Moreover, in young patients, the **histone H3-K27M mutation** often occurs and presents a poor prognosis; anyhow, in adults grades II and III gliomas are mostly IDH-mutant, while grade IV ones often display a IDH mutation only when they derive by a lower grade tumours and, for this reason, it is defined “secondary glioblastoma”; instead, the defined “primary glioblastoma”, that begins directly as a high grade tumour, is more recurrent and is properly IDH-wild type, as seen in the **Figure 1** (histone H3-K27M mutation = H; secondary glioblastoma = S, primary glioblastoma = P).

Mainly, some GBM grade IV typical molecular features are widespread among lots of diagnosticated grades II and III - IDH-wild type diffuse gliomas in adult patients (**Figure 1** = red box with exclamation mark). Furthermore, some astrocytic cancers which cannot be characterised

by tests or whose test results are not satisfying, are classified as **"not otherwise specified"** (**NOS**) astrocytoma or NOS GBM (**Figure 1** = hatched bar, number 1), tumours with mixed astrocytic and oligodendroglial phenotype and defined NOS oligoastrocytoma/anaplastic oligoastrocytoma (**Figure 1** = hatched bar, number 2); oligodendroglial glioma is specified as oligodendroglioma or NOS anaplastic oligodendroglioma in adults and as paediatric oligodendroglioma in young patients (**Figure 1** = hatched bar, number 3) [1].

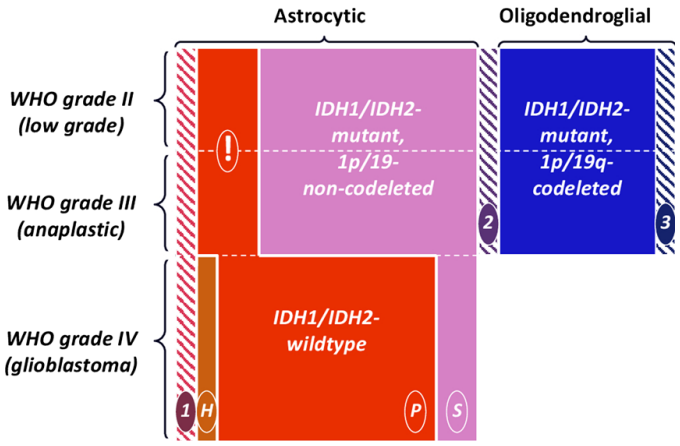

Figure 1: Classification of the diffuse glioma grades according to IDH mutation and 1p/19q deletion.
H = histone H3-K27M mutation; S = secondary glioblastoma; P = primary glioblastoma. Exclamation mark = grades II and III-IDH-wildtype diffuse gliomas with some glioblastoma molecular aspects; hatched bar, number 1 = NOS astrocytoma/NOS glioblastoma; hatched bar, number 2 = NOS oligoastrocytoma/anaplastic oligoastrocytoma; hatched bar, number 3 = oligodendroglioma or NOS anaplastic oligodendroglioma in adults and as paediatric oligodendroglioma in young patients (adapted from [1]).

1.2 Glioblastoma Multiforme

Glioblastoma Multiforme (**GBM, Astrocytoma IV, WHO**) is the most aggressive astrocytic brain tumour in adults, it is characterized by a high aggressiveness and a median survival which does not exceed 12 - 15 months [7,8]. As mentioned before, this tumour can arise either as primary GBM based on a *de novo* transformation, or as secondary GBM as evolution from already existing low-grade astrocytomas. GBM is hard to treat because of its tough microenvironment [9].

1.2.1. GBM Cell Heterogeneity

GBM is characterized by a significant tumour heterogeneity, in which several cell populations are involved; in particular, **GBM stem cells** (**GSCs**) are the most described for their self-renewal and multipotent differentiating feature [10]. The GBM tumour microenvironment, beyond the presence of malignant astrocytoma cell population and GSCs, is made of a high amount of residing and infiltrating immune cells (30-40 % of mass, in particular infiltrating macrophages, stromal and vascular endothelial cells and pericytes which all build up niches within the GBM itself) [9,11]. All these populations can stay in contact within the **extracellular matrix** (**ECM**) borders, where non-cellular fluidic- and macromolecules-based substrates harbour [12]. Of note, niches can be distinguished depending on cell composition, whose disposition within the tumour is strictly dependent on GBM *modus operandi*. In other words, it is always clearer that these several tumour and non-tumour cell types, as, respectively, highly proliferating and

infiltrating astrocytoma cells, GSCs ones, and macrophages, microglia, dendritic and lymphocytic cells, cooperate in remodelling different tumour components and its behaviour [13]. Focusing on a closer perspective, this microenvironment is characterised by the tumour core, which is featured by densely aggregated proliferating tumour cells, which expands to the more external (peri) necrotic zones, perivascular areas circumscribing vessels and (peri) hypoxic areas **(Figure 2)** [11].

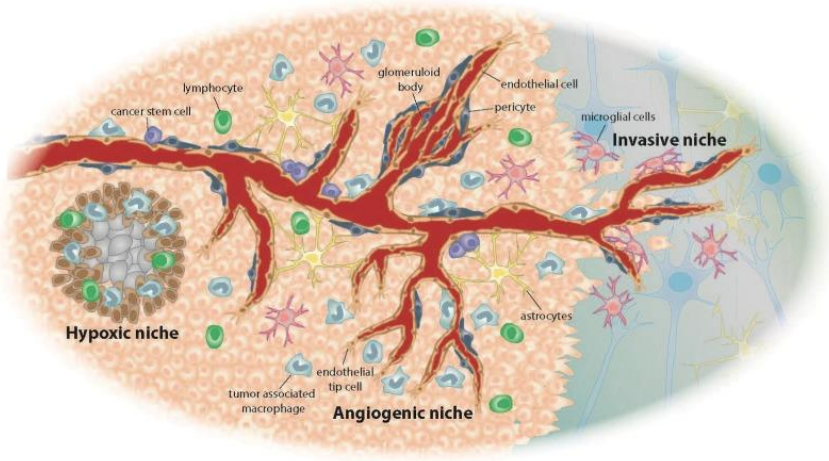

Figure 2. GBM tumour microenvironment niches.
GBM and glioma GSCs are embedded in a heterogeneous tumour microenvironment composed of different cell populations and compartmentalised in regions defined niches, which regulate metabolic needs, immune surveillance, survival, invasion and glioma stem cell maintenance. In the angiogenic niche GSCs are positioned very close to the abnormal angiogenic vasculature; in the invasive niche tumour cells stimulate normal blood vessels to migrate deep within brain parenchyma. In the hypoxic niche, a necrotic areas harbour, with surrounding hypoxic palisading tumour cells. (Adapted from [9]).

Moreover, GBM presents a **disrupted blood-brain barrier (BBB)**, which is caused by a **vascular endothelial growth factor (VEGF)**

notable **expression** and that is constituted by a neurovascular unit in which endothelial cells, astrocytes and pericytes are involved and all together cooperate to strictly modulate molecules and ions passage through blood and brain, phenomenon which significantly limits transfer of drugs for chemo-treatment [10,14]. VEGF over-expression, beyond to cause a BBB disruption, is responsible of abnormal vasculature formation, both in morphology and functionality, and also hinders GBM-reactive T cells extravasation and this developed immune-suppressive environment gives opportunity to GBM tumour to escape from host immunosurveillance [12,15]. More in deep, at the beginning of glioma proliferation, normal astrocytes are moved away from vasculature by astrocytoma cells, interrupting communication between astrocytes and vessels, factor which contributes to damage blood-brain barrier. Moreover, astrogliosis occurs, phenomenon which happens during CNS injuries, that consists of astrocytic cells circumscribing GBM cells, starting the proliferation, migration, and in the meanwhile several metabolites, growth factors and cytokines promoting gliomagenesis are produced [16]. Among all paracrine interplays between glioma cells and astrocytes, the connective tissue growth factor (CTGF), made by astrocytes, interacts with GSCs tyrosine kinase receptor type A (TrkA) and Integrin β1, and this binding induces both nuclear factor kappa B (NF-κB) activity and the zinc finger E-box binding homeobox 1 (ZEB1), an **epithelial–mesenchymal transition (EMT)** transcription factor able to favour GBM cells infiltration [17,18].

Of note, a damage to BBB provokes a permeabilization in vessels, which in turn causes a fluidic and plasma leaking which spills directly to the tumour tissue, originating cerebral oedema and increasing interstitial pressure [19]. Another mechanism that originates from this damaging is the blood flow braking in obstructed tumour vessels where a meaningful decreased oxygen partial pressure (pO_2) within tumour is observed [20]. This latter phenomenon, known as **hypoxia**, generates a pseudo-palisading necrosis, which in turn recruits principally pro-tumoral macrophages, that activate all those pro-angiogenic and immunosuppressive pathways able to enlarge GBM vessels network towards these necrotic areas [21]. Beyond these innate immune cells, even endothelial cells, already existing in tumour vessels, vasculature progenitors of bone marrow and GSCs are main contributors to neo-angiogenesis process [13]. From the molecular side, this angiogenic process is driven by the expression of a fundamental transcriptional factor: **hypoxia-inducible factor-1α (HIF-1α)** (see the paragraph **1.2.6**) [22].

1.2.2 GBM Genetic Characterisation

Both in primary and recurrent GBM, a pattern of genes results to be altered, as follows:

- **p53-dependent DNA damage** checkpoint response pathway and pRB-dependent cell cycle restriction point pathway [23]**,** where in particular, CDKN2A and CDKN2B genes are deleted [24,25]. In physiological condition, p53, poorly expressed, is modulated by MDM2 and MDM4 (in turn regulated by ARF)

through ubiquitination and degradation steps; but, under stress conditions as DNA damage, genotoxicity, oncogene activation, aberrant growth signals and hypoxia, the p53-MDM2 binding is interrupted, triggering to p53 activation. Moreover, according to The Cancer Genome Atlas (TCGA, [26]), ARF-MDM2-p53 pathway is deregulated in 84% of GBM and in more than 94.1% of GBM cell lines, while p53 is not regulated in in 22% of GBMs [25]. Under physiological conditions, kinases encoded by CDKN2A and CDKN2B genes are involved in the CDK4/6 inhibition through a hyperphosphorylation, causing cell cycle brakes at the late G1 phase checkpoint. Their deletion causes a cell cycle control missing and an abnormal cell cycle progression [27].

- **Epidermal Growth Factor Receptor (EGFR)**, that is hyperactivated through mutation or amplification. This receptor belongs to a larger family of ErbB receptors with tyrosine kinase activity and it is involved in a wide range of pathways, both ligand-dependent and -independent. In pathologic conditions, EGFR overexpression correlates to increased cell survival, proliferation, aggressiveness and invasion [28].
- **TERT promoter**, that results to be mutated. It is a guanine-cytosine rich (GC-rich) promoter which affects TERT expression in several frameworks, and it is featured by specific recognition sequences binding, for instance, to p53 and the aforementioned HIF-1α. When TERT promoter is mutated, its expression appears increased and this phenomenon provokes

a telomerase activity rescue, which in turn favours malignant progression [29].

- **RTK/Ras/PI3K signalling pathway**, which presents mutations and also a loss of function of the phosphatase and tensin homolog (PTEN) is common. For instance, catalytic and regulatory components of this pathway (PIK3CA - PIKC2B and PIK3R1, respectively) are mutated and amplified **(Table 1)** [24].

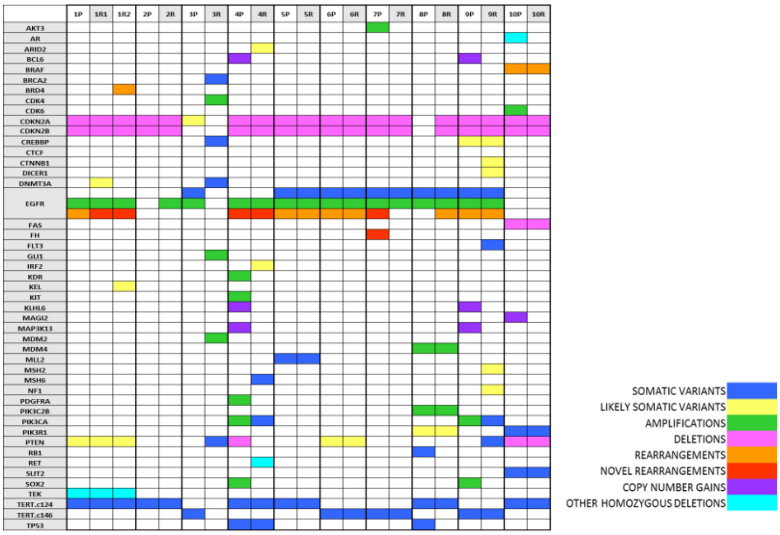

Table 1: Known and likely pro-tumorigenic genetic alterations in primary and recurrent GBM.
Table includes deletions, amplifications, mutations, and rearrangements within 315 genes and 28 introns found in 10 patients' primary and recurrent GBM (adapted from [24]).

RTKs result to be pivotal modulators of all those growth factors-mediated cascades involved in proliferation, survival and metabolism. Of note, GBM cells which surround pseudo-palisading necrotic regions, express a high level of HIF-1α

protein, which in turn contributes to VEGF release, that, as we described above, is implicated in neo-angiogenesis. In detail, type IV RTKs receptors, as VEGFR 1/2/3 and their co-receptors, through hypoxia both dependent and independent processes, are able to favour GSCs niche proliferation and in turn, cancer growth **(Figure 3)** [30].

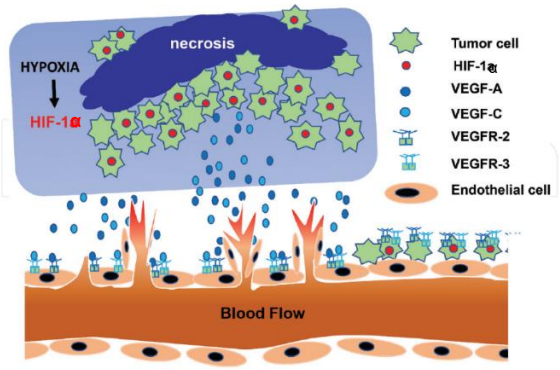

Figure 3: The tumour cells in hypoxic conditions induce neovascularisation in GBM.
Herein, tumour cells secrete enhanced levels of VEGF family members, as VEGF-A and VEGF-C. RTKs which are specific of endothelial cells, as VEGFR-2 and VEGFR-3, through ligand (VEGF-A, VEGF-C) binding, are able to stimulate proliferation and migration of endothelial cells. In the peri-vascular areas, GSCs harbour (adapted from [30]*).*

1.2.3 Standard Therapy based on Stupp Protocol

GBM standard therapy follows the Stupp protocol, finely tuned in 2005 [31]. It is characterized by surgical resection followed by **radiotherapy (RT)** with concomitant **Temozolomide (TMZ)**-based chemotherapy; however, prognosis remains dismal, entailing survival up to maximum

two years [7]. In general, GBM has a heterogeneous and infiltrative nature and, for this reason, it can acquire a resistant phenotype and its response to lots of treatment modalities is not predictable [32].

For what concerns radiotherapy, since GBM is characterised by elevated aggressiveness and proliferation rate, often radiation treatment results inefficient to defeat it [33]. Moreover, from biochemical side, GBM cells result to be strongly glycolytic also in normoxic conditions, phenomenon called “Warburg effect” [34]. In this microenvironment, high levels of **superoxide anion (O_2^-)** are mainly generated from mitochondria (mt), the high quantity of anion produced rapidly undergoes to dismutation to **hydrogen peroxide (H_2O_2)**, which in turn, translocating to the cytosol, mediates the radio-resistance [35]. Both O_2^- and H_2O_2 constitute some of the **Reactive Oxygen Species (ROS)**, which mediate several pathways, but when they overcome a threshold concentration within cell microenvironment, may cause the so called “oxidative stress”, which may damage cells [36]. In fact, GBM cells reply to this potential damage provoked by high levels of ROS, augmenting their antioxidant defences, activating a specific detox machinery composed of enzymes and molecules, as **catalase** and **superoxide dismutase 2 (SOD2)** enzymes, **glutathione (GSH)** molecule and GSH-related enzymes (see the paragraph **1.2.8**) [37]. Ionising radiations cause their cytotoxic effect by inducing ROS production, which in turn elicits nucleic acids damage and genomic instability. In this way, increased amount of catalase and SOD2 enzymes improves DNA damage-induced by radiation, contributing to the resistance produced by radiation-mediated cell damage.

Furthermore, the reduced GSH contribution is pivotal for protecting cells from ROS and enhancing radio-resistance. Moreover, lactate produced by aerobic glycolysis behaves as an antioxidant, strictly relating this molecule to radio-resistance [38]. Moreover, it is now always more evident GBM radio-resistance association to mitochondria-mediated stress and to consequential over-production of Reactive Oxygen Species (ROS) scavengers, that reply to radiotherapy shifting cell status to an anti-oxidative one [39].

In summary, radio-resistance is composed by a series of orchestrated cell replies turned to defend cells from increased ROS levels caused by ionizing radiations [40].

INSTRUMENTATION FOR RADIOTHERAPY

From a biological point of view, radiation represents a waves/stream of particle-dependent energy which works for damaging DNA in tumour cells, causing cell death. Radiations used for cancer treatment are defined "ionising" because they generate ions in cells and microenvironment, then "capturing" electrons from atom and molecules, and provoking with high likelihood cell damage and growth inhibition [41]*. External beam radiation is the most used technique for RT. Radiations are generated by a machine that focalizes the radiation waves to specific tissue volumes, for instance the tumour. Usually, the total dose is split in smaller doses, called for this reason fractions, which makes the therapy lasts for weeks and, in this way, damages to normal tissues are contained and radio-responsiveness is maximised* [42]*. Other radiotherapeutic approaches are available such as those related to brachytherapy or internal radiation. In this case, a radioactive material is placed directly within or close to the tumour area. Through this method, a high dose of radiation (compared to external beam radiation) can be focused directly on the small tumour area* [43]*. Finally some radiopharmaceuticals made up of a specific carrier labelled with a radioactive atom which decays produce a corpuscular emission can be used to provide RT at all the potential tumour sites (primary tumour and metastases) since the radiopharmaceutical is distributed by blood and localizes in relation to a specific molecular feature* [44]*.*
Although the availability of several RT options new opportunities in this scenario are necessary and some improvements attempts are in ongoing phase.

Temozolomide (TMZ, commercial name Temodal) is an alkylating agent, discovered for its antitumor activity for the first time in 1987 and approved after in 2005 by Food and Drug Administration (FDA) [45,46]; it is able to methylate some DNA bases, specifically Guanine in N7 and O6 positions and Adenine in N3 one, during its replication (70% for N7-Guanine, 10% for N3-Adenine and 5% for O6-Guanine) [7,47]. This molecule is a monofunctional alkylating agent, orally

administered as prodrug: TMZ is hydrolysed at physiologic pH, forming the 5-(3-methyltriazol-1-yl)imidazole- 4-carboxamide (MTIC) compound, whose hydrolysis to 5-amino-imidazole-4-carboxamide (AIC) and methyldiazonium ion reacts with DNA and releases its methyl group, causing methyl adducts formation in DNA **(Figure 4)** [47,48].

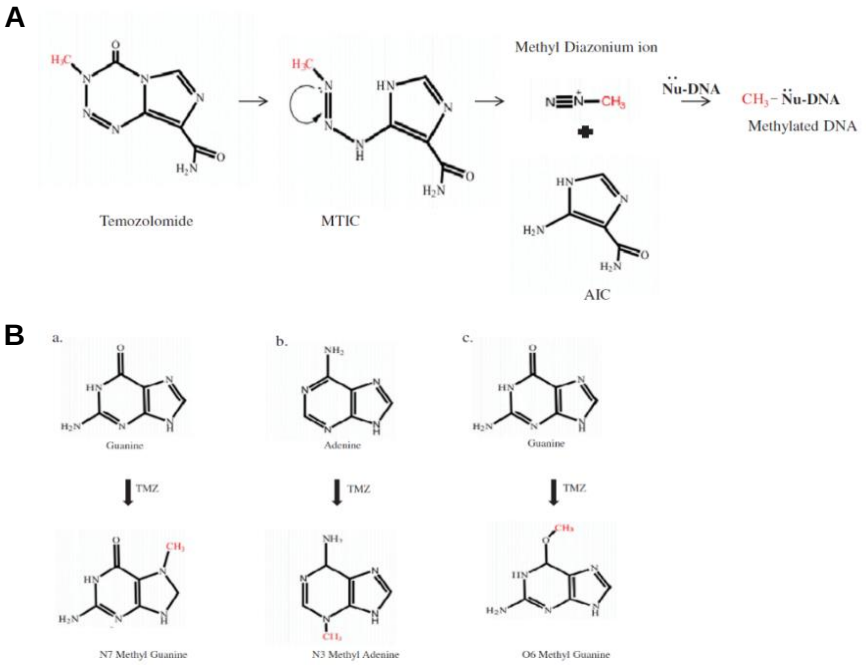

Figure 4: Temozolomide utilisation for treating GBM.
A: *Mechanism of action of the alkylating agent.* ***B:*** *Formation of methyl adducts on DNA bases (adapted from* [47]*).*

Despite TMZ is used in standard therapy, GBM resistance is an important problem, which varies depending on different cell features, as genotype, phenotype, mutational state and genetic profile [49].

1.2.4 Temozolomide-mediated Autophagy activation

Temozolomide, beyond to its alkylating action, is able to induce autophagy, which is a degradation and recycling process that cell adopts when it is exposed to stress conditions. In general, under stressors, cell reacts inducing this pathway for surviving, thus recycling intracellular proteins and organelles which are damaged, or, otherwise, for activating **apoptosis** (whose the main modulator factors are the pro-apoptotic ones **BAX** and **BAD** and the anti-apoptotic one, **BCL-2** [50,51]), because it is no longer able to sustain its vital functions [52]. This mechanism has been deeply studied among several works in literature, in particular contextualised in pathologic conditions as those of tumours: in detail, lots of papers have validated the autophagy pro-apoptotic trend in tumour conditions, in particular, TMZ-based GBM therapy has the potential to induce autophagic pathway, which in turn is followed by G2/M arrest and, consequently, apoptosis , thus favouring responsiveness to the treatment [53–55].

1.2.5 DNA repair mechanisms induced by Temozolomide action

It is well documented that resistance to TMZ occurs, due to DNA repair system activity. Main repair mechanisms are:

- **O6-methylguanine-DNA methyltransferase enzyme (MGMT)-mediated direct repair (DR)**
- **Mismatch repair (MMR)**
- **Base excision repair (BER)** [56].

These systems are strictly dependent to the formation of adducts, after TMZ administration. The N7 methyl guanine (N7MeG) and N3 methyl adenine (N3MA) are more frequent but less harmful compared to the less frequent but most dangerous O6 methyl-guanine (O6-MeG). In fact, although the high nucleophilic power of the first two adducts, they do not cause mismatches and rarely they are powerful to interfere with DNA replication with cytotoxic consequences [48]. O6 methyl adduct formation is reversed by the **MGMT** enzyme, a cytoplasmic protein which crosses the nucleus when the damage occurs and transfers an alkyl surrogate from the guanine oxygen to the Cysteine 145 (C145) within its catalytic site, inducing its own degradation through proteasome machinery [57]. MGMT has to be continuously expressed to ensure its detox activity but its transcription is strictly dependent by the methylation status of cysteine-phosphate-guanine (CpG) site in its promoter [47]. In fact, the less is the methylation in MGMT promoter the higher enzyme activity is guaranteed, thus counteracting TMZ effect. On the contrary, a higher promoter methylation percentage assures a lower enzyme activity, increasing GBM responsiveness to TMZ treatment [7]. For this reason, MGMT methylation promoter status has been defined as a TMZ therapy response biomarker in clinics **(Figure 5A)** [58]. Another repair system related to O6-methylguanine is the **MMR** one, which generally removes mismatches occurring during DNA synthesis. In specific cases, O6-MeG mispairs with thymine are recognized by MMR, which, instead to remove the O6-MeG cytotoxic adduct, removes the thymine from the new synthetized strand, provoking a mistaken O6-MeG inclusion during

replication phase; as consequence, futile cycles occur, which cause cell cycle block and apoptosis, mediating TMZ cytotoxic effect [59]. On the other hand, a loss of MMR function can be related to TMZ resistance, since it does not reply to TMZ-activated mispairing **(Figure 5B)** [60,61]. The last cell system repair, the **BER** one, is activated to repair single nucleotide modifications, specifically the N7MeG and N3MeA adducts. When this repair mechanism is not functioning in GBM cells, TMZ-mediated N7MeG adducts formation result to be cytotoxic to cells; furthermore, it has been described that BER intermediates able to maintain unpaired gaps are more toxic than the original methyl adducts formation. **(Figure 5C)** [62].

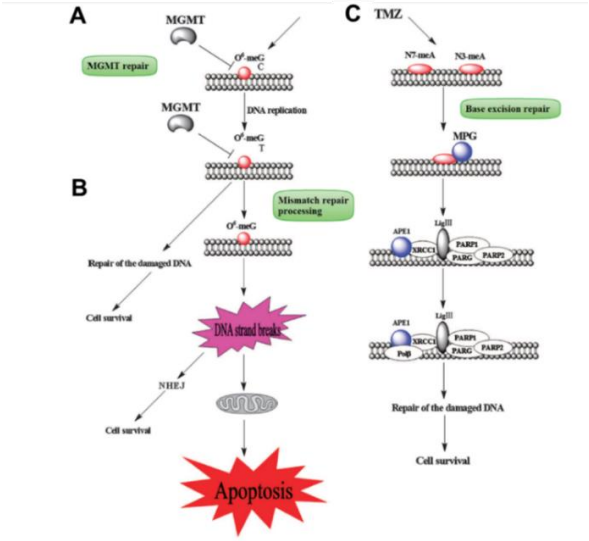

Figure 5: MGMT and other DNA repair mechanisms deal with DNA damage produced by the alkylating agent TMZ in cancer cells.
A: *MGMT-mediated direct repair system.* ***B:*** *Mismatch repair mechanism (MMR).* ***C:*** *Base-excision repair system (BER) (adapted from* [59]*).*

Among the several already described GBM mechanisms of resistance to radio-chemotherapy, a hypoxic microenvironment and HIF-1α activity result to be crucial in mediating it. [58,59,63–66].

1.2.6 Hypoxia and HIF-1α

As already mentioned, hypoxia, which is a decrease of partial O_2 pressure (pO_2) in organs and tissues and which is observed during several pathological conditions is a predominant GBM feature [67]. In detail, it is mostly resilient within the pseudo-palisading necrotic areas, where innate, endothelial, GSCs and bone marrow progenitor cell populations are harboured as well [9,22]. Hypoxia is also related to GBM resistance to treatment [68]. One of the most important factors induced during hypoxia is **Hypoxia Inducible Factor-1α (HIF-1α)** that plays a key role under hypoxic environment. In detail, HIF-1α is characterized by an Oxygen-sensor domain, that is highly modulated by O_2 concentration and it is featured by a short half-life of 5 minutes [69]. In normoxia, HIF-1α is continuously degraded, mainly through Prolyl-Hydroxylase (PHD) enzymes activity, that are dioxygenase which require molecular oxygen, Fe^{2+} and 2-Oxoglutarate as substrates to act, properly hydroxylating P402, P564 and N803 on HIF-1α. At this point, Von Hippel-Lindau protein (pVHL) is recruited, which in turn, retrieves the ubiquitin ligase protein complex consisted in elongin B, elongin C, and cullin, which ubiquitinate HIF-1α for 26S proteasome degradation. Moreover, among the PHDs, the isoform 2 has been identified as oxygen sensor which keeps steady state levels of HIF-1α under normoxia [70]. Conversely, during hypoxic conditions (or in condition in which iron levels are low), this regulatory mechanism

is inhibited because PHDs cannot hydroxylate HIF-1α, favouring a HIF-1α translocation into the nucleus, where, dimerizing to HIF-1β (even known as aryl hydrocarbon receptor nuclear translocator ARNT), binds to the cofactor p300/CBP. This new complex binds Hypoxia Response Element (HRE) in specific promoter sequences and induces genes expression for angiogenesis, glycolytic metabolism, mitophagy, stemness, invasiveness and cell cycle regulation **(Figure 6)** [71].

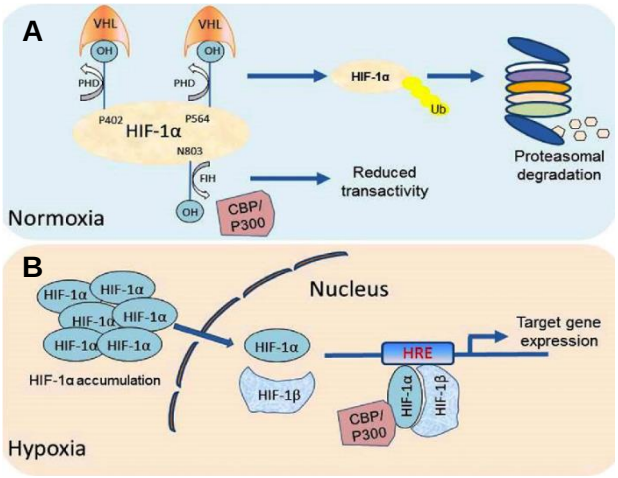

Figure 6: HIF-1α mechanism of action.
A: *During normoxia, HIF-1α is prolyl-hydroxylated in specific residues, reaction which allows its ubiquitination and transfer to proteasome for its degradation.* ***B:*** *In hypoxia, HIF-1α is not prolyl-hydroxylated and it is translocated into the nucleus where, with HIF-1β, binds HRE sequences on DNA and activates expression of genes related on different pathways (adapted from* [70]*).*

Among the several pathways activated in hypoxic conditions, HIF-1α is implicated also in **epithelial-mesenchymal transition (EMT)** pathway modulation, mediating an increase of the transcription of pro-

mesenchymal factors, as SLUG [72,73]. Among molecules involved in EMT transition process, beyond **SLUG**, **SNAIL** and **E-cadherin** are pivotal players. In detail, among the E-cadherin expression suppressors, SNAIL and SLUG are the main key players, and both belong to the transcriptional activators of SNAIL family and modulate the reduced expression of several epithelial markers and the augmentation of other different mesenchymal ones. In particular, SNAIL transcriptional activity is strictly dependent from its localization between nucleus and cytosol. In fact, its phosphorylation triggers to its inactivation but TGF-β factor secretion by mesenchymal cells induces its translocation into the nucleus via SMAD 2 and 3 proteins. SLUG is particularly involved in increasing the high invasion and migration power which characterises malignant gliomas [74]. E-cadherin, which in gliomas results to be poorly present, belongs to the cadherins family, which are transmembrane calcium-dependent cell-adhesion molecules, which are key players in tissue building up and morphogenesis. In particular, E-cadherin links to the cytosolic β-catenin, which in turn binds directly to the α-catenin, which binds the cadherin system to the actin in the cytoskeleton. An E-cadherin down-modulation in tumour conditions is related to its high invasiveness and metastasis **(Figure 7)** [75].

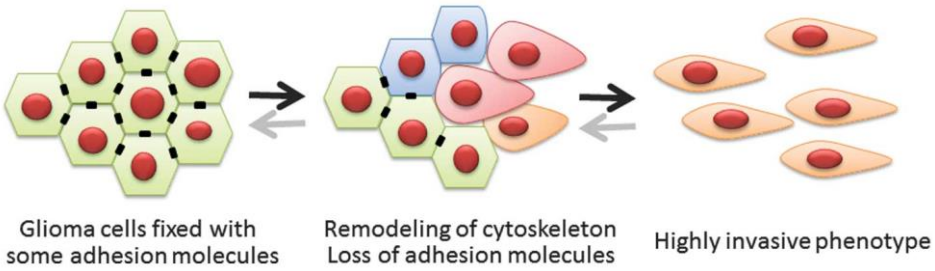

Figure 7: EMT in glioma cells.
Glioma cells lose adhesion molecules and alter their cytoskeleton through a reprogramming process. The EMT- reverse process, the Mesenchymal-Epithelial Transition, is pivotal for the formation of distant or disseminated tumour nodules (adapted from [74]*).*

In GBM HIF-1α covers a very crucial role even in responsiveness to TMZ treatment. In particular, HIF-1α activity has been suggested as biomarker of TMZ treatment efficacy in U251 TMZ-responsive cells [76]. Furthermore, since this pivotal role covered by HIF-1α, this transcription factor has been selected as target of cancer therapy in clinics, exploiting its inhibitors to target several cancer pathways as cell proliferation and invasion, apoptosis, glucose metabolism and angiogenesis [77]. In fact, in 2010, a Phase I clinical trial of PX-478 was completed at two sites in the US after having tested this drug against lymphomas and solid tumours [78]. PX-478 (S-2-amino-3-[4-N, N,-bis(2-chloroethyl)amino] phenyl propionic acid N-oxide dihydrochloride) derives from melphalan and is orally bioavailable. A suppression of HIF-1α levels in human tumour xenografts and of HIF-1α target genes, among which vascular endothelial growth factor (VEGF) and the glucose transporter-1 (GLUT-1), has been reported. Moreover, PX-478 abrogated HIF1α protein levels and its

transactivating activity in several cancer cell lines [79]. Of note, it has been reported that, among the proteins recognised by one of the three authophagy types, the Chaperone-Mediated Autophagy (CMA), HIF-1α is one of the most important [79]. In fact, in a work of Wen et al, a tight relation between a CMA phosphatase, the Pleckstrin homology (PH) domain and leucine-rich repeat protein phosphatase 1 (PHLPP1), and HIF-1α in colon cancer cells has been found: more precisely, hypoxia is able to down-modulate PHLLP1 promoting its degradation by proteasome and increasing HIF-1α activity able to mediate tumorigenesis in colon cancer cells [87].

1.2.7 Autophagy and CMA

Autophagy, albeit is characterised by three variants which differ from sequestration targets, however all of them end with the cargo delivery to the lysosomal compartment for its degradation and recycling [80]:

- **Macroautophagy**: it is characterised by cargo embedding in different double-membrane vesicles until its delivery to the lysosome
- **Microautophagy**: during this process, lysosomal membrane protrusions or invaginations occur for incorporating cargo
- **Chaperone-Mediated Autophagy (CMA)**: differently to the other aforementioned two ones, CMA process does not exploit membranous vesicles for embedding cargo, but chaperones are pivotal to identify only proteins, as targets, which contain a conserved pentapeptide domain (KFERQ, made of Lysine-Phenylalanine-Glutamate-Arginine-Glutamine).These

chaperone-bound proteins are then unfolded and one by one translocated across the lysosomal membrane for consequent degradation [81].

CMA is one of the three main autophagic processes carried out by cell in specific conditions of stress, such as lack of nutrients, oxidative stress and others [82–84]. CMA consists in the degradation of specific proteins carrying the KFERQ-like motif, which are selectively and individually delivered to lysosomes by chaperon proteins such as the **heat shock chaperone 70 kDa (HSC70)**, with the help of other co-chaperones. The target proteins are delivered to the lysosomes where they bind the **lysosome-associated membrane protein type-2A (LAMP-2A)**. This protein works as a receptor on lysosome membrane and after polymerisation, introduces the target protein into the lysosomal lumen for being degraded, with the contribution of lysosomal-HSC70 (lys-HSC70). CMA activity is strictly modulated by local LAMP-2A and lysosomal HSC70 amounts [85]**.** Several works have shown HIF-1α degradation in lysosomes through CMA pathway [86,87]. Of note, another CMA pivotal component is the **Pleckstrin homology (PH) domain and leucine-rich repeat protein phosphatase 1 (PHLPP1)**, belonging to phosphatase 2C (PP2C) group in the family of S/T phosphatase **(Figure 8)** [88]. In fact, it binds to lysosomal membrane and regulates CMA activity by dephosphorylating glial fibrillary acidic protein (GFAP) that in the phosphorylated form inhibits CMA [89].

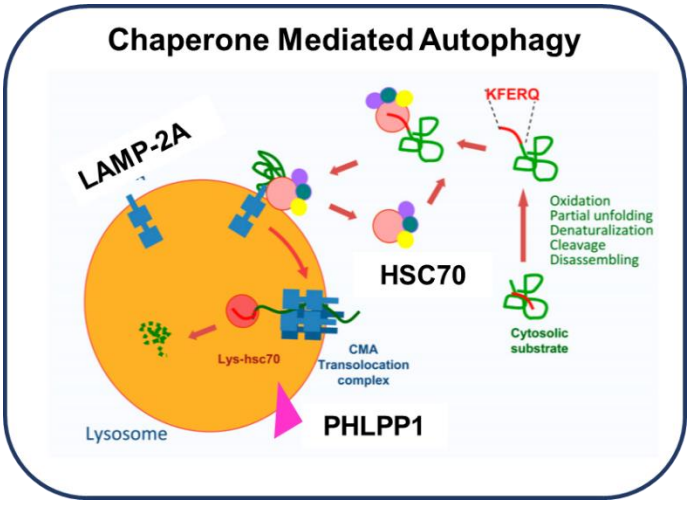

Figure 8: Chaperone-mediated autophagy schematic representation. *CMA, a form of selective autophagy, is involved in degradation of proteins containing KFERQ-like motif. Different chaperons, as HSC70, cooperate in shuttling target proteins to lysosomes. Herein, after LAMP-2A binding and multimerization, the target proteins are unfolded and degraded (adapted from* [80]*).*

CMA can be induced by lack of nutrients, and several stressors such as oxidative stress. In literature, a Reactive Oxygen species (ROS)-mediated CMA activation has been reported. Moreover, it has been shown that TMZ induces a ROS burst [90]. For this reason, in this thesis work, the involvement of oxidative stress in CMA activation is analysed.

1.2.8 Mitochondrial Oxidative Stress

It has been demonstrated that TMZ-mediated ER stress is responsible for the release by mitochondria of ROS and that their release is related to TMZ responsiveness [83,91]. Trying to describe a mechanism, a high ROS amount and Calcium (Ca^{2+}) overladen provoke

mitochondrial permeability transition (MPT) pore opening, which triggers mitochondrial membrane potential abrogation and cytochrome c and pro-apoptotic factors release, from mitochondrial inner membrane space into the cytosol, incrementing even more ROS generation and leading to ATP depletion. Mitochondria constitute the major ROS producers due to the activity of the respiratory chain. Here, molecular oxygen is partially reduced to superoxide anion, the hydroxyl radical (OH•) and hydrogen peroxide are generated within mitochondrial matrix and intermembrane matrix; in particular, superoxide is massively generated by mitochondrial complexes I and III through the transfer of a free electron to the O_2 [92]. These species, being highly reactive, are readily converted to the more stable H_2O_2 molecule by manganese superoxide dismutase (MnSOD/SOD2) located in the mitochondrial matrix or by the one situated in the cytoplasm, the Copper/Zinc SOD (CuZn/SOD1) [93]. Different studies have focused on assessing mitochondrial key role in ROS production, exploiting several molecules: among these, **MitoTEMPO (MitoT)**, which is a SOD2 mimetic, is able to abrogate mitochondrial ROS overproduction and it damages the mitochondrial **Oxidative Phosphorylation System (OXPHOS)** functionality and mitochondrial DNA (mtDNA) [94]. Moreover, H_2O_2 contributes to the activation of inflammatory pathways. It can be reduced by metal ions, as iron or copper, forming, through the Fenton reaction, the hydroxyl radical OH•, whose formation results highly reactive and dangerous for biological macromolecules [95]. Moreover, as shown in **Figure 9**, other hydrogen peroxide detoxification pathways have been described: in

detail, the H_2O_2 can be converted to molecular oxygen and water by catalase enzyme or to water and a reduced molecule by means of a peroxidase enzyme, as the **glutathione peroxidase (GPx)** [93,96].

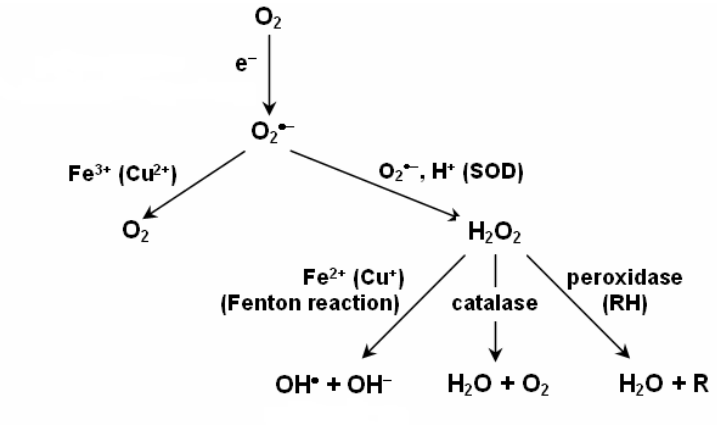

Figure 9: Reactions of O2- conversion to H_2O_2, including Fenton reaction.
After O_2^- conversion, H_2O_2, could be converted according to different reactions, including the Fenton one (adapted from [97]*).*

In particular, in GBM cells, since the content of flavoproteins which transfer electrons is high, massive amounts of hydrogen peroxide are constantly generated as consequence, make H_2O_2 also a “second messenger” [92]. In detail, ROS and, especially hydrogen peroxide, have the ability to induce autophagic pathway, which, depending on the intracellular status, can be pro-survival or pro-apoptotic. Furthermore, only a moderate ROS dose exposure favour autophagy activation [95]. Linked to this latter phenomenon, massive ROS produced at mitochondria level have the ability to cause a PHD activity inhibition, which in turn deactivates proteasome-mediated HIF-1α degradation, which, in turn, becomes an autophagic action [98].

In general, beyond the hydrogen peroxide, reactive oxygen species all contribute in activating antioxidant enzymes for protecting cells from an apoptotic destiny. These detox mechanisms have been therapeutic target in different studies [99,100]. At physiological levels, oxidative stress and detox system are regulated by a dynamic equilibrium. In brain tissue, the most important redox machinery is driven by the already described catalase and superoxide dismutase 2 enzymes, glutathione (GSH) and GSH-related enzymes: **GSH synthetase (GSS)**, **Glutathione Peroxidase (GPx)** and **GSH Reductase (GR)** [101]. As discussed in paragraph **1.2.3**, GSH protects cells against free radicals generated by radiotherapy [102]. In particular, a glutathione level increase in GBM cells after TMZ-treatment has been reported, showing its strictly relation to TMZ treatment resistance [103]. Moreover, intracellular levels of GSH *per se* and GSH-related enzymes are highly associated to TMZ resistance; in fact, resistance, together to the redox intracellular balance, is strictly dependent to GSH amount and to GSH-associated enzymatic system [99]. In particular, GSH synthetase (GSS) enzyme catalyses the condensation of gamma-glutamylcysteine and glycine to form glutathione and mutations in the GSS gene provokes the metabolic disorder called GSS deficiency in which production of glutathione is prevented [104]. The most abundant isoform of Glutathione peroxidase, the GPx1, which is located in eukaryotic cytosol and mitochondria, oxidises GSH (glutathione reduced form) to GSSG (glutathione oxidised form), reducing at the same time Hydrogen peroxide (H_2O_2) to H_2O. In turn, GSSG is reduced again to GSH by another key enzyme, glutathione

reductase (GR), by exploiting NADPH reducing power. By the way, GSH redox machinery is strictly associated to the intracellular redox status and energetic metabolism through thiol-disulphide bonds and NADPH-NADP system [102].

1.2.9 GBM models

To study GBM, different human and murine cell models are available. Commercially available cell models are characterized by different genetic feature for MGMT promoter methylation, PTEN, p53 and IDH1/2 mutations. These cells possess are useful models for the evaluation of molecular mechanisms driving resistance. During the experiments described in this thesis work, different glioma cell lines have been adopted: U251 and T98 GBM human cell lines, and murine CT2A cells (see The Global Bioresource Centre ATCC [105]).

HUMAN GBM U251 AND T98 CELLS

These cell lines have been widely used as cell models in several works and are already well characterized, because of their easy handling in terms of rapid cell growth and, thus, fast performing of assays in order to test several types of treatment with high congruency of replication for the same treatment [76,106–108]. From genetic side, these two cell lines result to be mutated in *PTEN* and *p53* genes, while they are wild type for *IDH1* gene [109,110].

MURINE GBM CT-2A CELLS

CT-2A cells are a murine GBM cell line already well characterized. This cell line derives from a non-metastatic murine glioma [111]. CT-

2A cell line has been produced from a malignant astrocytoma originated through the carcinogen 20-methylcholanthrene implantation in the cerebrum of a C57BL/6J mouse. Tumour has been kept via serial intracranial transplants prior to cell line isolation. Anyhow, beyond their mutation in PTEN gene as U251 and T98, CT-2A present no mutations in p53; contrarily to these two human glioblastoma cell lines, CT-2A show mutation in IDH1 [112,113].

2.1 Glioma in vivo Models

For studying GBM tumorigenesis and for evaluating new therapies for this tumour, cell cultures, beyond their easy handling and reasonable costs, cannot allow the multifactorial environment study which *in vivo* deeply affects tumour behaviour. Thus, brain tumour models in experimental animals are required, which need not only to reproduce as much as possible human GBM features accurately, but also to be reproducible per se as well. A glioma mouse model should have the following aspects [114]:

- **Cellular heterogeneity** and **genetic pattern** characterising glioma patients
- Needs to be **orthotopic**
- **Intraparenchymal growing**, comprising tumour-stroma interactions visualization
- **Non-immunogenic** in a host with an undamaged immune system
- **High reproducible power** with foreseen growing rate (accurate estimation of tumour location and dimensions), with

faithful imitation of the human glioma therapeutic and immune responses.

Consequently, a glioma mouse model needs to allow these analyses, which *in vitro* result to be limited or not feasible, as listed here below [115]:

- Assessment of all those signals and pathways involved in tumorigenesis, tumour maintenance and tumour resistance to therapy
- Faithfulness in reproducing tumour invasion, angiogenesis and metastasis
- Identification of all those local growth factors secreted by the tumour per se and the surrounding stroma able to favour tumour proliferation and therapy-resistance
- Self-renewing stem like cells contribution study in cancer recurrence.

Currently, three categories of preclinical glioblastoma models are available: xenografts, Genetically Engineered Mouse (GEM) and syngeneic murine models [116]. In turn, xenograft models can be produced by using cell-lines or patient-derived cells (PDX) [117]. Glioblastoma cell line xenografts derive from glioblastoma patients, cultured *in vitro* and implanted in immunodeficient mice (as instance, the nude ones); among the commercially available lines, U251 and T98 emerge [118–120]. These models, widely used both *in vitro* and *in vivo* context, are advantageous for their optimal capacity to establish and proliferate, to be reproducible for both physiological and

pathological conditions [121]. On the other hand, these xenografts do not recapitulate clinical aspects of patient tumour, both by genotypic and phenotypic sides [122]. PDX, contrarily to the previously described model, keeps not only genetic but also histological traits observed in primary tumours from which they are obtained: of note, they are not influenced by stressors to which instead cell cultures are by, because they are bred directly among mice generations. Moreover, they originate from injected fresh tumour tissues or from cultured tumour spheres implanted into immunodeficient mice and both these modalities reflect genetic and phenotypic aspects of original patient tumour including multicellularity. Although tumour spheres injection presents some difficulties, patient-derived xenografts are pivotal for translational approach of glioblastoma [123–126].

Glioblastoma biology and histology are faithfully recapitulated by genetically engineered mouse (GEM) models as well, where usually gene expression is modified to favour gene expression/inhibition at a precise time/duration or in chosen cells [127]. Also, they can be set up by retroviral/adenoviral vectors-mediated transfer of somatic cells genetic transfer. These models are helpful to monitor genetic modifications involved in tumour initiation and progression, consequently to study tumour microenvironment involvement and to test therapy efficacy. As for previously described models, even GEM present limits, particularly in the lack of perfectly mimicking pathways involved in glioblastoma progression and its heterogeneity [128–130].

The last category constituted by glioblastoma syngeneic models are generated by chemical induction of the tumour (as CT-2A) or by the

spontaneous development of a murine glioma [131]. In detail, these models retrace glioblastoma histology and biology and, exploiting immunocompetent mice, are helpful to study glioblastoma immunological and immunotherapy-based features [132]. The still-open challenge which surround syngeneic models is to deeply test their effective ability to mirror human glioblastoma [133].

Human GBM *in vivo* tumour models generated by intracranially or subcutaneously implanted glioma cell lines in rodents have been massively used for over 40 years and have currently been using [134]. As aforementioned, human GBM xenografts implanted in immunocompromised mice represents a candidate category among mouse models used; for instance, U251 cell model, belongs to this category, even if xenogeneic nature negatively affects immune-mediated anti-tumour strategies assessment. This latter limit is overcome by the use of syngeneic glioma models, as, for instance, CT-2A murine cell model [135].

2.2 In vivo Imaging

In vivo imaging represents a biomedical research field which acts on extending monitoring in living small animals to a more tangible view [136]. In other words, small animal imaging is a non-invasive and repetitive technique applied in living beings which allows biological and cellular processes characterisation and evaluation, both at cellular and sub-cellular (molecular) levels [137]. Molecular and cellular imaging comprises non-invasive imaging techniques as Magnetic Resonance Imaging (MRI), Positron Emission Tomography (PET) and the Single Photon Emission one (SPECT), Computed Tomography (CT) and

Ultrasound (US) imaging, and other procedures initially used for *in vitro* assays, comprising Nuclear Magnetic Resonance (NMR), Bioluminescence (BL) and Fluorescence (FL) methods [138]. Some of these techniques, as MRI, PET/SPET, CT, US, have been adapted and scaled from clinical side to preclinical animal models, going to augment their resolution and sensitivity in order to study organisms of smaller dimensions; some other *in vitro* approaches, as BL and FL, have been adapted from a cell cultures setting to use them in small animals, and sometimes also in humans as well (such as in imaging-guided surgery or for diagnosis during laparoscopy [139,140]), even if its use is still restricted to organs while whole body imaging is not yet applicable because of some physical limits [141] . Furthermore, MRI, CT and US are defined as anatomical techniques since they allow anatomical images of body structures production, while PET and SPECT are called functional imaging because they act imaging physiological processes and producing functional images. Also BL and FL are included among functional imaging techniques, since they allow to image gene expression, promoter and transcriptional activity in vivo: this analysis result to be very important because all these features represent starting points for several deregulated pathways in cancer [142]. These approaches have distinct features basing on various factors, as follows:

- **spatial and temporal resolution**
- **radiation energy and penetration depth**, which are functional to images production
- **availability or need of contrast agents**

- **threshold detection**

Moreover, they can be distinguished even for providing information type, if it is anatomical or functional, as already defined above in **Table 2** [143].

Imaging modality	Form of energy used and variable assessed	Main imaging agent or contrast	Primary use	Type of information	Main use small animal or clinical	Signal quantification capabilities	Anatomical, biochemical physiological and physical advantages and constraints
CT	X-rays Tissue density	Iodine	Whole-body clinical general imaging. Small animal phenotyping	Morphologic	Both	N/A	High anatomical resolution; lack of biochemical information; limited physiological information; fast and simple but not repeatable indefinitely because of radiation hazard
US	High-frequency sound waves Tissue impedance	Microbubbles, nanoparticles or liposomes	Abdominal, vascular and interventional clinical imaging	Morphologic Physiologic	Both	Low	Intermediate anatomical resolution; lack of biochemical information; good physiological information; fast, operator dependent; repeatable indefinitely, no radiation hazard
MRI/MRS	Radio frequency waves Tissue molecular composition	Gadolinium, Iron oxide, Europium, Manganese	Whole-body high contrast clinical general imaging and spectroscopy	Morphologic Physiologic Cellular	Both	Medium	High anatomical resolution; intermediate biochemical information (MRS); good physiological information (fMRI); not fast, requires significant supervision, repeatable indefinitely, no apparent radiation hazard
BLI	Visible to infrared photons Luminescence	Firefly and *Renilla* luciferase	Reporter gene expression, cell tracking	Cellular Molecular	Small animal	Low–medium	Limited anatomical resolution; good biochemical information, good physiological information; fast, simple, repeatable indefinitely, no radiation hazard; no endogenous background signal; requires exogenous substrates
FLI	Visible to infrared photons Fluorescence	Fluorescent proteins (GFP), near infrared fluorochromes or quantum dots	Reporter gene expression, cell tracking	Cellular Molecular	Small animal	Low–medium	Limited anatomical resolution; good biochemical information, good physiological information; fast, simple, repeatable indefinitely, no radiation hazard; no endogenous background signal; does not require exogenous substrates; requires external light source
PET	Annihilation photons Radioactivity distribution	^{18}F, ^{11}C, ^{15}O, ^{68}Ga, ^{64}Cu, ^{124}I	Whole-body clinical and research applications	Physiologic Cellular Molecular	Both	High	Limited anatomical resolution; good biochemical and physiological information; not fast, complex, not repeatable indefinitely owing to radiation hazard; high sensitivity and excellent quantitative potential; small probe mass
SPET	Gamma photons Radioactivity distribution	^{99m}Tc, ^{111}In	Whole-body clinical and research applications	Physiologic Cellular Molecular	Both	Medium–high	Limited anatomical resolution; good biochemical and physiological information; not fast, complex, not repeatable indefinitely owing to radiation hazard; excellent sensitivity but poor quantitative potential; small probe mass

Table 2: Main non-invasive modalities used for in vivo molecular and cellular imaging studies.
(Adapted from [143]*)*

Thereby, relating to the application, each of these methodologies should be used with a distinguished efficiency. Two macro-areas among molecular and cellular imaging have been developed:

- Technologies detection-related area
- Cell labelling strategies-linked area, including tracers, contrast agents and reporter genes/probes [143]

Moreover, a vastity of molecular imaging approaches have been reported, anyway all of them might be categorised in [144]:

- **Direct imaging**, where the image is due to the molecular probe localization at target level, in a direct manner. The image intensity is directly related to the target expression level and its binding to the specific molecular probe.
- **Indirect imaging**, which is based on reporter gene expression imaging. In detail, cells or animals are engineered to express a reporter gene which, in turn, codes for a reporter protein, whose expression results detectable and quantifiable by imaging, immunohistochemistry (IHC) and enzymatic assays without difficulties. Reporter expression is activated in relation to the occurrence of the molecular event which is studied. After reporter protein expression has occurred, a molecular probe, which might be a ligand or a substrate, and that is protein-specific (enzyme/receptor) is exploited in order to image it. Imaging reporter genes can code for proteins (enzymes, membrane receptors or membrane transporters) both of

intracellular type, for instance Luciferase [145], and membrane associated (i.e. the dopamine receptor D2R) [146].

- **Functional or tissue microenvironment imaging**, even defined “metabolic”, “physiological” or “surrogate”. After the probe injection, the downstream effect of one or more endogenous genes and/or activation/abrogation of molecular pathways involved, for instance, in metabolism can be monitored, with the aim to define physiologic and pathologic tissue conditions.

Most of the molecular imaging applications exploit the direct imaging principle, due to the long-term and well-established probe development practice and its wide utilisation in clinical nuclear medicine. Anyhow, new specific tracer development for detecting new targets is a long and expensive process for biologist, chemists, physics and physicians. For bypassing these limitations, the reporter systems utilisation has been suggested as a strategy for exploiting as simply as possible these non-invasive techniques, at least in small animals. New strategies linked to cell imaging have been developed: in detail, specific cell populations are labelled in order to monitor some key parameters as localisation, survival, distribution, proliferation and their function in the organisms. Labelling strategy can be done in two different ways:

- **Direct labelling**, where a detectable probe links to cell membrane or is internalised by isolated cells before they are

infused again in the model to be studied. Steps which need to be performed are as follows:

- Sample population harvesting
- Sample population *ex vivo* labelling through radiolabelled molecule/paramagnetic particles/ fluorescent probe
- Reinfusion
- Visualisation of labelled population distribution and behaviour by means of imaging approach

Direct strategy advantages reside in the easiness to label cells and the availability of clinically approved probes for accomplish this process. The big limit is that this protocol does not allow a long-term monitoring of cell proliferation in the body since the label loss or dilution which in turn is caused by, respectively, apoptosis or mitosis (moreover, after cell death the probe might be transferred to another cell population, such as macrophages, causing an imaging misinterpretation) [141].

- **Indirect labelling**, which provides genetic modification of the cell population to study, by inserting reporter genes, whose expression is utilised for studying genetically modified cells which contain a specific reporter probe. Here some steps are provided:
  - Cells harvesting
  - *Ex vivo* cells transduction with an exogenous reporter gene which encodes a reporter product
  - Transduced population reinfusion

- Specific tracer administration
- Visualisation of cell distribution and behaviour in the recipient subject by exploiting imaging approach

This strategy is pivotal for imaging proliferating cells since reporter gene is maintained form a cell to the daughter one. By using tis approach it could also be possible to non-invasively monitor cell activation or differentiation, by using specific promoters driving the expression of the reporter gene. No signal dispersion to other cell population will be allowed or visualised, only cell viability of the cell population of interest, over each monitoring, will be feasible. If this process could be advantageous for all the aforementioned aspects, anyway it is not so feasible in a clinic scenario.

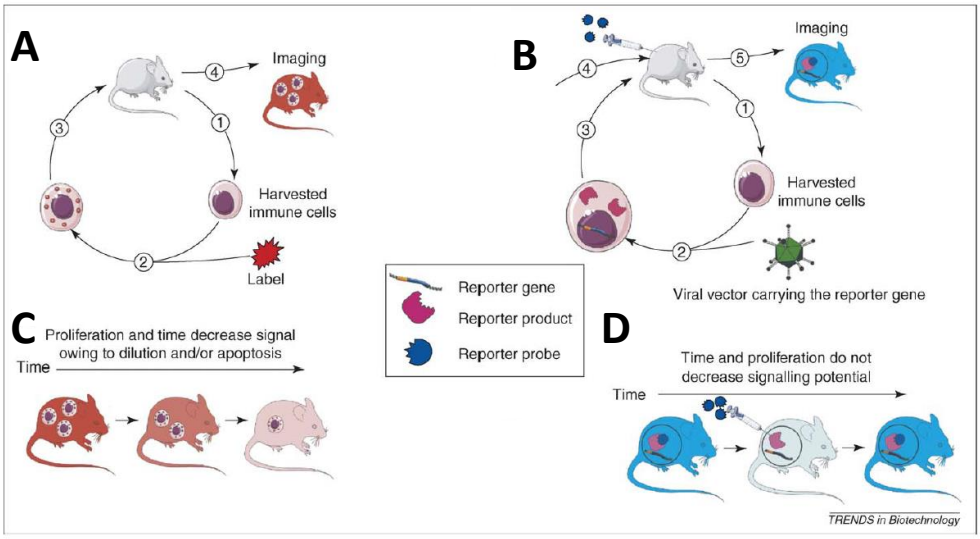

Figure 10: A schematic representation of the direct and indirect imaging strategies.
A: *Direct labelling.* ***B:*** *Indirect labelling.* ***C*** *and* ***D****: Imaging of cell progeny over time for, respectively,* ***A*** *and* ***B*** *(adapted from* [141]*).*

For sure, if *in vitro* approach remains pivotal for monitoring the target of interest through molecular and biochemical analyses, the *in vivo* molecular imaging is as much fundamental to evaluate the molecular event or the cell population in the whole organism. This latter aspect is not permitted by using the *in vitro* approach alone, because only molecular imaging *in vivo* is able to contextualise the specific *in vitro* data in a holistic approach, made of a sophisticated and dynamic network of biological functions and molecular mechanisms occurring in the whole body [122,123]. All these listed strategies, particularly in an oncological field, allow to carry out a non-invasive monitoring of tumour mass over time in individual animals. In this way, the 3R principle (Refine, Reduce, Replace) will be faithfully followed, because, the animal number for the experimental aim will be limited, permitting in the meantime to obtain all the information needed for tumour characterization thus increasing statistical power and decreasing experimental costs [149].

2.2.1 Magnetic Resonance Imaging

Magnetic Resonance Imaging (MRI) is a non-invasive imaging technique which furnishes structural and functional data on organ of interest; in particular, it is the reference modality through which diagnosis, treatment scheduling and plan and follow-up of neurological disease, is performed [150]. This technique uses signal produced by hydrogen atoms nuclei (^{1}H), for generating the images. The MRI signal is used to measure different variables to be used for image weighing **(Figure 11)** [151]:

- T1 longitudinal relaxation/recovery, or spin-lattice interaction, due to the energy dissipation of the nuclei to the surrounding environment (the lattice), since nuclei have to come back to their ground state.
- T2/T2* transverse relaxation, or spin-spin interaction: it is due to the fact that spins lose their phase coherence, without dissipating all their energy.
- Proton density (PD), which is the number of excitable spins in a unit volume, which defines the maximum signal which can be registered by a tissue. Lowering T1 and T2 parameters is possible to ameliorate proton density, for this reason the resulting images are named “proton density-weighted” or “proton density images”.

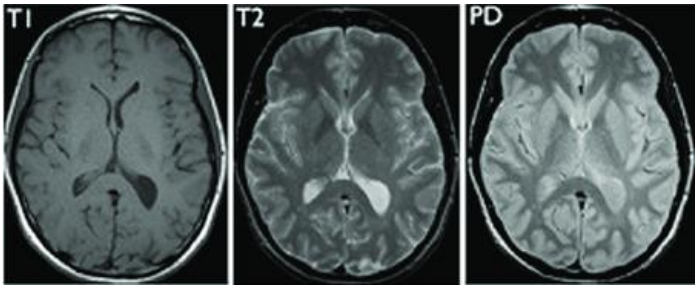

Figure 11: Sample of MRI images for a normal brain.
T1: *T1-weighted.* ***T2:*** *T2-weighted.* ***PD:*** *proton density (adapted from* [152]*).*

Depending on which of these three parameters are emphasised, MRI technique reveals to have a higher potential compared to the CT for discriminating soft tissues. Image contrast can be obtained both by changing acquisition parameters and sequences, both by administering an exogenous contrast medium [153]. Among MR

contrast medium agents, one of the most used is a Gadolinium based agent able to decrease both T1 and T2 time [154]. More advanced acquisition sequences have been developed by simply changing acquisition parameters and weighing the images in different variables. By using advanced sequences, it is now possible to monitor brain function (fMRI), perfusion (DCE), the presence of specific metabolites (MRS) and water diffusion (DTI) without the need of exogenous contrasts. In particular, diffusion imaging is very important in oncological studies since it provides information about tumour cellularity and early response to treatment by simply monitoring water ability/possibility to diffuse in all the directions. This measure can be used for tissue structure reconstruction in terms of cell density, cell swelling and fibre presence [155]. MRI technique, exploited from the mid-1980's, has been subjected to several improvements in term of resolution, in order to get more defined images of the injured brain region. Through this ameliorating process, a gradual transition from the first images got with 0.3-0.6 T MR scanner to the currently used 1-1.5 T or further 3T MRI (and also 7T MRI for small animal imaging), which comprises improved imaging quality and diagnostic accuracy but even a more rapid acquisition process [156]. The usual MacDonald and RANO criteria for glioma management are based on bi-dimensional tumour measurements made on CT or MRI scans, clinical history of patient, and modification in corticosteroid levels after treatment, and are utilised for GBM response evaluation. Nevertheless, they often provoke mistakable phenomena and wrong interpretation, as pseudo-progression or -response because of the

blood brain barrier (BBB) and vasculature changes, respectively, in integrity and permeability, because of the necrotic processes, post-operative infarcts and biological effect due to radiotherapy (RT) [157,158]. Starting from this consideration, the combination of MRI with another imaging technique, such as PET, could improve the information obtained by imaging approach [159].

2.2.2 Positron Emission Tomography

Positron Emission Tomography, PET, is a nuclear-based imaging technique, which exploits specific radiopharmaceuticals to produce an image describing a specific tissue feature depending on the radiopharmaceutical used; this technique is able to provide quantitative physiological information and can be used in particular for tumour evaluation. PET takes advantage of natural biomolecules, the radiotracers, which can be labelled with a positron-emitting isotopes, such as: ^{18}F, ^{15}O, ^{11}C, ^{13}N (other less frequently used ones are ^{14}O, ^{64}Cu, ^{62}Cu, ^{124}I, ^{76}Br, ^{82}Rb and ^{68}Ga) [160–162]. These natural radioisotopes decay generates a positron emission from their nucleus, which by interacting with a neighbouring electron produce a phenomenon called “annihilation”, which produces mass particle disappearance and the production of two 511 keV photons/γ-rays, which are emitted at the same time in an anti-parallel manner, which is 180° apart [160]. After radiotracer administration, it distributes to the body by blood and it will localize with a higher concentration at the target site. Its decay will produce high-energy anti-parallel photons acquired by a PET scanner core in the form of a ring-shaped array of

photoelectric crystals [163]. These scintillators convert this high energy into visible light: this light is captured by photomultiplier tubes, which are sensors fitted for converting light into electrons, to decipher and convert them in electronics and to translate processing units in image. The coincidence through which both photons are detected by the tomographic detector within a range of nanoseconds describes the line of response in space and the flight direction which contributes to define the γ-rays source (physic process defined “electronic collimation”). The software reconstructs an image in which the positron-emitted radionuclide is shown in a precise localisation and concentration within a plane of the scanned organ, easily measuring all those coincidence events at all linear and angular positions [164]. The most frequently used molecule in the last years for tumour study has been ^{18}F-Fluorodeoxyglucose (FDG), which enters the cells through GLUT-1 and GLUT-3 transporters, frequently up-regulated in cancer, and then it is phosphorylated by hexokinase enzyme in the cells, entrapping it. ^{18}F -FDG in relation to the cell glycolytic rate [165]. This tracer has been exploited to obtain information about tumour grading, extent and prognosis; however, its non-negligible limit is the high background in some healthy tissues such as brain (because of the glycolytic metabolism pf neurons), liver (again because of glucose metabolism), kidneys and bladder (because of tracer elimination) [166]. Moreover, even inflammatory cells are able to uptake this tracer once they are activators, leading to a misunderstanding in the image evaluation. Since these disadvantages, other classes of tracers such as amino acidic radiotracers and others have been considered to

identify GBM volume delineation, drive biopsy, plan radiotherapeutic protocols and evaluate patient follow-up [167]. Generally speaking, the identification of a biologically significant biomarker for the identification and enhancement of the tumour is needed to identify those tracers whose uptake in the lesion can be efficient and specific and can be in relation to response to treatment. These biomarkers should be specific also for each therapeutic option, since the therapeutics itself could interfere with the uptake of the tracer independently from tumour real response to the treatment. The accurate choice of both imaging and therapeutic strategy in a precision medicine view would improve the final results of the treatment [168]. In the effort to monitor GBM tumour response to treatment, different tracers have been proposed to monitor tumour aminoacidic uptake (FET, MET, FACBC), tumour energetic metabolism (DASA), hypoxia (FAZA, MISO) or inflammation (TSPO related agents) [168–171]. All these tracers can be used to delineate GBM and follow tumour growth and features. Only some of them have been proposed for the monitoring of GBM response to chemo-radio-immuno- treatments [172].

In particular, ^{18}F-Fluciclovine (FACBC) is acquiring a large consensus not only in the delineation of tumour volume but also as a strategy for the assessment of response to treatment [173].

^{18}F-FLUCICLOVINE RADIOTRACER

^{18}F-Fluciclovine (FACBC, commercial name Axumin, chemical name 1r, 3r-1- amino 3-^{18}F-fluorocyclobutane-1-carboxylic acid) is a radiotracer which contains an L-leucine amino acid analogue which is

radiolabelled with fluorine F-18 [174,175]. FACBC has been approved by Food and Drug administration in 2016 (FDA Investigational New Drug (IND) 72,437) for detecting prostate cancer [176]: in fact, Oka and colleagues have analysed the ^{18}F-Fluciclovine uptake mechanism in prostate cancer cell lines by *in vitro* approach [177]. They have shown that FACBC cell internalisation was mediated predominantly by Alanine, Serine, Cysteine transporters system, among which Alanine, Serine, Cysteine Transporter 2 (ASCT2) and L-Type Amino Acid Transporter-1 (LAT-1), which, depending on Sodium (Na+) availability, are both overexpressed in lots of cancer types [178–181]. FACBC has been tested very recently also in glioma, not only for detecting tumour volume, but also for prognostic intent, for the discrimination between recurrence and treatment-associated effects and for distinguishing low- and high- grade gliomas [182]. Unluckily, although no evidences for this radiotracer to show GBM response to treatment have been emerged yet, it is a very promising tracer because it is strictly involved, in most cases of primary GBM, in an uncontrolled PI3K (phosphatidylinositol 3-kinase)/AKT/mTOR (mammalian target of rapamycin) signalling pathway, that sustains tumour growth **(Figure 12)** [183]. New insights about this radiotracer are necessary to ameliorate prognosis of GBM treatment.

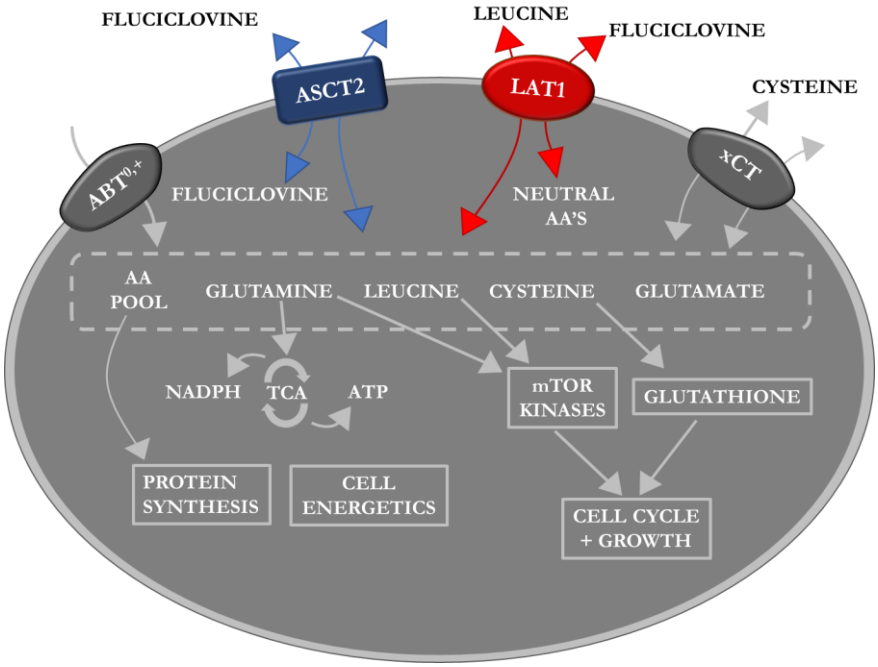

Figure 12: Internalisation mechanism of 18F-Fluciclovine.
Schematic representation of 18F-Fluciclovine cellular flux. Internalisation is mediated predominantly by system ASC transporters (such as ASCT2) or LAT1, depending on Na+ availability (adapted from [180]*).*

AIMS OF THE STUDY

The main purposes of the present study have been: 1) to understand the molecular mechanisms underlying GBM resistance to TMZ; 2) to investigate HIF-1α role in resistance and to assess a new strategy able to restore sensitivity to this treatment in previously resistant cells; 3) to set up and characterise an orthotopic model of GBM, resistant to TMZ; 4) to develop a multimodal non-invasive imaging procedure, including MRI and ^{18}F-Fluciclovine PET, for monitoring GBM features.

In detail, in line with the aforementioned purposes, a molecular characterisation of the cell lines has been crucial for identifying the relation between HIF-1α activity and the responsiveness to TMZ treatment. Once demonstrated this relation, since: TMZ, beyond its alkylating effect, is able to induce autophagy, chaperone mediated autophagy represents one of the main mechanisms through which HIF-1α is degraded; since, among CMA activators, ROS cover a pivotal role and TMZ is able to produce an ER stress inducing an increase or ROS release from the mitochondria, the identification of a molecular relation between ROS release, CMA activation and TMZ-responsiveness in GBM was hypothesised. Moreover, a treatment exogenously providing ROS has been positively tested for its ability in reverting resistance to TMZ. Results obtained herein will be aimed at identifying a new therapeutic approach able to induce a transitory ROS increase able to induce CMA, to down-regulate HIF-1α activity and recovering sensitiveness to TMZ. To this end, a TMZ resistant GBM murine model has been set up together with a strategy for non-invasive monitoring of its features, to test new therapeutic approaches also in combination with RT.

MATERIALS AND METHODS

1. *IN VITRO* EXPERIMENTS

1.1 Cell Lines

Engineered U251-HRE human glioma cells were kindly provided by Dr Giovanni Melillo, National Cancer Institute, Frederick (MD). These cells express luciferase reporter gene under the control of three copies of an HRE sequence, (through stable transfection with pGL2-Tk-HRE plasmid), and routinely selected adding G418 antibiotic (disulfate salt solution G418, 50 mg/ml, Sigma-Aldrich, St. Louis, MO, US) in culture medium. T98 cell lines were engineered for obtaining T98-HRE through transient transfection of 3.0 x 10^4 cells/well with 1 µg of DNA (pGL2-Tk-HRE), 24 hours (h) after cell plating.

Both cell lines have been maintained in Roswell Park Memorial Institute (RPMI) 1640 medium, supplemented with 10 % of heat-inactivated Foetal Bovine Serum (FBS) (EU approved, Euroclone Spa, Pero, MI, Italy), Penicillin/Streptomycin antibiotic mix (50 IU/ml, Euroclone Spa, Pero, MI, Italy), glutamine (2 mM, Euroclone Spa, Pero, MI, Italy).

Murine glioma cell line CT-2A (kindly provided by Prof. Susan Short, St James's University Hospital, Leeds, UK) has been transiently transfected for gaining CT-2A-HRE. Cells engineering has been performed through transfection of 5.0 x 10^4 cells/well, with a 1 µg of DNA (pGL2-Tk-HRE) and 2 µl of T-Pro P-Fect (T-Pro Biotechnology, Taiwan R.O.C.) for each well in 100 µl of DMEM without serum, 24 h after cell plating. 24 h after exogenous DNA incubation, transfection successful has been verified. Murine CT-2A cell lines were routinely maintained in Dulbecco's Modified Eagle Medium (DMEM)-High

glucose medium (Sigma-Aldrich, St. Louis, MO, US) supplemented with 10 % of decomplemented Foetal Bovine Serum (FBS) (EU approved, Euroclone Spa, Pero, MI, Italy), Penicillin/Streptomycin antibiotic mix (100X, Euroclone Spa, Pero, MI, Italy), glutamine (100X, Euroclone Spa, Pero, MI, Italy).
All these cells have been kept in a humidified atmosphere of 5% CO_2 at 37°C.

1.2 Drugs and compounds preparation for in vitro treatments

In vitro treatments have been carried out with the following doses and timing: for dose-dependent Temozolomide (TMZ) efficacy 0.1–200 μM for 24 hours (h); in all the other experiments, the TMZ dose used was 100 μM for 24 hours (h); 200μM or 1mM of Hydrogen Peroxide (H_2O_2) for 24h; 25 μM MitoTEMPO (MitoT) for 1h of pre-treatment (all these products have been provided by Sigma-Aldrich, St. Louis, MO, US); 50 μM S-2-amino- 3-[4'-N,N,-bis(chloroethyl)amino]phenyl propionic acid N-oxide dihydrochloride (PX-478), the HIF-1α translation inhibitor, for 24h (DBA Italia S.R.L, Segrate, MI, Italia). After treatments, samples have been analysed for testing cell viability through Trypan Blue exclusion assay (0.5 %, Euroclone Spa, Pero, MI, Italy). Glioma cells were transfected with 10 nM of *HIF-1α* or *LAMP2A* or *HSC70* or *PHLPP1* siRNA or a scrambled negative control (Product No. 1027280, Qiagen, Hilden, Germany). *LAMP-2A*, *HSC70* and *PHLPP1* siRNA have been realised custom-made by Eurofins company (Vimodrone, MI, Italy), while the *HIF-1α* siRNA has been provided from Qiagen (Cat. No. GS3091, Qiagen, Milan, Italy). Due to the high homology (>95%) between the human and murine HIF-1α sequences,

the same oligonucleotide used for human cells has been used also for the murine ones. All the mentioned siRNAs have been transfected utilising T-Pro P-Fect (T-Pro Biotechnology, Taiwan R.O.C.), as already described for obtaining T98- or CT-2A-HRE.

1.3 Cell Viability Assay

Cell viability was evaluated using the Trypan blue (Sigma-Aldrich, St. Louis, MO, US) exclusion test. During the hypoxia experiments, 1.0 x 10^4 seeded cells/cm^2 were incubated in a hypoxic chamber containing a 1% O_2 gas mixture.

1.4 HIF-1α activity evaluation-Luciferase Biochemical assay

HIF-1α activity evaluation has been performed lysing cell samples with lysis reagent (Lysis Reagent 1X, stock 5X, Promega, Madison, WI, US). Resulted lysates have been analysed with Luciferase Biochemical assay: 20 µl of lysates and 100 µl of Luciferin solution (mix made by: Luc Assay buffer 1X, Luciferin 10 mM, DTT 1M, ATP 200 mM, as described below), and photon emission has been measured through luminometer (GloMax-Multi Detection System, Promega, Madison, WI, US). Obtained values, expressed in counts, have been normalised for protein content, which in turn has been gained through Bradford assay (Comassie Plus Protein Assay Reagent, Thermo Scientific, Rockford, IL, US) and expressed as Relative Luminescence Unit (RLU=counts/mg of proteins). During the hypoxia experiments, 1.0 x 10^4 seeded cells/cm^2 were incubated in a hypoxic chamber containing a 1% O_2 gas mixture.

LUC ASSAY BUFFER 1X: 104 mg of $(MgCO_3)4Mg(OH)_2$ * 5 H_2O (Sigma Aldrich St. Louis, MO, US); 150 ml of distilled H_2O; 4 ml of Tricine 1 M (Life Technologies, Waltham, MA US) , 40 μl of EDTA 0.5 M and 534 μl of 1 M Magnesium Sulphate (both from Sigma Aldrich St. Louis, MO, US). The solution become clear at pH 7.8, then add distilled water to reach a final volume of 200 ml. Sterilization by means of a 0.22 μm filter and store at 4°C.

LUCIFERIN SOLUTION: 950 μl of Luc assay solution 1X, 550 μl of luciferin 10 Mm resuspended in distilled water (Promega, Madison, WI, US), 33.3 μl of DTT 1 M and 2.6 μl of ATP 200 mM (both from Amersham) for each ml of working solution (prepared at the moment of use).

1.5 Biochemical assay

The ROS content in each treatment described in section **1.2** has been measured utilising ROS-Glo™ H_2O_2 Assay kit (Promega, Milan, MI, Italy). Lysates were analysed through Luciferase Biochemical assay, measured using GloMax-Multi Detection System (Promega, Milan, MI, Italy). Treatments cytotoxicity has been assayed using CellTox™ Green Cytotoxicity Assay kit (Promega, Milan, MI, Italy) and CellTiter-Glo® Luminescent Cell Viability Assay (Promega, Milan, MI, Italy). Glutathione (GSH) detection and quantification has been carried out by the commercially available GSH-Glo™ Glutathione Assay (Promega, Milan, MI, Italy), after the treatment. Data has been expressed as GSH concentration.

1.6 HIF-1α Nuclear Quantification

An ELISA-based kit (TransAM Kit, Vinci-Biochem, Vinci, Italy) was used to detect and quantify HIF-1α transcriptional factor activity in accordance with the manufacturer's instructions. The data are expressed as the amount of HIF-1α protein in nuclear extract (OD 450 nm).

1.7 RNA extraction and real-time PCR

RNA has been extracted utilising a commercially available Illustra RNA spin Mini Isolation Kit (GE Healthcare, Milan, MI, Italy) according to the manufacturer's instructions. Total RNA was reverse-transcribed to cDNA through a High-Capacity cDNA Reverse Transcription Kit (Applied Biosystems, Monza, MB, Italy). The real-time PCRs has been accomplished in triplicate for each data point using the Sybr Green technique; the oligonucleotides used are shown in **Table 3**. Changes in target mRNA content in relation to the *β-ACTIN/β-Actin* housekeeping gene have been determined using the ΔΔct Method. *β-Actin*, *Hif-1α* and *Vegf* primer sequences have been used for real-time PCR on murine CT-2A samples **(Table 3)**.

1.8 Wounding assay

For this test, at the end of the treatment, a wound has been made by manually scraping confluent glioma cells monolayer with a p200 pipette tip. Images at time zero (t=0 h) were captured to record the wounds initial area, while the evaluation of the wounded monolayers recovery, due to cell migration toward the denuded area, has been

performed at 24 h (t=Δh). The wound zone has been quantified by Java's Image J software [184] and cell migration toward wounds has been expressed as wound closure percentage, as follows:

% wound closure=[(At=0h−At=Δh)/At=0h] × 100%, where, At=0h is the wound area measured soon after scratching, while At = Δh is the wound area measured 24 h after scratch.

1.9 Protein analyses

Samples have been prepared in Novex Bolt LDS sample buffer and Novex Bolt Reducing Agent and after boiled for 3 min. For protein quantification has been performed through Lowry method; proteins (10–30 μg) have been loaded in Precast Bolt® Bis-Tris Plus Gels 4–12% and run for 30 min at 200 V in Novex Bolt 1X MES/SDS Running buffer. A Trans-Blot® Turbo™ system (BioRad, Hercules, California, US) has been used for the transfer to nitrocellulose membrane. Membranes have been blocked in Odyssey® Blocking Buffer (LICOR, Lincoln, Nebraska, US) and incubated with secondary fluorescent antibodies (IRDye®). Protein bands have been observed by an Odyssey Fc device, model 2800 (LICOR Biosciences LICOR Biosciences, Lincoln, Nebraska, USA). Bands intensity quantification has been done by an Image Studio Lite Ver 5.2 software. Subcellular fractions of cells were obtained using Protein Fractionation Kits (Thermo ThermoScientific, Waltham, MA US) [185]. Probing with samples has been performed using the following antibodies: LAMP2A (51-2200 1:1000, Invitrogen, Carlsbad, California, US), HSC70 (MA1-26078 1:000, Invitrogen, Carlsbad, California, US), GAPDH (sc4772

1:1200, Santa Cruz, Santa Cruz, California, US), NDUFB8 (ab110242 1:1000, Abcam, Cambridge, UK), SDHB (ab14714 1:1000, Abcam, Cambridge, UK), UQCRC2 (ab14745 1:1000, Abcam, Cambridge, UK), MTCO2 (ab110258 1:1000, Abcam, Cambridge, UK), ATP5A (ab14748 1:1000, Abcam, Cambridge, UK), SDHA (459200 1:10000, Invitrogen, Carlsbad, California, US), COXIV (A21347 1:2000, Invitrogen, Carlsbad, California, US), SOD1 and CATALASE (ab179843 1:500, Abcam, Cambridge, UK), LAMP1 (ab25630 1:900, Abcam, Cambridge, UK), ACTIN (A2066 1:200, Sigma-Aldrich, St. Louis, MO, US) , GAPDH (sc4772 1:1200, Santa Cruz, Santa Cruz, California, US), and α-TUBULIN (3873S 1:800, Cell signalling Massachusetts, US) have been used as loading and fractionating controls.

1.10 Biochemical analyses

Protein extraction has been performed by sonication (50 W for 10 s, 3 times) after resuspending cell pellets in proper buffer (pH 7.2). Lysates have been centrifuged at 750g for 10 min and supernatant has been recovered. For protein quantification Lowry method has been used. A Lambda 2 spectrophotometer (Perkin Elmer, Massachusetts, US) has been used to determine enzymatic activities. Analyses were performed at specific wave lengths for each enzymatic activity after having prepared proper solutions, as previously described with mild modifications [185]. Experiments have been performed at 30 °C. A Perkin Elmer software has been exploited for performing the analyses. Measurements were normalized over the activity level of citrate synthase, a stable matrix mitochondrial enzyme; this latter step was

performed in order to normalize respiratory chain activity over mitochondrial mass.

Gene	**Forward**	**Reverse**
BAX	ATGGACGGGTCCGGGGAG	ATCCAGCCCAACAGCCGC
BAD	CCCAGAGTTTGAGCCGAGTG	CCCATCCCTTCGTCGTCCT
BCL-2	GATTGTGGCCTTCTTTGAG	CAAACTGAGCAGAGTCTTC
PHLPP1	CCTACCTTCTCCAGTGCACT	CCAGCAGTTCCAAGTTTCCT
LAMP-2A	TGCTGGCTACCATGGGGCTG	GCAGCTGCCTGTGGAGTGAGT
HSC70	ATTGATCTTGGCACCACCTA	GGGTGCAGGAGGTATGCCTGTGA
HIF-1α	TGATTGCATCTCCATCTCCTAC	GACTCAAAGCGACAGATAACACG
VEGF	CGAGGGCCTGGAGTGTGT	CGCATAATCTGCATGGTGATG
SNAIL	GCGAGCTGCAGGACTCTAAT	CCCGCAATGGTCCACAAAAC
SLUG	CATGCCTGTCATACCACAAC	GGTGTCAGATGGAGGAGG
E-CAD	GATCAAGTCAAGCGTGAGTCG	AGCCTCT CAATGGCGAACAC

SOD-2	TTAACGCGCAGATCATGCA	GGTGGCGTTGAGATTGTTCA
CATALASE	TAAGACTGACCAGGGCA	CAAACCTTGGTGAGATCGAA
GR	AACATCCCAACTGTGGTCTTCAGC	TTGGTAACTGCGTGATACATCGGG
GPX	CGCAACGATGTTGCCTGGAACTTT	AGGCTCGATGTCAATGGTCTGGAA
GSS	ATGCTGTGCAGATGGACTTCAACC	TGGATGTCAAACAGACGAGCGGTA
β-ACTIN	TCAAGATCATTGCTCCTCCTG	CCAGAGGCGTACAGGGATAG
β-Actin	AGGTCATCACTATTGGCAACGA	CACTTCATGATGGAATTGAATGTAGTT
Hif-1α	AGCCCTAGATGGCTTTGTGA	TATCGAGGCTGTGTCGACTG
Vegf	GAC CCT GGC TTT ACT GCT GTA	GTG AGG TTT GAT CCG CAT GAT

Table 3: Oligonucleotides used for real-time PCR.

2. *IN VIVO* EXPERIMENTS

2.1 Animal studies

Animal experiments have been performed in compliance with the University of Leeds institutional guidelines for the care and use of experimental animals. For intra-cerebral injections, an orthotopic

murine model was obtained by stereotaxic injection (coordinates: 1 mm rostral to bregma, 1.5 mm lateral and 3 mm deep) of 2 µl of Dulbecco's Modified Eagle Medium (DMEM)-High glucose medium (Sigma-Aldrich, St. Louis, MO, US), containing 1 x 10^5 CT-2A glioma cells into female C57BL/6J mice (also known as: Black 6, B6, B6J, C57 Black, Mouse Strain Datasheet: 000664, The Jackson Laboratories [186]) at day 0. For surgery, mice have been placed under isofluorane-based gaseous general anaesthesia (Baxter International, Deerfield, Illinois, US). Soon after anaesthesia step (through Isofluorane), Lubrithal Eye Gel (Dechra Pharmaceuticals PLC, Northwich, UK) has been applied on mouse eyes for avoiding their drying. Mice have been injected both with 20 µl of Baytril antibiotics 0.25% (intramuscular into the back leg; 1:10 of dilution with saline) (Bayer, Leverkusen, Germany) and with 10 µL of pain-killer Metacam 5% (subcutaneously at the mice back) (Boehringer Ingelheim, Ingelheim am Rhein, Germany). Cells were aspirated with a 10 µl Hamilton syringe (Hamilton Company, Nevada, US) just immediately before the injection. By pointing to a drill (Roboz, Gaithersburg, MD, USA)-made hole, Z axis has been fixed to 0 and the syringe gently inserted into the brain until reaching the correct coordinate (-3 mm depth). Cells were injected with a velocity of 1 µl/min. Syringe has been left for further 1 minute in the hole before to gently remove it, to avoid cell lift in the path of the needle. Hole has been closed using Bone wax (Harvard apparatus, St. Laurent, Quebec, Canada) and the wound with sterile and self-absorbing glue (3M Vetbond tissue adhesive, 3M, St. Paul, MN, USA); soon after,

Bacitracin-based antibiotics gel (Polyfax, GlaxoSmithKline, Middlesex, UK) has been applied on the wound closure. After surgery, were monitored for recovery until complete wakening. Animals have been monitored daily for adverse effects, especially for signs of neurological symptoms and ill-healthy signs due to chronic intra-cranial pressure, as: reduced mobility, hunching, decrease in food intake, hypersensitivity upon touching and handling, separation from cage mates and a considerable weight loss. In case of these symptoms and/or after the end of the experiments, mice have been euthanized by perfusion before with saline and soon after with 4% paraformaldehyde (PFA) into the heart right ventricle. Brains have been collected in 4% PFA and embedded in paraffin for consecutive ImmunoHistoChemistry (IHC) analyses.

2.2 In vivo imaging study design

In vivo experiments have been carried out on different groups (negative controls, controls and RT-treated mice). MRI and PET imaging has been used for monitoring tumour growth, effect of RT treatment and ^{18}F-Fluciclovine uptake, as described below.

2.3 MRI analyses

The MRI scans exploited for confirming the presence of an intra-cranial tumour have been performed through a Bartec M7 Machine (1 Tesla, Bartec, Bad Mergentheim Germany) located in SBS animal facility. For each animal, pictures obtained have been acquired in T2, with 16 slices in total, 0.8 mm for each slice thickness and 10 minutes-long lasting scan as parameters. During acquisitions, mice have been

under gaseous inhalation--based general anaesthesia (Baxter International, Deerfield, Illinois, US). Tumour ROI volumes have been calculated through VivoQuant software [187].
MRI imaging was performed on these two groups:

- **Control group**: (n=6) (defined in results and graphs as “control”), tumour cells were injected as previously described, and no RT has been carried out, but only multiple 1T-MRI acquisitions in order to monitor the tumour growth and to compare it to the RT-treated mice cohorts. Moreover, in an experimental point, dynamic and static PET scans have been performed for evaluating ^{18}F-Fluciclovine radiotracer distribution and uptake in brain tumour.
- **Cohort 1 – RT-treated group 1** (n=6): tumour-bearing mice have been treated with RT (three 5Gy-hemibrain radiotherapy fractions with SARRP, 15 Gy in total along the entire experiment) and the expected tumour mass volume decrease has been monitored with several 1T-MRI scans.

2.4 Radiotherapy

Radiotherapy has been performed by using the Small Animal Radiation Research Platform, SARRP (Xstrahl Life Sciences, Camberley, Surrey, UK [188]), according to the following plan:

- For **cohort 1, RT-treated group 1:** mice have undergone to three 5Gy-hemibrain radiotherapy fractions with Small Animal Radiation Research Platform, SARRP, 15 Gy in total along the

entire experiment. Each mouse has received the radiotherapy in a precise temporal window: days 9,10,11.

The angle to which radiation beam has been set was from +60° to -60°. Treatment duration, for which mice have been anaesthetised by isofluorane inhalation, took approximatively 2 minutes. SARRP machine is implemented with a CT scan, which has been useful to better direct radiation beam on brain.

2.5 Radiotracer availability and PET analyses

FACBC (^{18}F-Fluciclovine) PET tracer (FDA Investigational New Drug (IND) 72,437), which permits in clinics to allows distinguish between low and high-grade gliomas (LGGs and HGGs) [182], has been provided by Blue Earth Diagnostic Company (Oxford, OX4 4GA, UK) through an agreement with University of Leeds (Principal Investigator: Prof. Andrew Scarsbrook, Leeds Teaching Hospitals NHS Trust, Leeds, UK). Before use, radiotracer has been purified by elution on chromatographic column. For each mouse, radiotracer has been intravenously injected (tail vein) at the beginning of the 90 minutes-long-lasting PET dynamic scan or one hour before the 20 minutes long-lasting PET static acquisition. At the end of each PET, both dynamic and static, an extra 10 minute-Computed Tomography (CT) scan has been performed. The PET detection system is made by a piece of the Albira Si imaging platform (Bruker, Massachusetts, US): this machine contains PET, SPECT (Single Photon Emission Tomography) and CT (Computed Tomography) imaging capabilities only in one instrument. Mice were anesthetized with isofluorane (Baxter International, Deerfield, Illinois, US) and they have been

undergone multiparametric MRI scans through a next generation Bruker Biospec 7T preclinical MRI machine (Bruker, Massachusetts, US) on one day. Anaesthesia times reflect those ones of the 7T MRI scans.

PET imaging was performed on these two groups:

- **Negative Group** (n=3), the mice will be injected with only 2 µl saline i.c. injection (n=2; sham operated mice) or without any i.c. injection (n=1; healthy mouse). This group (defined in results and graphs as “non-tumour bearing mice”) has been carried out in order to test specific radiotracer localisation at tumour injection site.
- **Control group**: (n=4) (defined in results and graphs as “control”/ ”tumour bearing mice”), tumour cells were injected as preciously described, and no RT has been carried out.

For what concerns regions of interest chosen for PET analyses, the following considerations have been done: are the following healthy brain region, corresponding to the mid-brain, which is the central back of the brain away from tumour injection site, has been used as primary control. Liver has been added as the primary metabolic region on ^{18}F-Fluciclovine. The region of interest was chosen at the bottom lobe of the liver for consistency. The tumour, healthy brain and liver regions of interest are chosen at the same size for consistency (2 mm diameter spheres). The salivary glands and nasal passages are a region of interest sized to match the anatomy.

2.6 Immunohistochemistry

Brains collected in 4% PFA at 4 C° temperature have been washed twice in Ethanol 70 % and soon after immersed in fresh 4% PFA at room temperature for the consecutive paraffine embedding. After this passage, embedded brains have been cut in 5 µM slices and soon after they have put on glass slides and, in order to monitor tumour detection along slices cutting, a fast Haematoxylin and Eosin staining has been performed. Immunostaining for ASCT2 (concentration 1/100, Abcam, Cambridge, UK) was performed.

2.7 Statistical analysis

In vitro experiments have been repeated at least three times and have brought to reproducible results. The mice number for each experimental group for the *in vivo* analyses have been defined in the paragraphs above. Data are shown as the mean values ± SD of independent experiments and were statistically analysed utilising a t test or one- or two-way analysis of variance, followed by Dunnett's or Bonferroni's multiple comparison and Prism 4 software (GraphPad Software Inc., San Diego, CA, US).

RESULTS

1. *IN VITRO* RESULTS

1.1 GBM cell profiling of responsiveness to TMZ treatment

In vitro characterisation of TMZ responsiveness was assessed in two glioma cell lines (U251 and T98) that have different percentage in MGMT promoter methylation (65 % and 40%, respectively). U251 and T98 GBM cell lines have been treated with TMZ for 24 hours. In U251 MGMT-highly methylated cells, the viability was significantly reduced after treatment with TMZ, while in the T98 MGMT-low methylated cells, TMZ did not influence cell viability **(Figure 13)**.

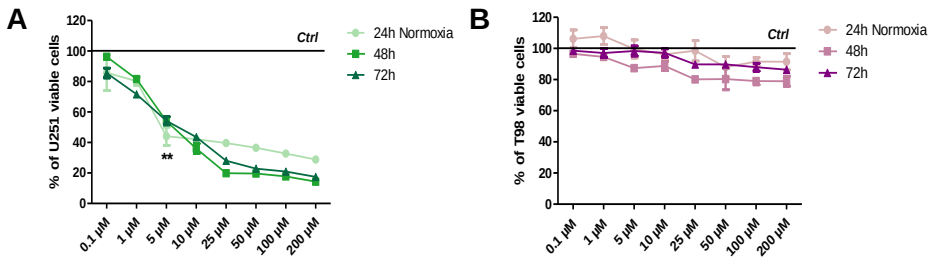

Figure 13: Dose–response viability of responsive and resistant cells after TMZ treatment under normoxic conditions.
Cell viability has been assessed through a Trypan blue exclusion test and expressed as the percentage of viable cells after 24, 48, or 72 h of treatment at increasing doses of TMZ under normoxic conditions. ***A:*** *U251 cells.* ***B:*** *T98 cells. **p < 0.01 TMZ-treated cells vs untreated cells. Mean values ± SD.*

TMZ responsiveness was also investigated in hypoxic condition, showing that U251-responsive cells became more resistant to TMZ compared to their trend in normoxia: indeed, in hypoxia five times higher dose of the drug is needed to induce a significant cytotoxicity even in methylated cells **(Figure 14)**.

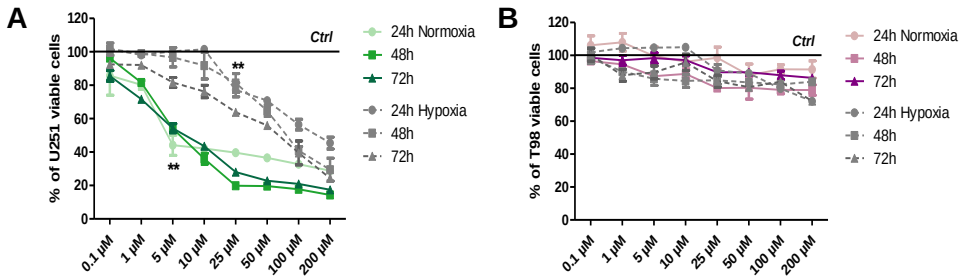

Figure 14: Dose–response viability of responsive and resistant cells after TMZ treatment under normoxic and hypoxic conditions.
*Cell viability has been assessed through a Trypan blue exclusion test and expressed as the percentage of viable cells after 24, 48, or 72 h of treatment at increasing doses of TMZ under normoxic and hypoxic (grey-coloured) conditions in **A:** U251 cells and **B:** T98 cells. **p < 0.01 TMZ-treated cells vs untreated cells. Mean values ± SD.*

As shown in **Figure 14**, since hypoxia is able to modulate TMZ treatment, we have focused on assessing the contribution of the main factor driving cell response to hypoxia, HIF-1α, in responsiveness to TMZ treatment, selecting one TMZ dose (100 µM), which will be used for all the following results reported. Firstly, HIF-1α levels in the nucleus have been monitored and, only in responsive cells, both in normoxia and hypoxia, TMZ treatment produced a reduction of the nuclear HIF-1α amount **(Figure 15A and B)**. Moreover, sensitivity to TMZ was also related to a modulation of HIF-1α activity. In fact, in both normoxic and hypoxic conditions, while in sensitive cells a reduction in the activity of this transcription factor after treatment was also detected, in resistant cells TMZ treatment failed in modulating HIF-1α activity **(Figure 15C)**.

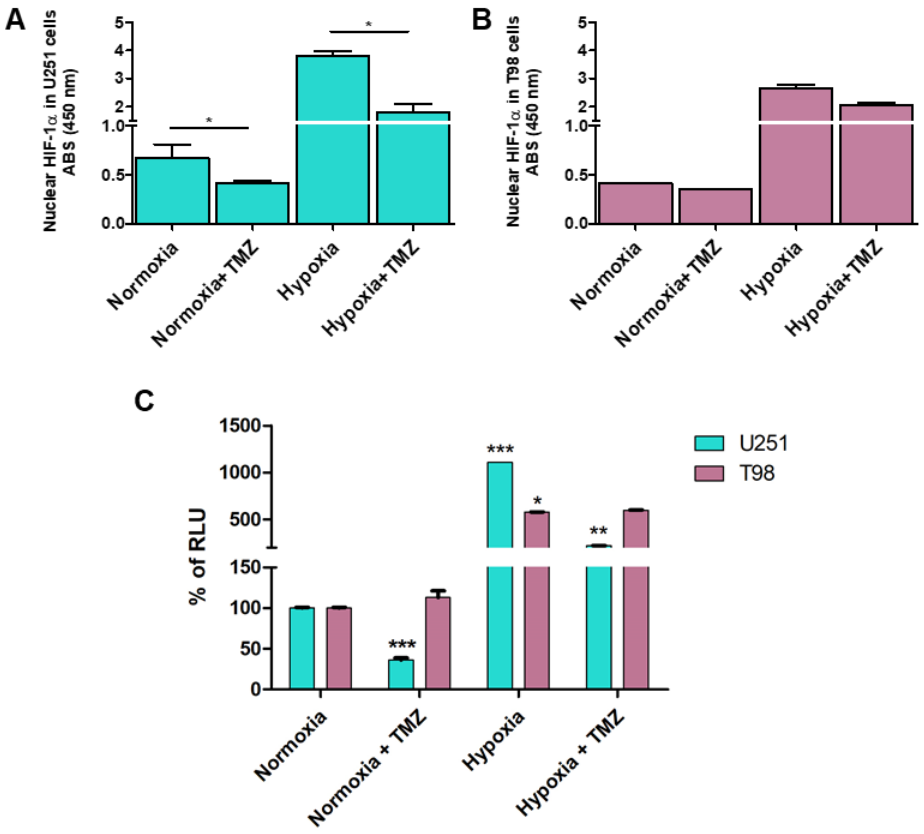

Figure 15: Nuclear HIF-1α localisation of responsive and resistant cells after TMZ treatment, both in normoxic and hypoxic conditions.
ELISA-based HIF-1α nuclear quantification after TMZ treatment under normoxic and hypoxic conditions has been carried out in ***A:*** *U251 cells and* ***B:*** *T98 cells. The data are expressed as absorbance at 450 nm. *p < 0.05 vs control under normoxic/hypoxic conditions.* ***C:*** *Luminescent assay applied to evaluate HIF-1α activity, both in untreated cells and after treatment with 100 μM TMZ, both in normoxia and hypoxia. Data were expressed as Relative Luminescence Units (RLU) obtained by luciferase counts normalised to the amount of proteins quantified by Bradford assay. *p < 0.05, **p < 0.01, ***p < 0.001 treated vs control under normoxic/hypoxic conditions. Mean values ± SD of three independent experiments.*

The effect of TMZ treatment on cell viability was also confirmed by the analysis of the gene expression profile for some apoptotic genes (*BCL-2*, *BAX* and *BAD*). Indeed, real-time PCR showed that TMZ treatment was able to significantly induce pro-apoptotic genes such as *BAX* and *BAD* with the down-regulation of the expression of the anti-apoptotic *BCL-2* gene. This expression pattern has been defined a “sensitive-like” expression profile.

In hypoxic condition, since hypoxia itself dramatically changed HIF-1α expression and activity as well as *BCL-2* expression profile, TMZ treatment reduced only partially the amount of nuclear HIF-1α producing a partial resistance as confirmed by the lower induction of proapoptotic genes and the lack of negative modulation of *BCL-2* expression compared to normoxic untreated controls.

In T98 cells, the TMZ-resistance was also confirmed in hypoxic condition. For what concerns their apoptotic expression pattern, in resistant cells, both hypoxia and TMZ induced the up-regulation of *BCL-2* anti-apoptotic gene that we associated with a “resistant-like expression pattern” **(Figure 16)**.

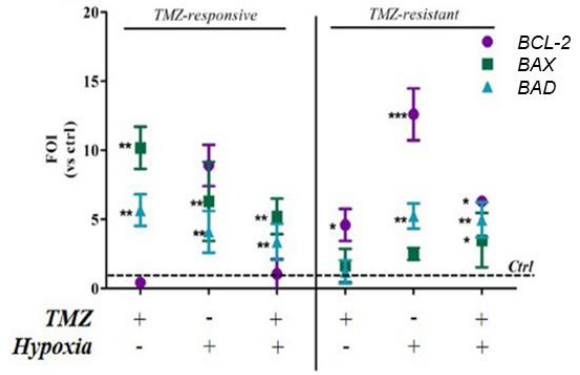

Figure 16: Gene expression of the apoptosis-related genes (BAX, BAD, BCL-2) in TMZ-responsive and -resistant cells treated with TMZ under both normoxic and hypoxic conditions.
*The induction of anti-apoptotic (BCL-2) and pro-apoptotic genes (BAX and BAD) was analysed by means of real-time PCR. Data were normalised to β-actin, and the ΔΔCt values were expressed as FOI of the ratio between treated and control cells. *p < 0.05, **p < 0.01, ***p < 0.001 treated vs control cells. #p < 0.05, ##p < 0.01, ###p < 0.001 vs TMZ-treated cells. Mean values ± SD of three independent experiments.*

1.2 HIF-1α degradation and chaperone-mediated autophagy involvement in GBM responsiveness

TMZ treatment, as already described (see the **INTRODUCTION-1.2.4-1.2.6**), is able to induce autophagy and within the different molecular pathways involved in HIF-1α degradation, Chaperone-mediated Autophagy plays an important role [86].

Taking into account that TMZ induces autophagy, that HIF-1α is a Chaperone-mediated Autophagy (CMA) target and its activity decreased in relation to TMZ responsiveness, a connection among HIF-1α activity modulation, TMZ-responsiveness and CMA has been hypothesised. Firstly, a gene expression profile for the main CMA-related genes, *LAMP-2A*, *PHLLP1* and *HSC70, and for HIF-1α* has

been performed in U251-sensitive and T98-resistant cells after treatment with TMZ. Gene expression analysis showed that treatment was able to increase *LAMP-2A*, *HSC70* and *PHLPP1* expression, and concomitantly, to reduce the *HIF-1α* transcript in TMZ-sensitive cells, while in resistant cells, alkylating agent produced an opposite response.

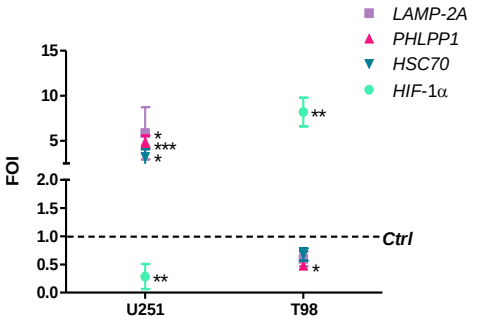

Figure 17: Gene expression of the CMA-related genes (LAMP-2A, PHLLP1 and HSC70) and of HIF-1α in TMZ-responsive and -resistant cells treated with TMZ.
*Gene expression analysis for CMA-related genes (LAMP-2A, HSC70, PHLPP1) and HIF-1α analysed by means of real-time PCR in U251 and T98 cells after treatment with 100 μM TMZ. Data were normalised to β-actin, and the ΔΔCt values were expressed as FOI of the ratio between treated and control cells. *p < 0.05, **p < 0.01, ***p < 0.001 treated vs control cells. #p < 0.05, ##p < 0.01, ###p < 0.001 vs TMZ-treated cells. Mean values ± SD of three independent experiments.*

Furthermore, in order to better define protein levels of two of the CMA key-players, LAMP-2A and HSC70, after alkylating agent treatment, a Western Blot analysis in U251-sensitive cells and T98-resistant ones, both in presence and absence of TMZ, has been performed. A statistically significant increase has been detected in both CMA proteins level in U251 cells after TMZ treatment compared to their

respective controls, whereas in T98 cells, after TMZ treatment, LAMP-2A and HSC70 amounts did not show any change in their level that resulted to be reduced compared to basal levels, although in a no statistically significant manner. Thus, these data support crucial CMA engagement in responsiveness to TMZ treatment **(Figure 18).**

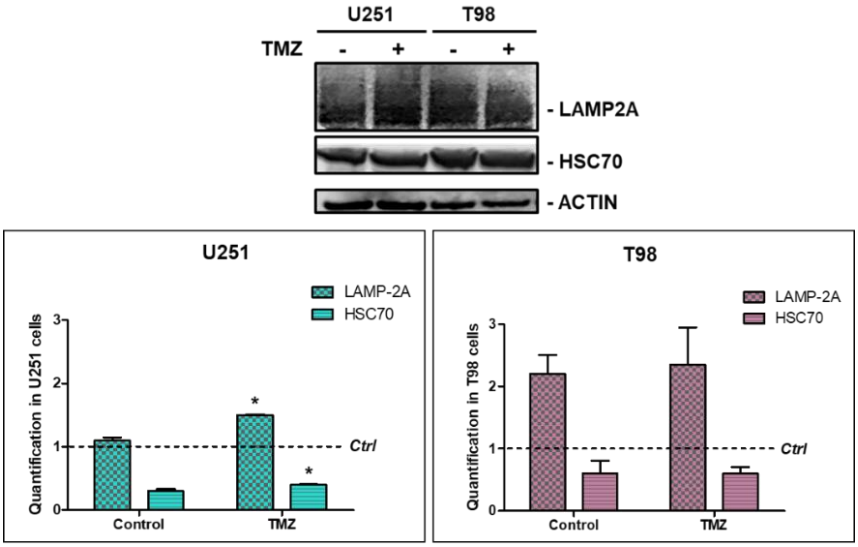

Figure 18: LAMP2A and HSC70 quantification.
*Western blot analysis of LAMP2A and HSC70 in protein lysates from untreated (-) and TMZ-treated (+) U251 and T98 cell lines. Protein signals were normalised to actin levels. Histograms show mean values of protein arbitrary units evaluated in independent experiments. Errors bars indicate standard deviation. * $p < 0.05$ treated versus untreated. Mean values ± SD of three independent experiments.*

In order to assess LAMP-2A and HSC70 intracellular localisation, a cell fractionation has been performed in U251 and T98 cells under control condition and after TMZ treatment. Results showed an increase in LAMP2A and HSC70 proteins in the lysosomal fraction in U251 cells after TMZ treatment. This increase was not detected in T98

resistant cells after TMZ treatment. At the same time, we studied also GAPDH levels to monitor CMA activity since it is a CMA substrate [89]. Cytosolic GAPDH level was decreased only in sensitive cells after treatment with TMZ and increase in the lysosomal fraction in the same condition thus confirming the selective involvement of CMA only in U251 cells **(Figure 19)**.

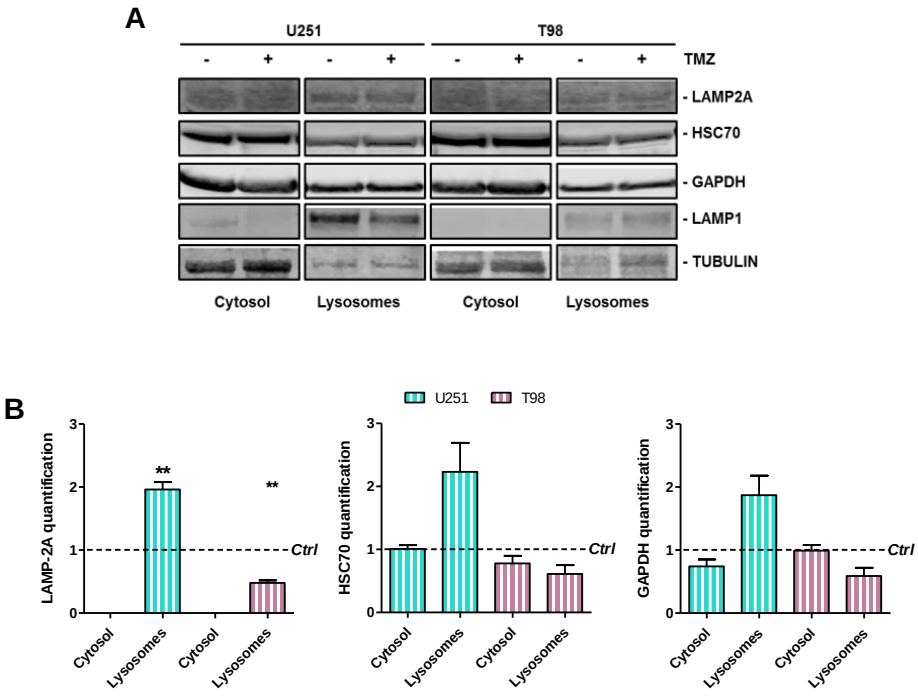

Figure 19: Essential CMA-related gene involvement in TMZ response. ***A:*** *Western blot analysis of* LAMP2A*,* HSC70 *and* GAPDH *protein levels in subcellular fractions obtained from untreated (-) and TMZ-treated (+) U251 and T98 cell lines.* ***B:*** *Protein signals were normalised to respective fraction markers:* TUBULIN *(cytosol) and* LAMP1 *(lysosomes). Histograms show the distribution of target proteins in the fractions after 24 hours of TMZ treatment compared to untreated control levels. **p < 0.01 treated versus untreated control levels. Mean values ± SD of three independent experiments.*

To further analyse CMA role in responsiveness to TMZ, we silenced different CMA-related genes (*LAMP-2A*, *HSC70* AND *PHLPP1*) both in sensitive and resistant cells and silenced cells were treated with TMZ. In U251-responsive cells, CMA-related genes silencing produced the acquisition of a TMZ-resistant behaviour **(Figure 20)**.

In detail, blocking CMA activity through the silencing of the CMA-related genes, cytotoxicity normally due to TMZ-treatment was abrogated, as shown in a missing reduction in viability **(Figure 20A)**, as well as in HIF-1α activity **(Figure 20B)**. In T98-resistant cells, TMZ-responsiveness and HIF-1α activity was not changed under the same experimental conditions **(Figure 20C and D).**

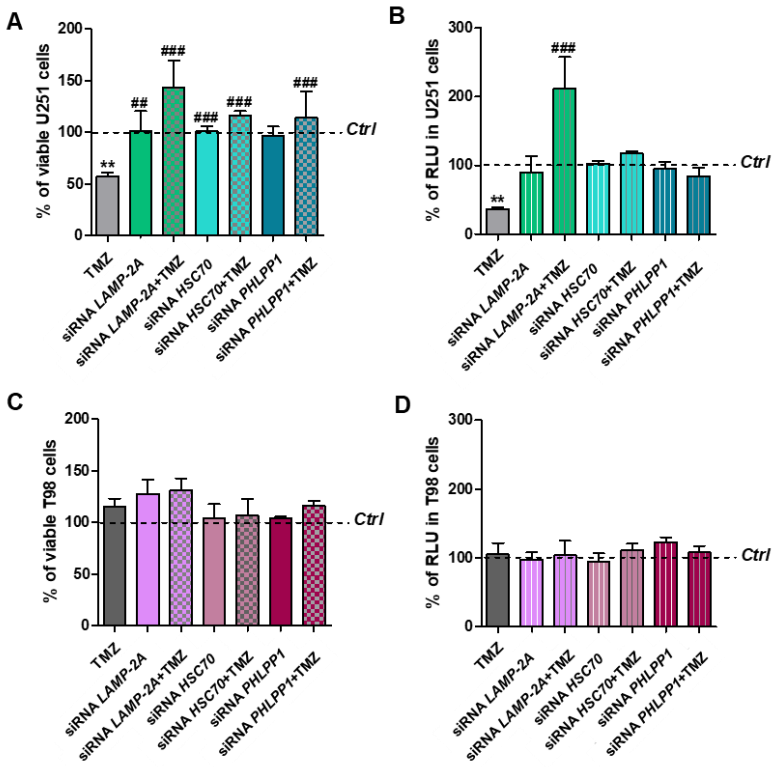

Figure 20: Viability analysis in U251 (A) and T98 (C) and Luminescent Assay on U251 (B) and T98 (D) after LAMP-2A, PHLPP1 or Hsc70 silencing ± 100 μM TMZ treatment.

A *and* ***C*** *have been assessed by means of Trypan blue exclusion test. Data were expressed as percentage of viable cells. **p < 0.01 treated vs control cells. ###p < 0.001 vs TMZ-treated cells.* ***B*** *and* ***D*** *have been performed through Luminescent assay applied to evaluate HIF-1α activity, both in untreated cells and after 24h treatment with 100 μM TMZ. Data were expressed as Relative Luminescence Units (RLU) obtained by luciferase counts normalised to the amount of proteins quantified by Bradford assay. **p < 0.01 vs control cells. ###p < 0.001 vs TMZ-treated cells. Mean values ± SD of three independent experiments.*

Also, gene expression analyses of CMA-related genes, of *HIF-1α* and one of its primary target genes, *VEGF*, under the same conditions confirmed the acquisition of TMZ-resistance in TMZ-treated U251 cells

after *LAMP-2A*, *HSC70* or *PHLPP1* silencing. In particular, it seems that *PHLPP1* silencing, more than the *LAMP-2A* one, has increased the *HIF-1α* and *VEGF* expression in these cells, showing again the CMA engagement in responsiveness to TMZ treatment **(Figure 21A, B)**. On the other hand, silencing of *LAMP-2A*, *HSC70* and *PHLPP1* genes did not change responsiveness to TMZ in T98 and these cells maintained their resistant-like behaviour even for *HIF-1α/VEGF* gene expression **(Figure 21 C, D)**.

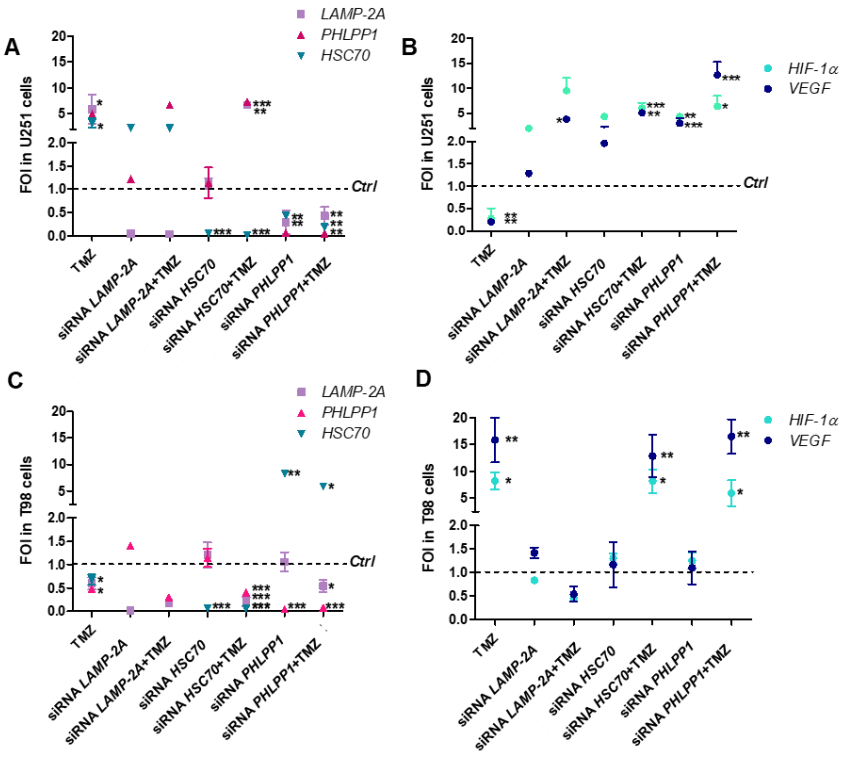

Figure 21: Gene expression of the CMA-related genes (LAMP-2A, PHLLP1 and HSC70) and of HIF-1α and VEGF after silencing of CMA-related genes ± TMZ in U251 and T98 cells.

*Gene expression analysis for CMA-related genes (LAMP-2A, HSC70, PHLPP1) and HIF-1α and VEGF were analysed by means of real-time PCR in U251 and T98 cells. Data were normalised to β-actin, and the ΔΔCt values were expressed as FOI of the ratio between treated and control cells. *p < 0.05, **p < 0.01, ***p < 0.001 treated vs control cells. #p < 0.05, ##p < 0.01, ###p < 0.001 vs TMZ-treated cells. Mean values ± SD of three independent experiments.*

EMT-linked (*SNAIL*, *SLUG* and *E-CAD*) gene expression profile investigation reported no changes among these genes in *LAMP-2A*, *HSC70* and *PHLPP1*-silenced U251 cells; the situation was different after TMZ treatment, in fact a *SNAIL* and *SLUG* expression increased and *E-CAD* mRNA amount decreased confirming a mesenchymal-like expression profile induction, which generally is obtained in TMZ-resistant cells **(Figure 22A)**. Contrarily, T98-resistant cells did not produce any alteration in EMT genes modulation neither after *LAMP-2A*, *HSC70* and *PHLPP1* silencing *per se*, nor after TMZ treatment **(Figure 22B)**.

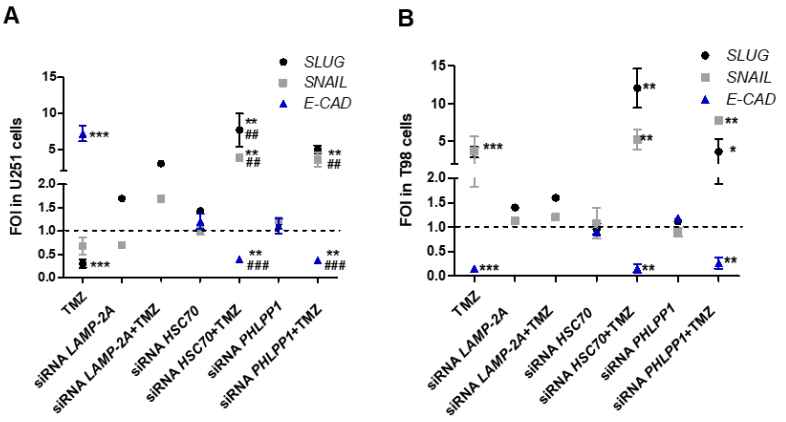

Figure 22: Gene expression of the EMT-related genes (SLUG, SNAIL and E-CAD) after silencing of CMA-related genes ± TMZ in U251 (A) and T98 (B) cells.

*Gene expression analysis for EMT-related genes (SLUG, SNAIL and E-CAD) were analysed by means of real-time PCR in U251 and T98 cells. Data were normalised to β-actin, and the ΔΔCt values were expressed as FOI of the ratio between treated and control cells. *p < 0.05, **p < 0.01, ***p < 0.001 treated vs control cells. #p < 0.05, ##p < 0.01, ###p < 0.001 vs TMZ-treated cells. Mean values ± SD of three independent experiments.*

The same silencing and TMZ treatment scheduling has been performed for *HIF-1α*, both in sensitive and resistant cell lines. Viability assay in U251 cell line has been shown that the silencing of *HIF-1α* alone did not reduce cell viability and, after TMZ treatment, no silencing mediated-additive effects have been observed **(Figure 23A)**. From what concerns HIF-1α activity evaluation, it was reduced by TMZ only in sensitive cells, and further decreased after *HIF-1α* silencing **(Figure 23B)**. On the other hand, *HIF-1α* silencing has significantly decremented cell viability after TMZ treatment in the resistant T98 cells **(Figure 23A)**. This result was confirmed from biochemical luciferase assay, where TMZ treatment alone was not able, as expected, to

decrease *HIF-1α* activity in T98 cells and the result was overturned only in simultaneous presence of TMZ and *HIF-1α* silencing, reverting the previous resistant-like behaviour in a sensitive-like one **(Figure 23B)**. The molecular consequences of *HIF-1α* silencing have been assessed by monitoring the expression of the apoptosis-related genes (*BCL-2, BAX*, *BAD*). Moreover, TMZ treatment activated an inverse modulation of pro- and anti-apoptotic genes in U251 and T98 cells. However, *HIF-1α* silencing in U251-responsive cells has not induced any further modulation of apoptosis-related genes beyond that obtained after TMZ treatment, but *HIF-1α* silencing in resistant cells restored a “sensitive-like pattern” in apoptosis-related gene expression, with the upregulation of *BAX* and *BAD* expression, and a reduction in *BCL-2* transcript levels **(Figure 23C)**.

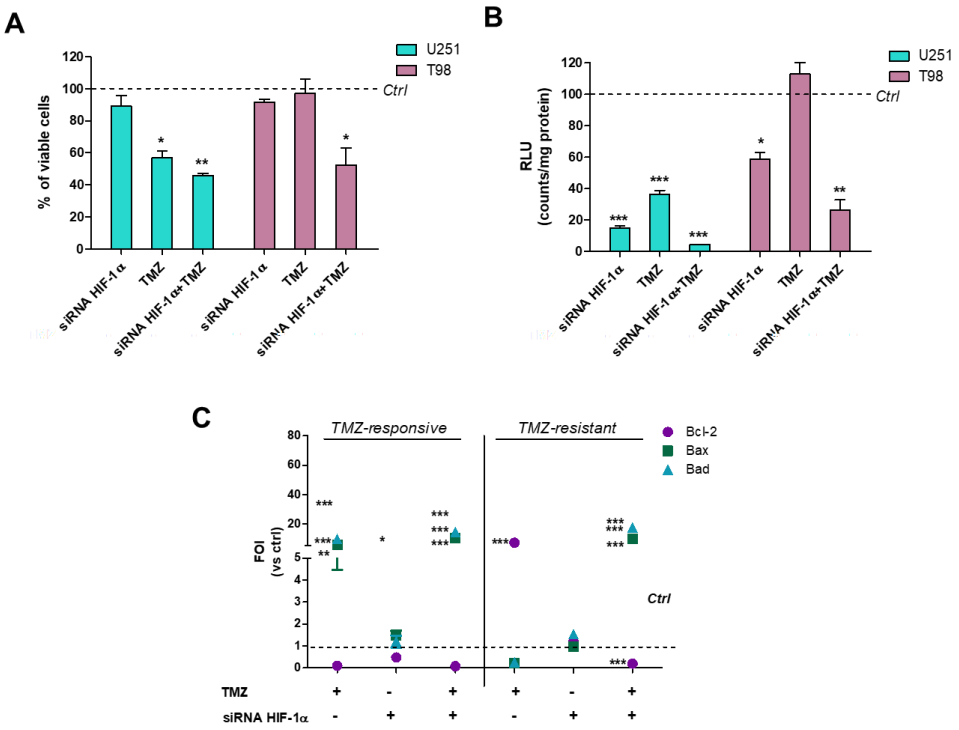

Figure 23: HIF-1α silencing induces a responsive-profile in TMZ-resistant cells.

A: *Viability of U251 and T98 was assessed by means of Trypan blue exclusion test and expressed as the percentage of viable cells after HIF-1α silencing. *p < 0.05, **p < 0.01, ***p < 0.001 vs control cells.* ***B:*** *HIF-1α dependent luciferase activity in U251 and T98 was analysed in cell lysates and expressed as the percentage variation in relative luminescence units (RLUs). *p < 0.05, **p < 0.01, ***p < 0.001 vs control cells.* ***C:*** *After silencing, the cells were treated with TMZ and the induction of BCL-2, BAX and BAD and genes was analysed by means of real-time PCR. The data were normalised to β-actin, and the ΔΔCt values were expressed as FOI of the ratio between treated and control cells. Results of sensitive and resistant cells were presented as FOI mean values ± SD. *p < 0.05, **p < 0.01, ***p < 0.001 treated vs control cells. Mean values ± SD of three independent experiments.*

With the aim to assess whether HIF-1α pharmacological inhibition could produce the same consequences of *HIF-1α* gene silencing, T98

cells have been treated with a specific HIF-1α inhibitor, PX-478. Cell viability data showed a statistically significant reduction of cell viability, compared to the untreated controls, both after PX-478 treatment *per se* and after combined treatment with TMZ, recovering cell sensitivity to TMZ **(Figure 24A)**. This trend was in line with HIF-1α activity reduction measured with the biochemical assay **(Figure 24B)**.

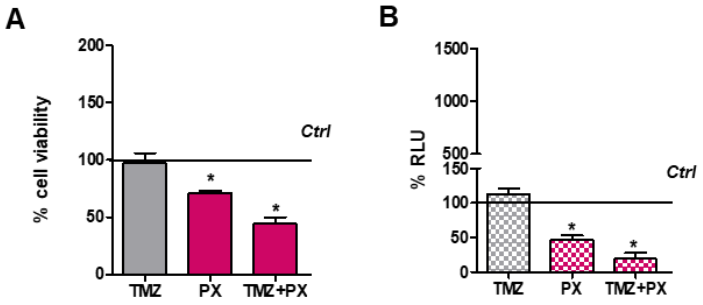

Figure 24: HIF-1α pharmacological inhibition, in particular after TMZ treatment, affects T98-resistant cells viability and HIF-1α activity.
A: *Cell viability of resistant cells was assessed by means of Trypan blue exclusion test and expressed as the percentage of viable cells after PX ± TMZ. *p < 0.05 vs control cells.* ***B:*** *HIF-1α dependent luciferase activity was analysed in cell lysates and expressed as Relative Luminescence Units (RLU) obtained by luciferase counts normalised to the amount of proteins quantified by Bradford assay. *p < 0.05 vs control cells. Mean values ± SD of three independent experiments.*

1.3 ROS are key player in TMZ-response contribution

Recent studies show that TMZ is able to induce an increase in cytoplasmic ROS levels that is important for the induction of cell toxicity [84]. At the same time, other papers report that a transitory increase in ROS levels can induce CMA activity [83,103,189].

Endogenous ROS levels were measured in TMZ-responsive U251 and TMZ-resistant T98 cell lines both in control condition and after treatment with TMZ. These cells exhibited a different intracellular ROS basal level, which in the resistant ones is 8-fold higher compared to the sensitive ones. After 24h-TMZ treatment, in responsive cells, ROS amount resulted statistically increased, while in T98 ones TMZ treatment was not able to further increase cytoplasmic ROS **(Figure 25A)**. The experiment has been replicated by treating cells with the selective mitochondrial (mt) ROS scavenger MitoTEMPO (MitoT), which has been able to reduce ROS levels in both cell lines, confirming their mitochondrial origin. However, ROS levels remained still higher in TMZ-resistant cells **(Figure 25B and C)**.

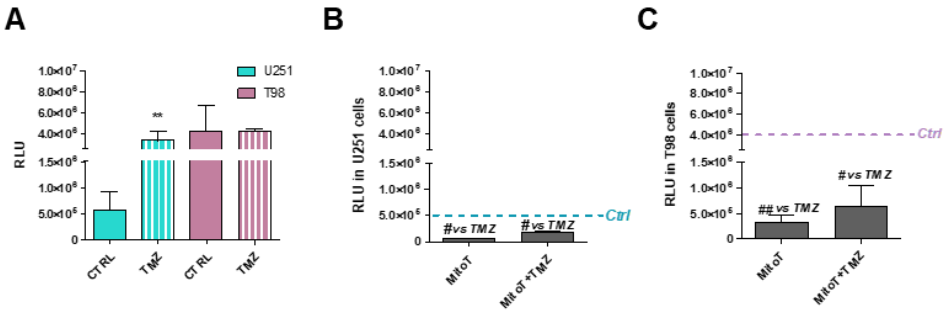

Figure 25: Mitochondrial ROS involvement in TMZ-responsiveness. ***A:*** *Luminescent assay applied to measure H_2O_2 levels in cell culture medium of U251 and T98 cells in untreated cells and after 24h treatment with 100 µM TMZ. Data were expressed as Relative Luminescence Units (RLU) obtained by luciferase counts normalised to the amount of proteins quantified by Bradford assay. **p < 0.01 vs control cells.* ***B and C:*** *ROS levels measured in U251 and T98 cells after 1h of treatment with MitoT 25µM ±TMZ for 24h. Data were expressed as RLU. #p < 0.05, ##p < 0.01 vs TMZ-treated cells. Mean values ± SD of three independent experiments.*

Once confirmed that intracellular ROS-related to TMZ treatment originate from mitochondria, U251 and T98 cells were treated with MitoT to analyse their role in response to treatment. In U251 cells, MitoT was able to reduce cell sensitivity to the TMZ treatment, observed both as regards cell viability and toxicity tests as well as in relation to HIF-1α activity which did non decrease **(Figure 26A, B and C)**. Moreover, TMZ-induced pro-apoptotic gene expression pattern observed in U251 cells was abrogated through MitoT treatment, conferring a resistant -like apoptosis-related gene expression profile to these cells, as shown in **Figure 26D**.

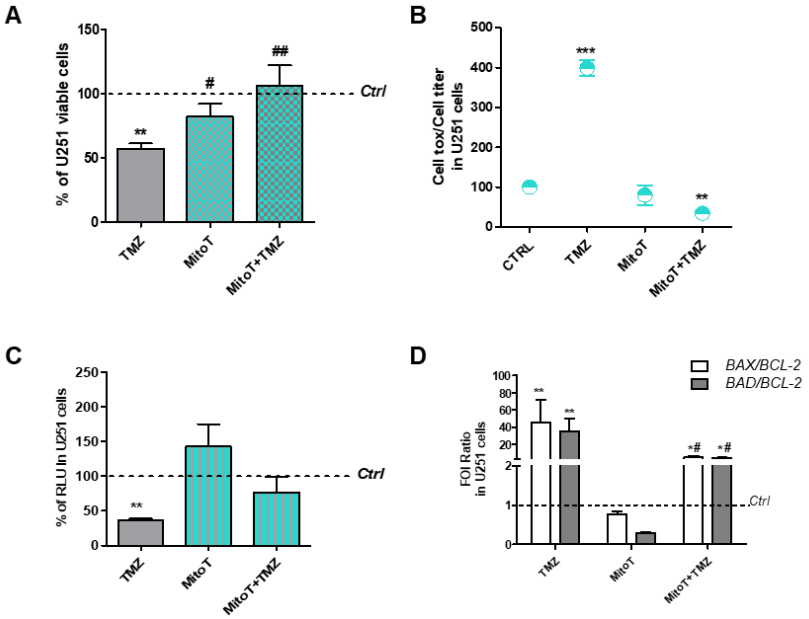

Figure 26: Crucial role of mitochondrial ROS in TMZ-responsiveness in U251 cells.

A: *Viability of U251 analysed through Trypan blue exclusion test and expressed as the percentage of viable cells after treatment with 100 μM TMZ ± 25 μM MitoT. **p < 0.01 vs control cells; #p < 0.05, ##p < 0.01 vs TMZ-*

treated cells. ***B:*** *Cell toxicity in U251 assessed by Cell Tox Green normalised on Cell Titer Glo and expressed as percentage compared to control cells. **p < 0.01, ***p < 0.001 vs control cells.* ***C:*** *Biochemical assay for HIF-1α activity in U251-responsive cell line. Data were expressed as RLU, obtained normalising luciferase counts to the amount of proteins quantified by Bradford assay. **p < 0.01 vs control cells.* ***D.*** *Gene expression analysis for BAX, BAD and BCL-2 analysed through Real-time PCR in U251 cells after treatment with 100 μM TMZ ± 25 μM MitoT. Data were normalised to β-actin, and the ΔΔCt values were expressed as FOI of the ratio between treated and control cells and then as the ratio BAX/BCL-2 and BAD/BCL-2. *p < 0.05, **p < 0.01 treated vs. control cells. #p < 0.05 vs TMZ-treated cells. Mean values ± SD of three independent experiments.*

A different result was observed in T98 cells, where after MitoT treatment no changes neither in cell viability nor in cell toxicity were observed even after treatment with TMZ. Similar results were obtained not only in HIF-1α activity evaluation but even in apoptosis-related gene expression profile analysis: in fact, *BAX/BCL-2* and *BAD/BCL-2* ratio after TMZ treatment maintained a “resistant-like profile”, also in combination with the SOD-mimetic **(Figure 27)**.

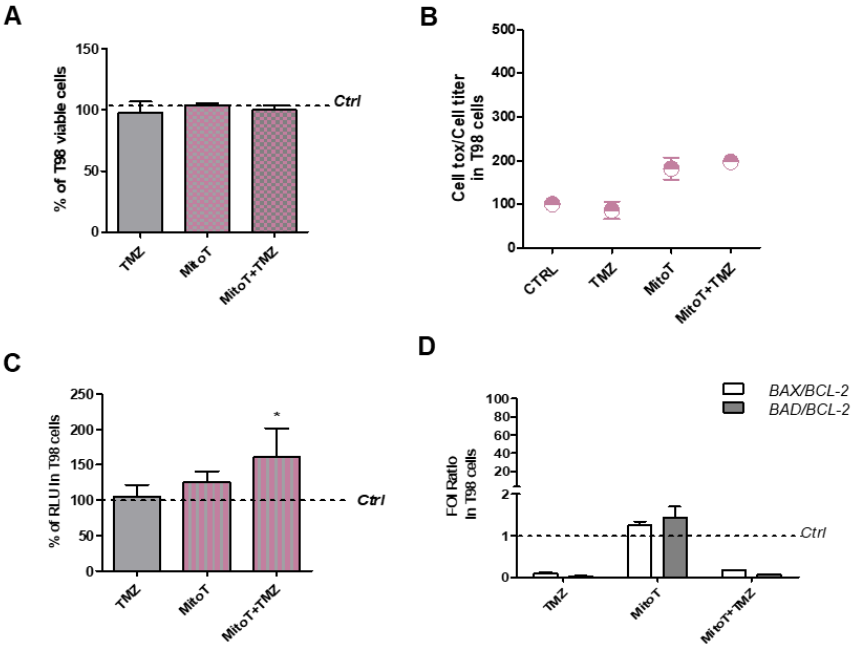

Figure 27: Crucial role of mitochondrial ROS in TMZ-responsiveness in T98 cells.
A: *Viability of T98 analysed through Trypan blue exclusion test and expressed as the percentage of viable cells after treatment with 100 μM TMZ ± 25 μM MitoT.* ***B:*** *Cell toxicity in T98 assessed by Cell Tox Green normalized on Cell Titer Glo and expressed as percentage compared to control cells.* ***C:*** *Biochemical assay for HIF-1α activity in T98-resistant cell line. Data were expressed as RLU, obtained normalising luciferase counts to the amount of proteins quantified by Bradford assay. *p < 0.05 vs control cells.* ***D.*** *Gene expression analysis for BAX, BAD and BCL-2 analysed through Real-time PCR in T98 cells after treatment with 100 μM TMZ ± 25 μM MitoT. Data were normalised to β-actin, and the ΔΔCt values were expressed as FOI of the ratio between treated and control cells and then as the ratio BAX/BCL-2 and BAD/BCL-2. Mean values ± SD of three independent experiments.*

In line with these data, we investigated the role of mtROS in regulating CMA activity. Specifically, CMA-related (*LAMP2A, PHLPP1, HSC70*) and hypoxia-linked (*HIF-1α* and *VEGF*) gene expression was analysed by real-time PCR in U251 and T98 cells. In U251 cells, *LAMP-2A*,

HSC70 AND *PHLPP1* genes, as expected, were up-regulated after TMZ-treatment, whereas the co-treatment with MitoT reverted the gene expression profile **(Figure 28A)**. This resistant-like expression profile can be observed also for *HIF-1α* and *VEGF* gene expression, which increased as in resistant cells **(Figure 28B)**.

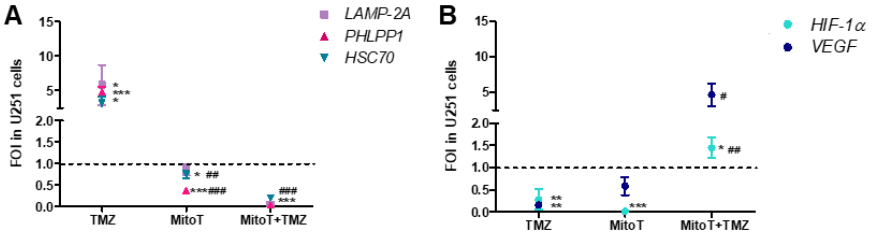

Figure 28: Gene expression analysis for CMA-related genes (LAMP-2A, HSC70, PHLPP1) and HIF-1α and VEGF in U251 cells.
*These genes have been analysed by means of real-time PCR in U251 after treatment with 100 μM TMZ ± 25 μM MitoT. Data were normalised to β-actin, and the ΔΔCt values were expressed as FOI of the ratio between treated and control cells. *p < 0.05, **p < 0.01, ***p < 0.001 treated vs control cells. #p < 0.05, ##p < 0.01, ###p < 0.001 vs TMZ-treated cells. Mean values ± SD of three independent experiments.*

In resistant T98 cells, MitoT by itself induced a statistically significant reduction in *LAMP-2A* expression and in combination with TMZ a further significant reduction in the expression of all CMA-related genes was observed **(Figure 29A)**. Moreover, in T98 cells MitoT treatment did not exert any influence on *HIF-1α* mRNA modulation both as single treatment and in combination with TMZ **(Figure 29B)**.

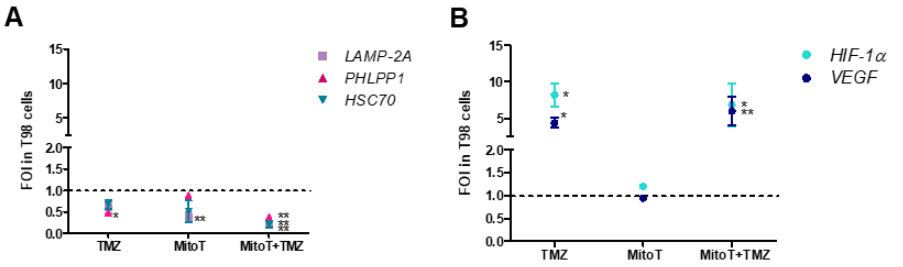

Figure 29: Gene expression analysis for CMA-related genes (LAMP-2A, HSC70, PHLPP1) and HIF-1α and VEGF in T98 cells.
*These genes have been analysed by means of real-time PCR in T98 after treatment with 100 μM TMZ ± 25 μM MitoT. Data were normalised to β-actin, and the ΔΔCt values were expressed as FOI of the ratio between treated and control cells. *p < 0.05, **p < 0.01 treated vs control cells. Mean values ± SD of three independent experiments.*

Since HIF-1α is also involved in the regulation of EMT, we performed a scratch test in both cell lines, to observe how differently the treatment might influence wound healing. EMT gene expression was analysed as well. In U251 cells TMZ treatment inhibited the closure of the scratch even at 24h, while MitoT treatment was able to prevent TMZ-mediated cell toxicity provoking the complete scratch closure in 24 hours **(Figure 30A)**. Results were supported by EMT gene expression analyses (*SNAIL*, *SLUG* AND *E-CAD*). In fact, while TMZ induced an epithelial-like expression profile in U251 cells with high expression of *E-CAD* and low expression of *SNAIL* and *SLUG* genes, the combination with MitoT produced an opposite mesenchymal-like pattern with an increase in *SNAIL* and *SLUG* expression and a reduction of *E-CAD* mRNA level **(Figure 30B)**.

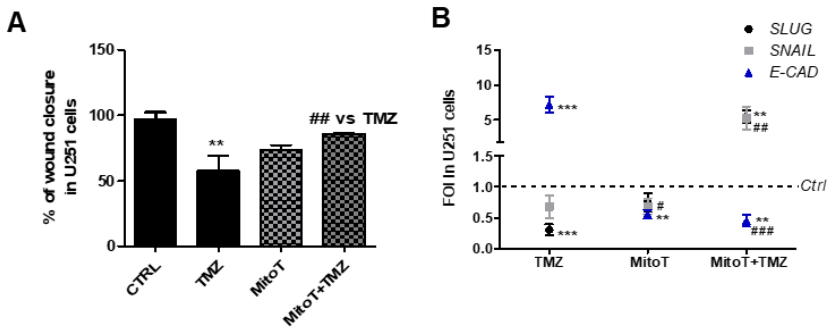

Figure 30: EMT involvement in TMZ response in U251 cells.
A: *Scratch test performed after treatments in U251 cells. Wound closure percentage compared to controls was analysed with ImageJ software. **p < 0.01 treated vs control cells. ##p < 0.01 vs TMZ-treated cells.* ***B:*** *Gene expression analysis for EMT-related genes (SLUG, SNAIL, E-CADHERINE) analysed by means of real-time PCR in U251. Data were normalised and expressed as mentioned above. **p < 0.01, ***p < 0.001 treated vs control cells. ##p < 0.01, ###p < 0.001 vs TMZ-treated cells. Mean values ± SD of three independent experiments.*

In T98 cells, MitoT treatment did not change neither wound healing kinetic and EMT-related gene expression, both as single treatment and in combination with TMZ **(Figure 31)**.

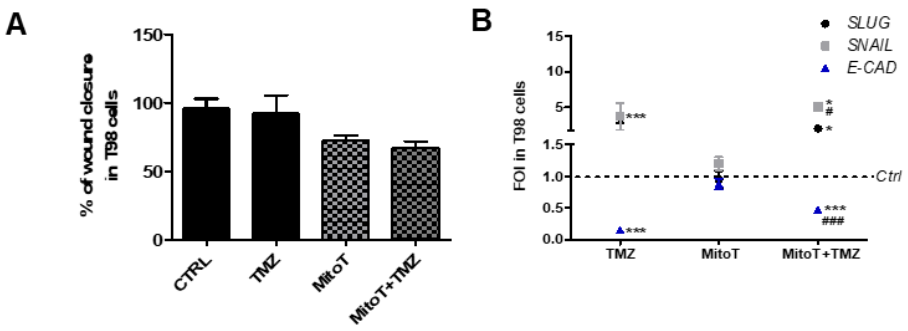

Figure 31: EMT involvement in TMZ response in T98 cells.
A: *Scratch test performed after treatments in U251 cells. Wound closure percentage compared to controls was analysed with ImageJ software. **p < 0.01 treated vs control cells. ##p < 0.01 vs TMZ-treated cells.* ***B:*** *Gene expression analysis for EMT-related genes (SLUG, SNAIL, E-CADHERINE) analysed by means of real-time PCR in U251. Data were normalised and expressed as mentioned above. **p < 0.01; ***p < 0.001 treated vs control cells. ##p < 0.01, ###p < 0.001 vs TMZ-treated cells. Mean values ± SD of three independent experiments.*

1.4 Redox-balance deregulation association to GBM TMZ-responsiveness

For a better investigation of the processes contributing in ROS increase after TMZ treatment in responsive cells, mitochondrial and cytosolic detox mechanisms were evaluated. Due to the dependence of the ROS production and, consequently, of the redox-homeostasis by the respiratory chain, the mitochondrial respiratory chain complexes activities (I, II, I+II and IV) have been measured both in U251 and T98 cells, both basally and after 24 h of TMZ-treatment. Complexes I, III and IV basal activities resulted to be significantly higher in resistant cells compared to the sensitive ones; this discrimination was kept even after alkylating agent treatment **(Figure 31A)**. No variations have been detectable in citrate synthase amounts,

showing no changes in mitochondrial global content (data not shown). T98 treated with TMZ did not show any appreciable reduction in complex activities (**Figure 31B**).

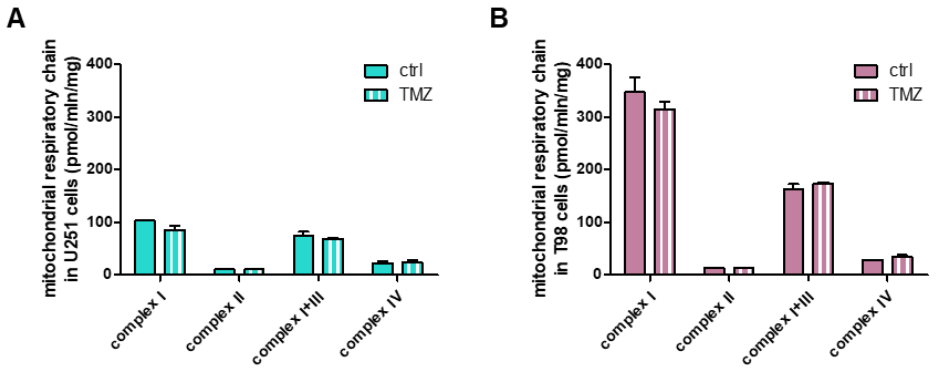

Figure 32: Deregulation of redox-homeostasis.
Spectrophotometric analysis of mitochondrial respiratory chain complex activities measured before and after 24 hours of treatment with TMZ in U251 (A) and (B) T98 cells. Values are expressed as mean values of complex I, II, I+III and IV normalised to citrate synthase activities (pmol/min/mg of proteins). Mean values ± SD of three independent experiments.

For testing whether these differences among mitochondrial complexes are due to altered stability in mitochondrial respiratory chain complexes, SDS-PAGE analysis of the key-player OXPHOS subunits has been performed in the same samples used for the biochemical approach. No consistent differences between U251 and T98 cell lines have been appreciated neither in basal conditions nor after TMZ treatment **(Figure 32)**; these findings support the idea that augmented OXPHOS activities and TMZ reduction observed in T98 cells might derive from deregulated OXPHOS homeostasis and/or altered ROS

management while steady state levels of mitochondrial proteins are conserved.

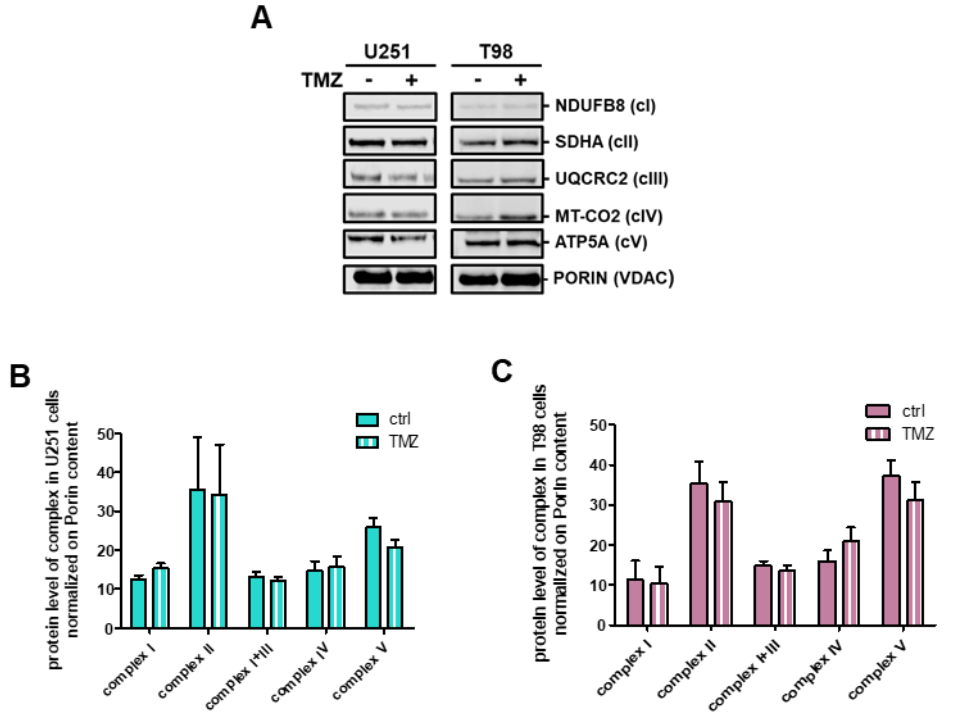

Figure 33: Western Blot analyses of OXPHOS subunits.
A: *Western Blot image of representative subunits of the mitochondrial respiratory chain analysed before and after 24 hours of TMZ treatment.* ***B:*** *Quantification of the aforementioned subunits in U251 cells.* ***C:*** *Quantification of these subunits in T98 cells. Values are expressed as mean values of protein content (arbitrary units) normalised to the signal of Porin (VDAC). Mean values ± SD of three independent experiments.*

Since the importance of ROS level modulation within the cells and its dependence from the cellular redox system, the expression of the main enzymes involved in detoxification from ROS were analysed by both real-time PCR and activity assays. In U251 cell line, the expression of glutathione peroxidase, synthetase and reductase (*GPX*, *GSS and*

GR), superoxide dismutase 2 (*SOD2*) and *CATALASE* genes resulted to be down-modulated after TMZ treatment. On the other hand, in T98 TMZ-resistant cells, an up-regulation in the expression of *CATALASE*, glutathione synthetase and reductase genes has been observed **(Figure 34A)**. Intracellular GSH levels were monitored in U251 and T98 cells and it has been shown that T98 cells possessed a higher GSH level compared to U251 at control condition. However, while in U251 cells TMZ treatment decreased GSH level compared to controls, GSH level did not change after treatment in T98 cells **(Figure 34B)**.

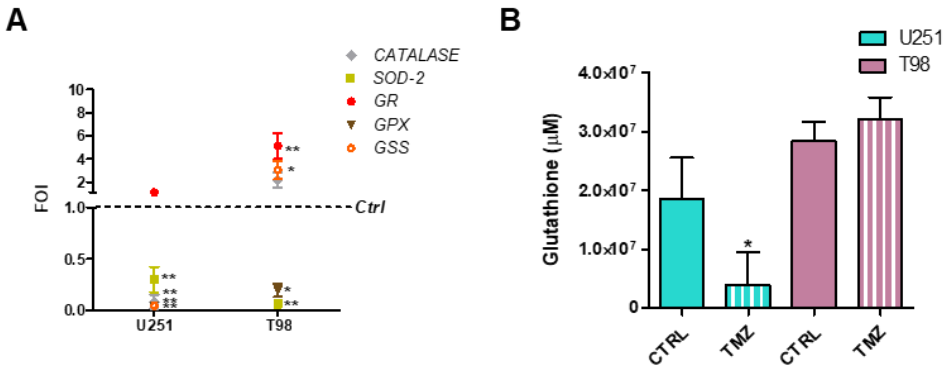

Figure 34: Investigation on ROS level modulation within the cells and its dependence from the cellular redox system.
A: *Gene expression profile for Detox enzymes (SOD-2, CATALASE, GR, GPX and GSS) after treatment with 100 µM TMZ in U251 and T98 cells. Data were normalised to β-actin, and the ΔΔCt values were expressed as FOI of the ratio between treated and control cells. *p < 0.05, **p < 0.01 vs control cells.* ***B:*** *Glutathione concentration assessed after TMZ treatment in both cells by means of a commercially available kit. Data were expressed as glutathione concentration (µM). *p < 0.05 treated vs control cells. Mean values ± SD of three independent experiments.*

In order to define the redox-homeostasis role in TMZ responsiveness, the protein levels of the key players of the detox machinery have been

assessed: in detail, we showed decreased CATALASE and SOD-1 residual levels after TMZ treatment only in U251 responsive cells, differently from T98 resistant ones, where SOD-1 resulted to be statistically augmented after 48 hours of TMZ-treatment. Herein, SOD cytosolic isoform protein, SOD-1, has been studied in relation to ROS presence into the cytosol **(Figure 35)**.

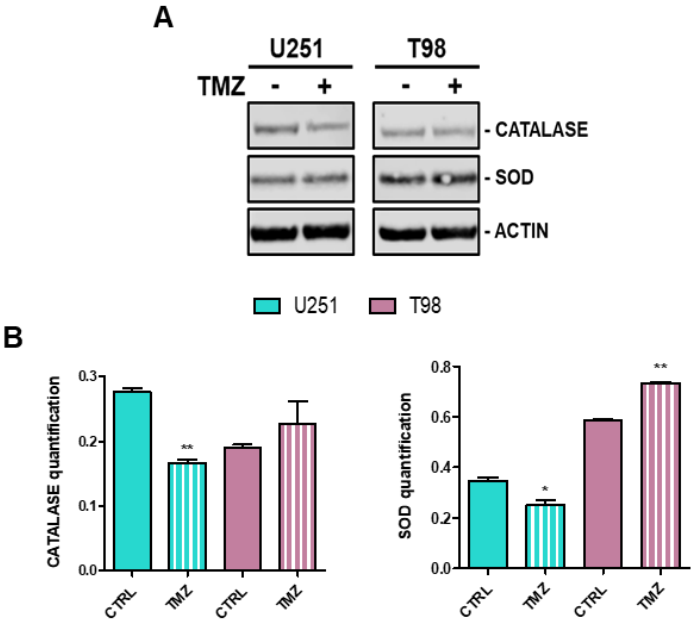

Figure 35: Analyses of the protein levels of the key players of the detox machinery in responsiveness to TMZ.
A: *Western blot analysis of CATALASE and SOD in protein lysates from untreated (-) and TMZ-treated (+) U251 and T98 cell lines at 24 hours of treatment.* ***B:*** *Quantification of the aforementioned proteins. Protein signals were normalised to actin levels. * p<0.05, ** p<0.01 treated vs control. Mean values ± SD of three independent experiments.*

1.5 Induced-oxidative stress helps to sensitise T98 cells in TMZ-treatment

Since it was well described the involvement of a transitory increase in ROS levels in inducing CMA activity, a treatment with H_2O_2 has been used to evaluate its ability in inducing CMA activity, especially in T98 cells, also in combination with TMZ. Firstly, a H_2O_2 dose response has been performed for testing which H_2O_2 doses showed the most significant results both in responsive and resistant cell lines, however, for better summarising this work, the dose response data are not shown. Cell viability has been carried out for monitoring both TMZ-responsive and -resistant cell lines after treatment with a “mild” and a “high” H_2O_2 dose also in combination with TMZ. Both the treatments have been previously described in literature [190–193].

In detail, “mild” H_2O_2 oxidative stress (200 µM) did not affect cell viability compared to controls and did not increase cell cytotoxicity in combination with TMZ in U251 cells; on the other hand, the use of the “high” H_2O_2 oxidative stress caused a reduction in cell viability comparable to what obtained also in combination with TMZ **(Figure 36A)**. Results were confirmed by the apoptotic gene expression assay **(Figure 36B)**. For what concerns T98 resistant cells, mild H_2O_2 (200 µM) oxidative stress, produced no effect in cell viability; while after the high H_2O_2 (1 mM) dose, a decrement in cell viability was observed, both in single and in TMZ-combined treatment **(Figure 36C)**. Moreover, apoptosis-related gene expression analysis showed that only the higher H_2O_2 dose in combination with TMZ had the potential

to change gene expression towards a “pro-apoptotic” phenotype **(Figure 36D)**.

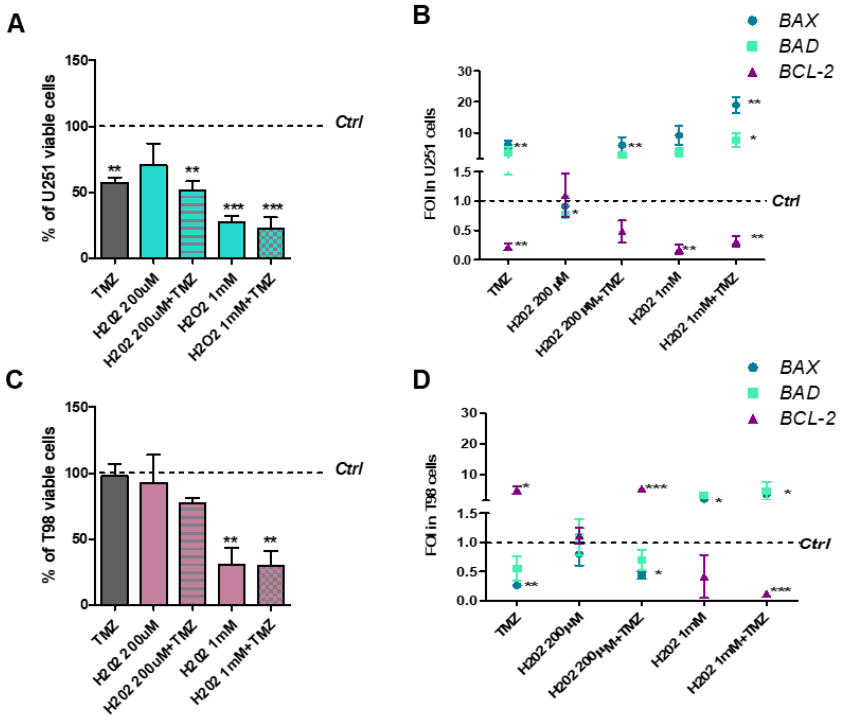

Figure 36: Induced oxidative stress and its role in overcoming resistance to TMZ.
A and B: *Viability analysis and gene expression profile for apoptotic-related genes (BAX, BAD and BCL-2) in U251 cells.* ***C and D:*** *The same analyses performed in U251 have been done in T98 cells. Viability was assessed through Trypan blue exclusion test after treatment with 200µM or 1mM H_2O_2 ± 100 µM TMZ. Data of viability were expressed as percentage of viable cells; **p < 0.01, ***p < 0.001 treated vs control cells. All data of gene expression were normalised to β-actin, and the ΔΔCt values were expressed as FOI of the ratio between treated and control cells. *p < 0.05, **p < 0.01, ***p < 0.001 treated vs control cells.*

As regards CMA, “mild” H_2O_2 treatment triggered an increment in CMA-linked genes expression, except for *HSC70* with a consequent significant expression rise in *HIF-1α* and *VEGF* mRNA levels

compared to controls. Differently, oxidative stress induced by 1 mM H_2O_2 was able not only to significantly activate *LAMP-2A* and *HSC70* expression, but even to significantly decrease the *HIF-1α* and the *VEGF* ones, while no modulation in *PHLPP1* expression was appreciated. Its expression was up-regulated only after concurrent treatment with "high" H_2O_2 and TMZ **(Figure 37A and B)**. In T98 cells, only the "high" H_2O_2 dose induced a "sensitive-like" expression pattern in CMA-related genes, that was completed only in combination with TMZ, with a significant decrease both in *HIF-1α* and *VEGF* expression **(Figure 37C and D)**.

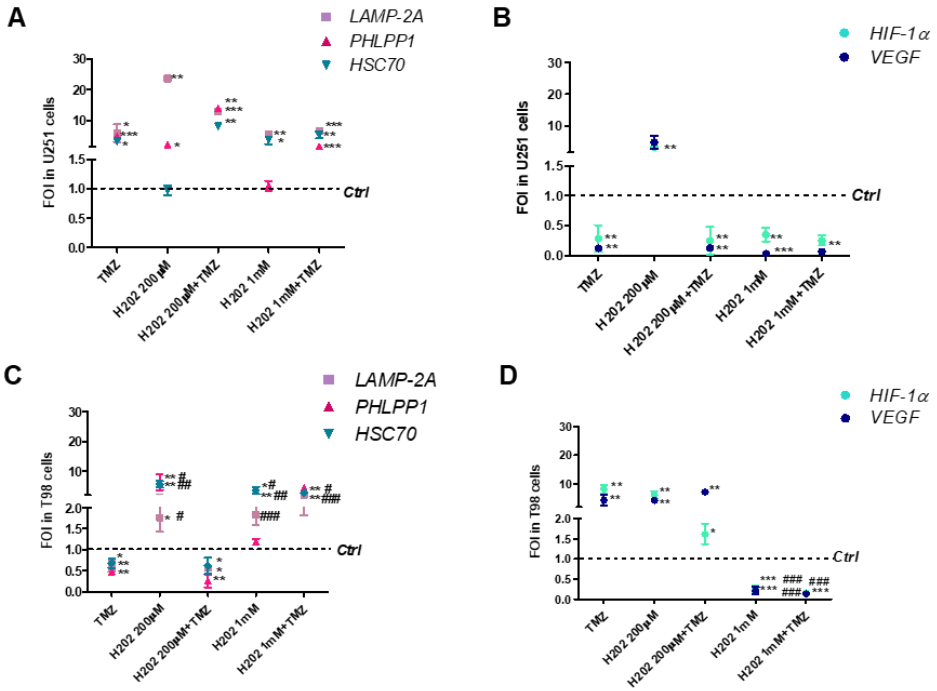

Figure 37: Gene expression profile for CMA-related genes (LAMP2A, HSC70, PHLPP1), and for HIF-1α and VEGF.
A and B: *Gene expression profile of the previously mentioned genes in U251.* ***C and D:*** *Gene expression profile of the previously mentioned genes*

*in T98 cell. **A-D** all performed after treatment with 200μM or 1mM H_2O_2 ± 100 μM TMZ. All data of gene expression were normalised to β-actin, and the ΔΔCt values were expressed as FOI of the ratio between treated and control cells. *p < 0.05, **p < 0.01, ***p < 0.001 treated vs control cells. #p < 0.05, ##p < 0.01, ###p < 0.001 vs TMZ-treated cells. Mean values ± SD of three independent experiments.*

Finally, as regards EMT evaluation, in U251 cells "mild" H_2O_2-mediated oxidative stress did not induce any therapeutic effect as single treatment, while, even as a single treatment, the "high" H_2O_2 dose induced an epithelial-like expression pattern similar to that obtained with TMZ single treatment and a concomitant delay in wound closure. Combination with TMZ did not provide any further effect different from those already obtained with the only TMZ treatment **(Figure 38A, B)**. In T98 cells on the other hand, only the "high" H_2O_2 dose favoured a delay in the scratch closure and a concomitant EMT expression profile close to an epithelial-like one. Once again, only in combination with TMZ, "high" H_2O_2 dose produced a complete epithelial-like expression pattern with down-regulation of *SNAIL* and *SLUG* expression and an increase in *E-CADERINE* mRNA **(Figure 38B and C)**.

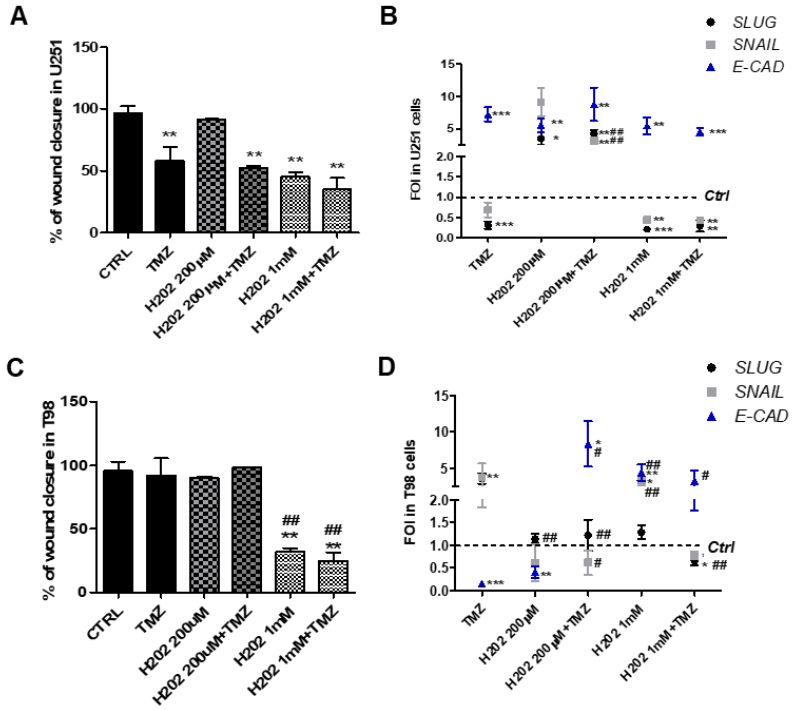

Figure 38: EMT role in induced oxidative stress related to TMZ treatment.
A and B: *Scratch test and gene expression for EMT-related genes (SLUG, SNAIL, E-CADHERINE) performed after treatments in U251.* ***C and D:*** *The same experimental procedures have been adopted also for T98 cells. Wound closure percentage compared to control was analysed with ImageJ software. **p < 0.01 treated vs control cells. ##p < 0.01 vs TMZ-treated cells. Data of gene expression were normalised and expressed as mentioned above. *p < 0.05, **p < 0.01, ***p < 0.001 treated vs control cells. #p < 0.05, ##p < 0.01 vs TMZ-treated cells.*

1.6 CT-2A characterization

Murine GBM CT-2A cell line has been characterised in an *in vitro* experimental setting to characterise their responsiveness to TMZ. MGMT methylation promoter analysis reported a 28% of promoter methylation. TMZ treatment, as shown in **Figure 39**, was not able to

induce a reduction in cell viability and *Hif-1α* expression and activity (related to one of its primary target, *Vegf*), demonstrating that these GBM murine cells are characterised by TMZ resistance similarly to T98 cells. Moreover, in CT-2A cells, as already demonstrated for T98 resistant cells, *HIF-1α* silencing allowed the recovery of cell sensitivity to TMZ **(Figure 39)**.

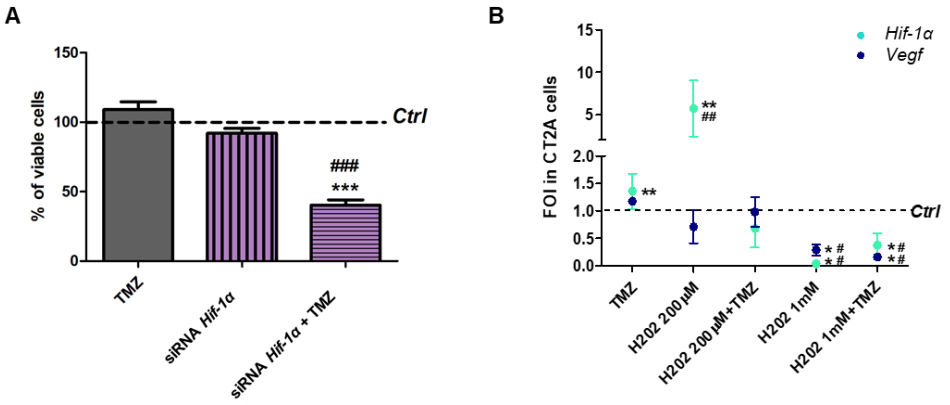

Figure 39: CT-2A cell line characterisation in relation to responsiveness to TMZ.
A: *Viability analysis in CT-2A after Hif-1α silencing ± 100 µM TMZ treatment. Viability test has been assessed by means of Trypan blue exclusion test. Data were expressed as percentage of viable cells. ***p < 0.001 treated vs control cells. ###p < 0.001 vs TMZ-treated cells.* ***B:*** *Gene expression analysis for Hif-1α and Vegf were analysed by means of real-time PCR in CT-2A cells. Data were normalised to β-actin, and the ΔΔCt values were expressed as FOI of the ratio between treated and control cells. *p < 0.05, **p < 0.01 treated vs control cells. #p < 0.05, ##p < 0.01. Mean values ± SD of three independent experiments.*

Finally, according to the H_2O_2-mediated-oxidative stress data reported in T98 cells (see the paragraph ***1.5***), CT-2A treated with the "mild" H_2O_2 dose were not affected by the treatment, both for their viability and in HIF-1α activity. On the other hand, the use of the high H_2O_2

concentration triggered a significant decrease not only in *Hif-1α* and *Vegf* expression **(Figure 39B)**, but also in cell viability and in HIF-1α activity, especially in combination with TMZ **(Figure 40A, B)**. As regards wound healing in CT-2A cells, as already described for T98 cells, only 1mM H_2O_2 treatment in combination with TMZ induced a significant wound closure delay **(Figure 40C).**

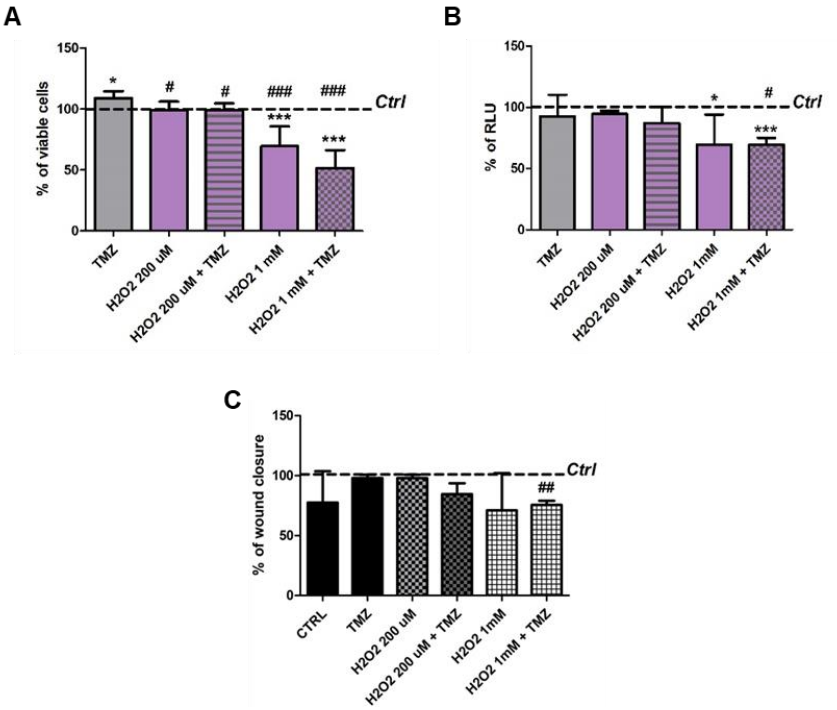

Figure 40: Induced oxidative stress and its role in overcoming resistance to TMZ in CT-2A murine cells.
A: *Viability assay has been assessed by means of Trypan blue exclusion test. Data were expressed as percentage of viable cells. *p < 0.05, ***p < 0.001 treated vs control cells. #p < 0.05, ###p < 0.001 vs TMZ-treated cells.*
B: *HIF-1α activity evaluation has been performed through Luminescent assay applied to evaluate HIF-1α activity, both in untreated cells and after 24h H_2O_2 treatment ± 100 μM TMZ (A). Data were expressed as Relative Luminescence Units (RLU) obtained by luciferase counts normalised to the*

*amount of proteins quantified by Bradford assay. *p <0.05, ***p < 0.001 vs control cells. #p < 0.05 vs TMZ-treated cells.* ***C:*** *Scratch test performed after treatments in CT-2A. Wound closure percentage compared to control was analysed with ImageJ software. ##p < 0.01 vs TMZ-treated cells. Mean values ± SD of three independent experiments.*

2. *IN VIVO* RESULTS

2.1 In vivo non-invasive GBM model characterization by MRI

CT-2A cells were used to implement a murine model of GBM resistant to TMZ, since it has been already reported that T98 cells cannot be used to produce ortothopic models [194–196].

C57Bl/6J mice received an intracranial (i.c.) stereotaxical injection with CT-2A murine cells, then tumour growth was monitored by using MRI, 9 and 15 days after cell injection, as shown in **Figure 41**.

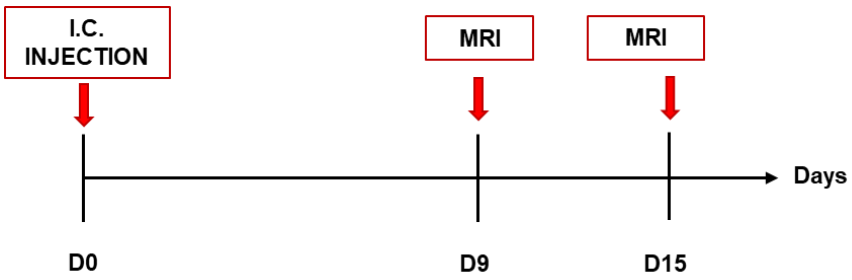

Figure 41: Timeline of the MRI acquisitions.
The procedures, shown in red contoured squares, are described following the days. D0 represents *the i.c. injection day. Two consecutive MRI scans were performed at days 9 and 15, the first one to check if the tumour was grown after surgery and the second one to monitor the tumour growing.*

Data analysis from MRI acquisitions showed an average tumour volume of 1.27 mm^3 ± 0.93 at day 9 post-injection which increased

after further six days to an average volume of 13.62 mm^3 ± 3.03, **(Figure 42A, B, C)**. MRI images have been performed in T2 (T2-weighted images, T2W), where brighter regions represent tumour sites. T2W-MRI data quantitation showed about a 25% increase in T2 values in tumours compared to unaffected contralateral regions **(Figure 42B and C)**. In fact, the bright signal in the T2W data represents a combination of tumour and oedema. DTI representative data showed the tumour disrupting normal white matter pathways with a visible ring of high FA that points to the tumour margin **(Figure 42D)**.

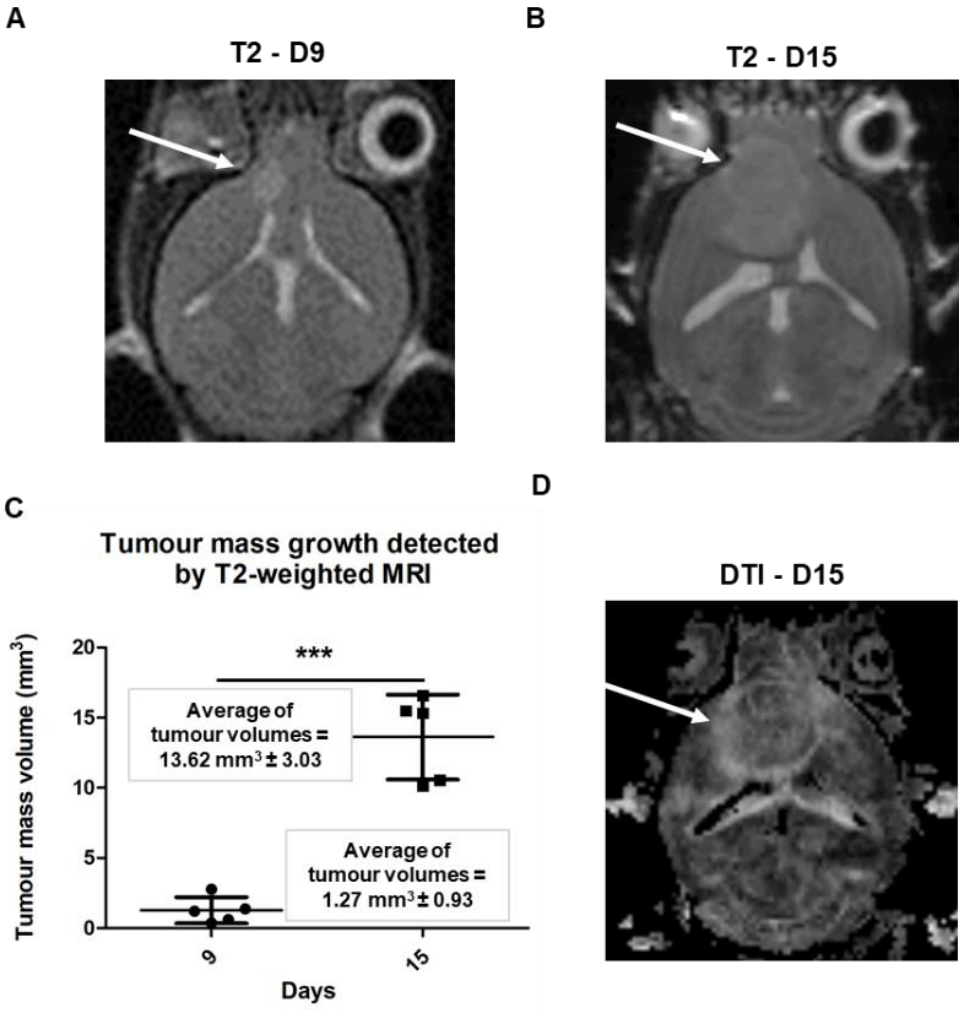

Figure 42: MRIs analyses on orthotopic mice models set up by i.c. injection of CT-2A murine cells.

T2W-MRI have been carried out on days 9 and 15. ***A:*** *T2-MRI at day 9 after i.c. injection.* ***B:*** *T2-MRI at day 15 after i.c. injection.* ***C:*** *Quantification of tumour growth monitored by MRI. T2W-MRI data showed about a 25% increase in T2 values in tumours compared to unaffected contralateral regions. ***p < 0.001 tumour volumes at day 15 vs tumour volume at day 9. In figure* ***D:*** *representative DTI acquisition showing the tumour disrupting normal white matter pathways with a visible ring of high FA that points to the tumour margin. Tumour ROI volumes have been calculated through VivoQuant software.*

2.2 CT-2A murine cells represent a good cellular model for the in vivo analyses for GBM responsiveness to radiation therapy

In order to assess the efficacy of an external radiation treatment, 15Gy-hemibrain radiation therapy (RT) has been fractionated into three sessions at days 9,10,11. GBM bearing mice, both controls (tumour-bearing mice without RT) and treated were monitored by MRI for tumour volume assessment. RT induced a significant reduction in tumour volume as clearly shown in **Figure 43A**. Moreover, the treatment induced also an increase in the OS of all the treated mice **(Figure 43B)**.

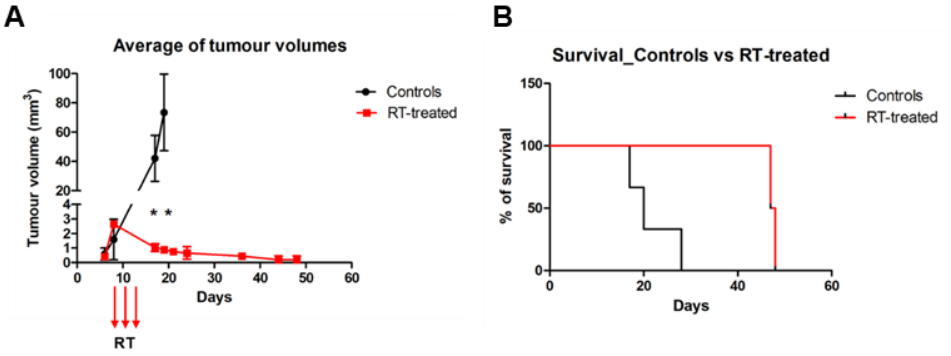

Figure 43: Evaluation of RT efficacy.
A: *Tumour volume monitored by MRI in controls (tumour-bearing mice) and RT-treated mice. *p < 0.05 RT-treated vs controls. Mean values ± SD.* ***B:*** *Kaplan-Meier survival curves showing OS of controls versus treated tumour bearing mice.*

In summary, these data have shown that murine glioma CT-2A cells are responsive to radiotherapy and can be used as a model of TMZ-resistant, RT-sensitive GBM *in vivo*.

2.3 Validation of ^{18}F-Fluciclovine as a tracer for GBM monitoring by PET

The same orthotopic models already described for MRI studies were used to set up a PET acquisition with ^{18}F-Fluciclovine to evaluate this tracer for GBM volume monitoring and potentially response to treatment. To this end, a first evaluation of tracer uptake during time has been carried out by performing a dynamic 90 minutes-PET acquisition 16 days after cell stereotaxic injection. Radiotracer has been injected i.v. (intravenously) when PET acquisition started. As shown in **Figure 44**, activity measurement was carried out in different Regions of Interest (ROIs): Healthy brain (blue), Tumour (green), Nasal passages (yellow), Salivary glands (purple), Liver (the region of interest is chosen at the bottom lobe of the liver for consistency). Image has been scaled between 0 and 3 SUV.

Time activity curves have shown radionuclide uptake in different ROIs during the 90 minutes acquisition **(Figure 44A)**. A high uptake has been observed in salivary glands and nasal passages, however tumour uptake increased progressively overcoming that of other organs from 60 minutes after injection. These curves have been helpful to set up the following static acquisition in order to maximise tumour to background ratio **(Figure 44B)**.

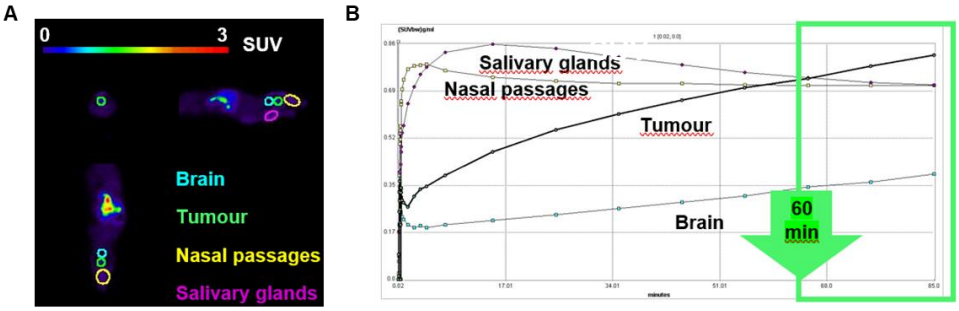

Figure 44: Dynamic PET.
A*: 90 minutes-PET on a representative tumour bearing mouse.* ^{18}*F-Fluciclovine PET has been done 16 days after cell stereotaxical injection. Radiotracer has been injected i.v. when PET acquisition started. Activity measurement was carried out in different Regions of Interest (ROIs): Healthy brain (blue), Tumour (green), Nasal passages (yellow), Salivary glands (purple), Liver (the region of interest is chosen at the bottom lobe of the liver for consistency).* ***B:*** *Time activity curves showing radionuclide uptake in different ROIs. Tumour uptake (green line) was higher than that of other organs from 60 minutes after injection (green square). Data are expressed in SUV.*

Static PET acquisitions started 60 minutes after ^{18}F-fluciclovine injection in both negative control and tumour bearing mice. SUV has been measured in different ROIs and averages of ratios between each tissue SUV Max and the respective liver SUV Max, have been reported **(Figure 45)**. Maximum intensity projection images has shown the ability to identify tumour volume in tumour bearing mice by ^{18}F-Fluciclovine uptake while no specific uptake in the brain has not been found in negative control animals. A high uptake of the tracer was detected in the liver, as expected because of tracer metabolism **(Figure 45A and C)**. SUV Max quantification and normalization on liver SUV Max showed that tumours are characterized by a specific higher uptake of this tracer compared with all the other organs **(Figure**

45B). The evaluation of tumour-to-brain ratio demonstrated the possibility to discriminate the tumour from normal brain, being statistically different **(Figure 45D)**.

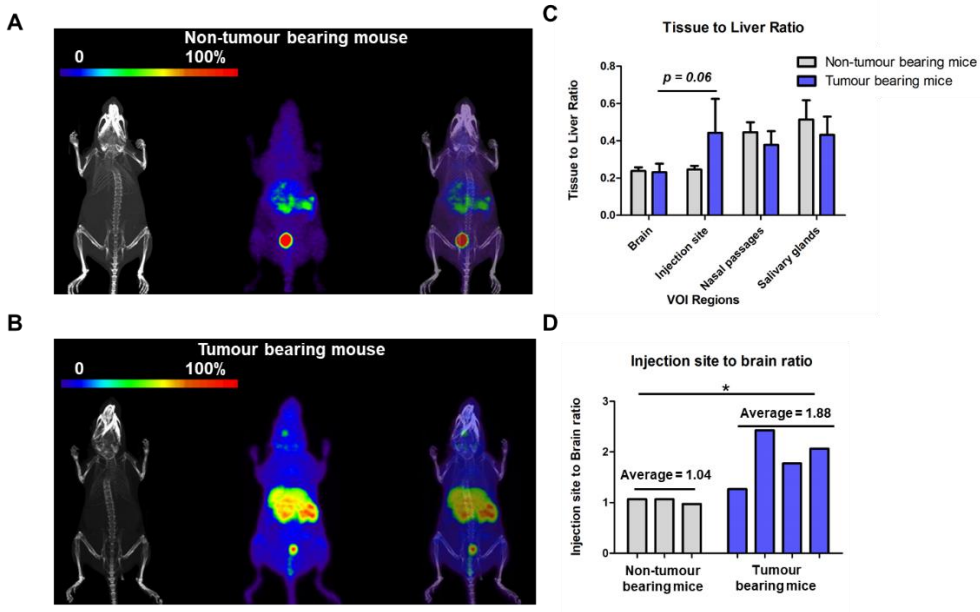

Figure 45: Static PET scans performed on non-tumour and tumour bearing mice.
Acquisition started 60 minutes after 18F-Fluciclovine injection. Acquisition included Static PET (20 minutes) and a CT (10 minutes). Images are expressed in Maximum Intensity Projection (MIP). ***A****: MIP for non-tumour bearing mouse.* ***B:*** *MIP for tumour bearing mouse.* ***C:*** *Maximum Standardized Uptake Value (SUV Max) in different ROIs for tumour bearing mice. Each SUV max has been normalised with the respective liver SUV Max.* ***D****: Ratios between the SUV Max measured at the injection site both in control and in tumour bearing mice and the respective SUV Max measured in normal brain. *p < 0.05 tumour bearing mice vs non-tumour bearing mice.*

2.3 Preliminary results about the IHC

From preliminary results of IHC of untreated vs RT-treated mice brains, the amino acid transporter ASCT-2 staining seemed to reveal,

at tumour bulk area, a higher cellularity levels in untreated mice brains compared to those ones RT-treated. Representative IHC data of untreated and treated mice brains are shown in **Figure 46**.

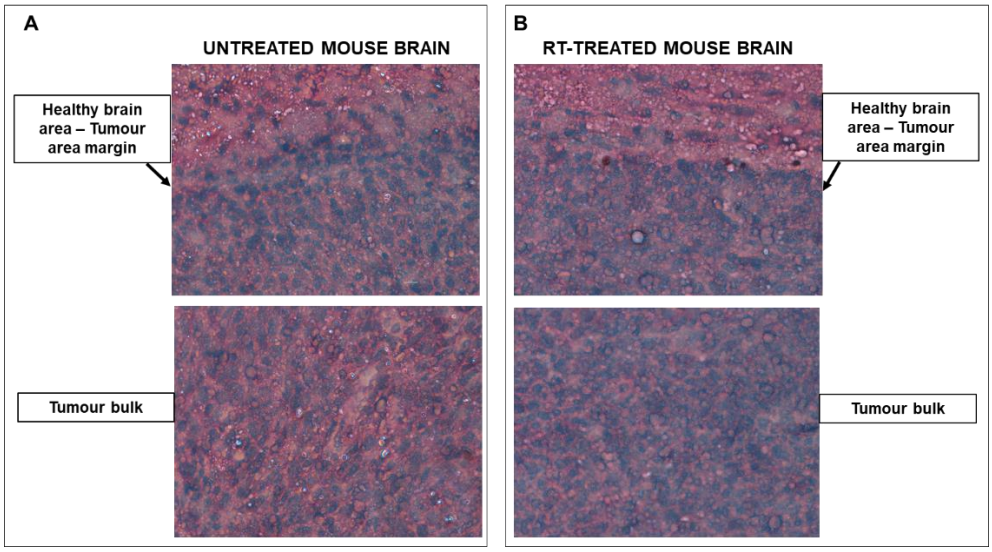

Figure 46: Representative IHC data on ASCT-2 staining of untreated and treated mice brains.
A: *IHC staining for ASCT-2 in representative untreated mouse brain.* ***B:*** *IHC staining for ASCT-2 in representative RT-treated mouse brain.*

DISCUSSION

Up to date, TMZ is the reference drug used in GBM patients in combination with radiotherapy [31]. The development of resistance is still a challenge since there are no equally valid alternative therapies [8]. In this thesis work, different GBM cell lines have been characterised in order to elucidate molecular mechanisms related to their responsiveness or resistance to TMZ. Main aim, in fact, has been the definition of a mechanism which was useful to modulate a switch of resistant cells toward a “sensitive-like” GBM phenotype. O6-MethylGuanine Methyl-Transferase promoter methylation has been considered as the key prognostic factor in GBM patients handling [58], but, not necessarily this situation has been always confirmed: indeed, in different cases, MGMT-methylated cells resulted to be resistant to TMZ-treatment and, instead, low MGMT methylated ones resulted to be sensitive to the alkylating agent [197,198]. Thus, there is the need of identifying new predictive biomarkers, to foresee GBM responsiveness to TMZ with higher reliability. A different TMZ-response between two human GBM cell lines, the U251 cells and the T98 ones, respectively TMZ-sensitive and TMZ-resistant, has been observed, both in normoxia and hypoxia. The higher resistance to TMZ in hypoxic conditions, led us to focus on the role of HIF-1α, the main character conducing cell response to hypoxia. Results showed that HIF-1α expression and activity were in relation to cell responsiveness to TMZ: in fact, we confirmed the early reduction of both its expression and activity specifically observed only in sensitive cells, as already reported in literature [76,199]. Through apoptosis-related gene expression profile evaluation, after TMZ treatment, in normoxia a

reciprocal expression pattern in TMZ-responsive and -resistant ones has been observed; on the other hand, hypoxia seemed to produce an anti-apoptotic profile also in sensitive cells. This pattern is similar to the one observed in T98 cells after TMZ treatment both in normoxia and in hypoxia. This data allowed to propose not only HIF-1α as an early biomarker of tumour response to TMZ treatment [199], but it also elicited a new interest about HIF-1α related mechanisms potentially accountable for GBM resistance to TMZ.

Since it is well known that temozolomide is capable of inducing autophagy and HIF-1α is a target protein for a specific kind of autophagy called Chaperone mediated autophagy (CMA) [86,87], we have wondered if CMA itself might be the key-mechanism which regulates responsiveness to TMZ. This molecular mechanism has three different steps, whose impairment might result in an alteration of the activity. The first potential alteration could involve the activity and availability of the carrier proteins which bind target proteins exposing KFERQ-like motif, as HSC70 and other related proteins, vehiculating them to the lysosomal compartment. The second control step includes LAMP-2A expression and activity, since LAMP-2A role consists in the translocation of CMA target proteins within the lysosomes [85]. The third target accountable for a modulation of CMA is represented by PHLPP1, a phosphatase responsible for the direct regulation of CMA [88]. The expression of the genes encoding these proteins resulted to differentiate sensitive and resistant cells after TMZ treatment [200]. Sensitive cells show an overexpression of all the CMA-related genes while in resistant cells TMZ treatment reduced their expression. These

results confirmed the involvement of CMA in responsiveness to TMZ. CMA selective induction in sensitive cells has been confirmed by Western Blot analyses showing a statistically significant increase in LAMP-2A and HSC70 level after treatment with TMZ. In detail, only in U251 sensitive cells this increase is specific for the lysosomal fraction and involved also an already described CMA protein target, GAPDH confirming also the activation of this mechanism. Silencing experiments demonstrated that the lack of even one of the three CMA-players would result in the abrogation of the entire CMA mechanism. In fact, we have demonstrated that the silencing of *HSC70*, *PHLPP1* or *LAMP-2A* is sufficient for abrogating CMA activity, driving U251 sensitive cells toward a “resistant-like” behaviour. Notably, *PHLPP1* silencing not only was able to impair CMA activity but induced also a negative regulation of both *LAMP-2A* and *HSC70* expression even after treatment with TMZ demonstrating its important regulatory role. These results confirmed the importance of CMA in GBM responsiveness to TMZ. On the other hand, in T98-resistant cells, CMA-related genes silencing has not brought any changes in responsiveness to TMZ; however, by the molecular side, *PHLPP1* silencing resulted in an overexpression of *HSC70,* probably due to the correspondent activation of a phosphorylation-dependent pathway which plays in *HSC70* modulation, but further investigations of the whole mechanism need to be carried out. On the other hand, *LAMP-2A* silencing abrogated the TMZ dependent HIF-1α down-regulation in U251 and was crucial in their switch, as regards apoptosis-related and EMT-related genes expression profile, after TMZ treatment toward a

“resistant-like” phenotype. CMA gene silencing in T98 did not provide any change in comparison to controls even after TMZ treatment. The only change was observed in the *HIF-1α* expression in *LAMP-2A* silenced cells after TMZ treatment. In fact, TMZ did not increase *HIF-1α* expression level which remained at the control level. The same results were observed for EMT-related genes in the same condition and will need further studies going beyond the aim of this work.

As for CMA-related genes, *HIF-1α* silencing has been accomplished [199], and showed important results being able to revert T98 resistant phenotype to a sensitive one, both for cell viability, HIF-1α activity and apoptosis-related gene expression pattern, demonstrating once again the pivotal role covered by this transcription factor which acts as switch between cell survival and cell death after TMZ treatment. Of note, the PX-478-mediated pharmacological inhibition of HIF-1α has confirmed the possibility of a pharmacological modulation driving TMZ responsiveness in resistant cells.

Since the importance of CMA activity in mediating GBM responsiveness to TMZ, we focused our attention on the mechanisms involved in its activation such as oxidative stress. CMA, as reported from literature, is an important oxidative stress sensor, because it is involved in removing proteins which have been modified and damaged by ROS activity into the cells and this process hugely contributes to cell homeostasis modulation, by specific proteins selective degradation [78–80]; of note, LAMP-2A and HSC70, the two CMA key-players, result to be up-regulated under oxidative stress [201]. In this work, a different cytoplasmic ROS content between sensitive and

resistant cells has been detected and reported, which is in relation to the different cell responsiveness to TMZ treatment and, as well, to CMA activity regulation. In detail, U251 TMZ-sensitive cells showed an increase in intracellular ROS after TMZ treatment while T98 resistant cells did not. The investigation on the role of the released ROS has demonstrated that ROS augmentation is strictly dependent to their mitochondrial release: in fact, MitoT (the mitochondrial ROS scavenger) exploitation abrogated their release in both cell lines. Moreover, the concurrent treatment of GBM cells with MitoT and TMZ, avoided the increase in cytoplasmic ROS in U251 sensitive cells and at the same time abrogated also cell cytotoxicity due to the drug. Further investigations will be accomplished in order to analyse in depth all those processes involved in this scenario: in fact, mitochondria, beyond to be an important cell ROS source, are key mediators of oxidative metabolism as well, and are even implicated in the apoptotic switch [202]. In the same sensitive cells (U251), MitoT treatment avoided TMZ-mediated reduction of HIF-1α activity and prevent the increase of pro-apoptotic gene expression after treatment. As regards CMA, mitochondrial ROS scavenger reverted TMZ-mediated expression pattern of the CMA-related genes both as single treatment and after TMZ treatment in U251 cells. Even in T98 cells, MitoT containing treatment induced a decrease in CMA related gene expression confirming the importance of ROS fluctuation for their expression. In line with these molecular results, also HIF-1α expression and activity and, as well, *VEGF* expression level have been modified by MitoT to a reciprocal modulation compared to that of

control cells sensitive to TMZ. Once again, HIF-1α activity and, in this example, *VEGF* transcript levels, might have been proposed as biomarkers for CMA activity determination and sensitivity to TMZ treatment. The absence of ROS fluctuation after TMZ treatment in U251 cells induced also a modification in EMT gene expression, changing the profile from an epithelial one to a mesenchymal one, confirming once more the crucial role of this ROS-related mechanism [83,91].

In this work, we have tried to elucidate all those mechanisms rounding cytoplasmic ROS increase after TMZ treatment; as we already mentioned, mitochondrial respiratory chain is the main ROS source, although cells have devised different processes to neutralise their intracellular damaging effect [92,99,100]. Through our data, we have been able to show that differences between U251 sensitive cells and the T98 resistant ones in ROS steady state level are related to an OXPHOS different activity, but that ROS increase after TMZ is not due to a to transitory change in OXPHOS activity. Neither OXPHOS complexes stability resulted to be altered by alkylating agent treatment and it is not accountable for the increase in ROS release due to TMZ treatment. In different studies, chemotherapy resistance has been put in relation to the cellular anti-oxidant machinery [102], even in GBM context, and, associated to this notion, Glutathione Reductase, Catalase and SOD-2 activation were evaluated and resulted to be higher in T98 cell line, supplying their contribution in mediating drug therapy resistance. A ROS detoxification machinery gene expression profile (*GSH, GSS, GPX, CATALASE, SOD-2*) confirmed the

differential involvement of this detox system between the two types of cell lines.

Associated to the crucial role of this detox machinery in therapy resistance, several approaches for lowering this machinery activity have been reported in literature, as well as lots of treatments with the power, on the contrary, to augment oxidative stress in tumour cells (as, for instance, for Stupp protocol) [31,203]. In this work, an exogenously-derived oxidative stress has been performed, to understand if an exogenously induced ROS fluctuation was able to activate the same pathways induced by TMZ-mediated ROS release in U251 cells and if it could be able to overcome detox systems activity in T98 ones. Hydrogen peroxide, H_2O_2, has been used for the chemically induced oxidative stress and a careful dose-response analysis, whose results have not been reported for better recapitulating this work, has been carried out; a 200 µM, named “mild”, and a 1 mM, defined “high”, concentrations have been chosen. In literature, several works have reported different doses of H_2O_2 administered in glioma cell lines [204–206]: in particular, it seems that doses up to 200 µM did not significantly affect cell viability [207,208]. In a study of Zhang et al., it has been shown that treatment with H_2O_2 at a high dose (1 mM) for 24 hours had the power to halve cell viability in U251 cell line, similarly to what occurred in cell viability assays in U251 cells treated with TMZ after 24 hours [208]. For this reason, we moved on with our analyses not only to confirm data reported in the Zhang’s work but also to evaluate a potential synergic effect due to the combination of H_2O_2 and TMZ administration in U251 e T98 cell lines.

Of note, H_2O_2 “high” dose had the power to activate, both as single treatment and in combination with TMZ, a pro-apoptotic expression pattern, to induce CMA-related gene expression, to reduce HIF-1α activity and to allow an epithelial-like expression profile in TMZ-sensitive cells, as it occurred after TMZ treatment. For what concerns T98 resistant cell line, beyond the fact that “high” dose had the effect to decrease cell viability and induce pro-apoptotic gene expression, it had the capacity to upregulate also CMA gene expression and an epithelial-like profile of expression in EMT expression pattern. Notably, only H_2O_2 “high” dose in combination with TMZ was able to completely induce a sensitive-like expression pattern both in CMA related and EMT-related gene expression confirming TMZ as a reference drug for GBM treatment but only in combination with ROS level fluctuation. In summary, all these results put in light the increase in oxidative stress associated to TMZ treatment, as a fundamental step for activating CMA pathway, for down-modulating HIF-1α activity and, thereby, to allow TMZ to exert its toxic effect.

The evaluation of such a combined treatment in an orthotopic model could help in improving new therapeutic approaches for resistant GBM. To set up this *in vivo* model, resistant cells already used for *in vitro* studies cannot be used since it has already been described that human T98 cells do not growth, after intracranial (i.c.) implantation, in murine models [196]. Thus, murine CT-2A cell line, which contrarily can be used for the production of orthotopic models [209], has been chosen in order to validate it as an *in vivo* model to assess the efficacy of ROS inducing treatments. *In vitro* CT-2A cell characterization

showed that these murine cells emulated the same response trend observed in T98 cells, both in cell viability and in HIF-1α activity after TMZ, different doses of H_2O_2 and in combined treatments, clearly confirming their resistant character. Moreover, *Hif-1α* silencing, as already reported for human GBM cell lines, was able to revert CT-2A resistant cells to a “sensitive-like” behaviour, supporting, even for the murine cells, the HIF-1α key role in mediating TMZ-responsiveness.

CT-2A were used for the establishment of a TMZ-resistant murine orthotopic model. These experiments were performed during my stage at the University of Leeds in UK, where a fully equipped facility for non-invasive imaging and radiotherapy for small animals is available.

CT-2A cells were stereotaxically injected in syngeneic immune-competent mice and tumour growth was monitored by MRI at different times after cell injection. Tumour growth rate was reproducible showing a good linearity during the considered time period.

RT treatment showed that these tumours were sensitive to RT, as expected by *in vitro* tests after oxidative stress. Mice treated with 3 fractions (5Gy each) had a statistically longer survival compared to untreated controls, confirming responsiveness to this oxidative stress inducing treatment. These results were confirmed by the reduction of tumour mass in treated mice, as detected by MRI.

With the aim of identifying an imaging strategy able to describe the biological modifications occurring after treatment to responsive tumours, ^{18}F-Fluciclovine-based PET imaging has been selected. In fact, it is strictly involved with primary GBM metabolism, that is, in turn, modulated by CMA activity.

This tracer is internalised by the cells in relation to the transport rate of specific amino acids, such as glutamine, through ASCT2 transporter [210,211]. This tracer has been already described for its ability in delineating tumour volume in GBM [182] but no data are available about its ability in reporting also GBM response to treatments.

Preliminary results showed interestingly that RT was able to downregulate the expression of ASCT2 transporter as shown in IHC images. For this reason, we started implementing, in collaboration with ePIC imaging centre of the University of Leeds and the Blue Earth Diagnostics, the ^{18}F-Fluciclovine producing company, a protocol for GBM non-invasive monitoring by PET with this tracer, in order to follow ASCT2 expression and activity *in vivo*, as a biomarker of responsiveness to an oxidative treatment able to non-invasively and repetitively describe biological and functional GBM features related to a specific metabolism.

Herein, I have described the setting up of this imaging procedure by a first dynamic study of tracer biodistribution and localisation and a consecutive static analysis of tracer uptake by un-treated tumours. Results are encouraging since there is a statistically significant difference in the tumour to brain ratio in tumour bearing mice with a low background in controls and in surrounding tissues.

Further studies will be performed in the next future to assess GBM response to radio- and radio-chemotherapies using CT-2A orthotopic model and ^{18}F-Fluciclovine.

CONCLUSIONS

In this research project, in conclusion, the findings have demonstrated the crucial role played by HIF-1α activity in supporting TMZ resistance, the importance of CMA activity in determining HIF-1α negative modulation after TMZ treatment. In fact, since HIF-1α can be degraded by Chaperone-Mediated Autophagy and TMZ induces autophagy, a relation between HIF-1α activity decrease, CMA activation and responsiveness to TMZ has been hypothesised. Through CMA-related (*LAMP-2A, HSC70, PHLLP1*) gene expression profile and Western Blot analyses, it has been demonstrated a pivotal CMA engagement in TMZ responsive cells. Moreover, this result has been confirmed by means of the gene silencing of CMA key-factors, *LAMP-2A, HSC70* and *PHLPP1*. The absence of even one of these proteins induced resistance in cells which were previously sensitive to TMZ, confirming CMA crucial role in mediating responsiveness to the alkylating agent. On the contrary, *HIF-1α* gene silencing reverted T98 phenotype from a previously resistant to a sensitive one, allowing TMZ to exert its cytotoxic effect even on these cells. Here it has been demonstrated also that PX-478 mediated pharmacological inhibition of HIF-1α activity is able to revert resistance to TMZ. Sensitivity and resistance to treatment have been identified by specific expression patterns of both apoptosis-, CMA- and EMT-related genes as well as by the kinetic of scratch closure. CMA induction can be activated by an increase of ROS cytoplasmic levels. In fact, responsiveness to TMZ is associated to a ROS release from the mitochondria resulting in a transitory increase of their cytoplasmic level and inducing CMA. The lack of this transitory increase was able to induce resistance to treatment in

previously sensitive cells. In the same way, the exogenous H_2O_2-mediated increase in intracellular ROS levels has been able to restore not only CMA activation, but even a completely responsive profile in resistant cells. Transition from sensitivity to resistance and from resistance to sensitivity have been accompanied by parallel changes in gene expression pattern similar to those already reported. From these results, it is possible to assert that TMZ drives the burst of mitochondrial ROS in sensitive cells driving cell responsiveness, moreover the increase of ROS is crucial for CMA activation and then responsiveness. As regards *in vivo* results, data reported herein demonstrate that CT-2A derived orthotopic tumour bearing mice represent a good model of TMZ resistant tumours for the assessment of new treatments aimed at reverting resistance to TMZ, for example they resulted to be radio-responsive. Further assessment of new treatments will be helped by the use of a multimodal non-invasive imaging procedure based on the use of MRI and PET with ^{18}F-fluciclovine. In fact, ^{18}F-fluciclovine has revealed to be a good radiotracer able to delineate tumour mass, consistently to tumours observed through MRI scans. Finally, preliminary IHC data of untreated and RT-treated mice brains have shown a decreased ASCT2 expression in RT-treated samples compared to the untreated controls. This finding provided a first molecular clue of a potential connection between CMA and the activity of this transporter, leading to new potential relations between CMA itself and tumour cell metabolism.

As future perspectives:

- New methods are needed to better characterize GBM by non-invasive functional imaging strategies. Mechanism underlying ^{18}F-Fluciclovine uptake will be studied to analyse if it could be in relation to CMA activity;
- New therapeutic approaches will be tested in the orthotopic resistant model to evaluate the ability to overcome resistance by inhibiting HIF-1α or inducing CMA activity;
- The importance of CMA will be studied also in relation to cell metabolism and the level of already identified miRNAs [212].

BIBLIOGRAPHY

[1] Wesseling P, Capper D. WHO 2016 Classification of gliomas. Neuropathol Appl Neurobiol 2018;44:139–50. doi:10.1111/nan.12432.

[2] Wood MD, Halfpenny AM, Moore SR. Applications of molecular neuro-oncology - a review of diffuse glioma integrated diagnosis and emerging molecular entities. Diagn Pathol 2019;14:29. doi:10.1186/s13000-019-0802-8.

[3] Iranifar E, Seresht BM, Momeni F, Fadaei E, Mehr MH, Ebrahimi Z, et al. Exosomes and microRNAs: New potential therapeutic candidates in Alzheimer disease therapy. J Cell Physiol 2019;234:2296–305. doi:10.1002/jcp.27214.

[4] Labreche K, Kinnersley B, Berzero G, Di Stefano AL, Rahimian A, Detrait I, et al. Diffuse gliomas classified by 1p/19q co-deletion, TERT promoter and IDH mutation status are associated with specific genetic risk loci. Acta Neuropathol 2018;135:743–55. doi:10.1007/s00401-018-1825-z.

[5] Forst DA, Nahed B V, Loeffler JS, Batchelor TT. Low-grade gliomas. Oncologist 2014;19:403–13. doi:10.1634/theoncologist.2013-0345.

[6] Sim H-W, Morgan ER, Mason WP. Contemporary management of high-grade gliomas. CNS Oncol 2018;7:51–65. doi:10.2217/cns-2017-0026.

[7] JIAPAER S, FURUTA T, TANAKA S, KITABAYASHI T, NAKADA M. Potential Strategies Overcoming the Temozolomide Resistance for Glioblastoma. Neurol Med Chir (Tokyo) 2018;58:405–21. doi:10.2176/nmc.ra.2018-0141.

[8] Thakkar JP, Dolecek TA, Horbinski C, Ostrom QT, Lightner DD, Barnholtz-Sloan JS, et al. Epidemiologic and Molecular Prognostic Review of Glioblastoma. Cancer Epidemiol Biomarkers Prev 2014;23:1985. doi:10.1158/1055-9965.EPI-14-0275.

[9] De Vleeschouwer S, Bergers G. Glioblastoma: To Target the Tumor Cell or the Microenvironment? 2017.

[10] Vescovi AL, Galli R, Reynolds BA. Brain tumour stem cells. Nat Rev Cancer 2006;6:425–36. doi:10.1038/nrc1889.

[11] Hambardzumyan D, Bergers G. Glioblastoma: Defining Tumor Niches. Trends in Cancer 2015;1:252–65. doi:10.1016/j.trecan.2015.10.009.

[12] Virga J, Szivos L, Hortobágyi T, Chalsaraei MK, Zahuczky G, Steiner

L, et al. Extracellular matrix differences in glioblastoma patients with different prognoses. Oncol Lett 2019;17:797–806. doi:10.3892/ol.2018.9649.

[13] Schiffer D, Annovazzi L, Casalone C, Corona C, Mellai M. Glioblastoma: Microenvironment and Niche Concept. Cancers (Basel) 2018;11:5. doi:10.3390/cancers11010005.

[14] Harder BG, Blomquist MR, Wang J, Kim AJ, Woodworth GF, Winkles JA, et al. Developments in Blood-Brain Barrier Penetrance and Drug Repurposing for Improved Treatment of Glioblastoma. Front Oncol 2018;8:462. doi:10.3389/fonc.2018.00462.

[15] Motz GT, Coukos G. Deciphering and reversing tumor immune suppression. Immunity 2013;39:61–73. doi:10.1016/j.immuni.2013.07.005.

[16] Watkins S, Robel S, Kimbrough IF, Robert SM, Ellis-Davies G, Sontheimer H. Disruption of astrocyte–vascular coupling and the blood–brain barrier by invading glioma cells. Nat Commun 2014;5:4196. doi:10.1038/ncomms5196.

[17] Edwards LA, Woolard K, Son MJ, Li A, Lee J, Ene C, et al. Effect of Brain- and Tumor-Derived Connective Tissue Growth Factor on Glioma Invasion. JNCI J Natl Cancer Inst 2011;103:1162–78. doi:10.1093/jnci/djr224.

[18] Du L, Tang J-H, Huang G-H, Xiang Y, Lv S-Q. The progression of epithelial-mesenchymal transformation in gliomas. Chinese Neurosurg J 2017;3:23. doi:10.1186/s41016-017-0086-3.

[19] Warth A, Simon P, Capper D, Goeppert B, Tabatabai G, Herzog H, et al. Expression pattern of the water channel aquaporin-4 in human gliomas is associated with blood–brain barrier disturbance but not with patient survival. J Neurosci Res 2007;85:1336–46. doi:10.1002/jnr.21224.

[20] Gérard M, Corroyer-Dulmont A, Lesueur P, Collet S, Chérel M, Bourgeois M, et al. Hypoxia Imaging and Adaptive Radiotherapy: A State-of-the-Art Approach in the Management of Glioma. Front Med 2019;6:117. doi:10.3389/fmed.2019.00117.

[21] Leblond MM, Gérault AN, Corroyer-Dulmont A, MacKenzie ET, Petit E, Bernaudin M, et al. Hypoxia induces macrophage polarization and re-education toward an M2 phenotype in U87 and U251 glioblastoma models. Oncoimmunology 2016;5:e1056442.

doi:10.1080/2162402X.2015.1056442.

[22] Nigim F, Cavanaugh J, Patel AP, Curry WT, Esaki S, Kasper EM, et al. Targeting Hypoxia-Inducible Factor 1α in a New Orthotopic Model of Glioblastoma Recapitulating the Hypoxic Tumor Microenvironment. J Neuropathol Exp Neurol 2015;74:710–22. doi:10.1097/NEN.0000000000000210.

[23] Ramis G, Villalonga-Planells R, Serra-Sitjar M, Brell M, Fernández de Mattos S, Villalonga P. The tumor suppressor FOXO3a mediates the response to EGFR inhibition in glioblastoma cells. Cell Oncol 2019;42:521–36. doi:10.1007/s13402-019-00443-1.

[24] Neilsen BK, Sleightholm R, McComb R, Ramkissoon SH, Ross JS, Corona RJ, et al. Comprehensive genetic alteration profiling in primary and recurrent glioblastoma. J Neurooncol 2019;142:111–8. doi:10.1007/s11060-018-03070-2.

[25] Zhang Y, Dube C, Gibert M, Cruickshanks N, Wang B, Coughlan M, et al. The p53 Pathway in Glioblastoma. Cancers (Basel) 2018;10:297. doi:10.3390/cancers10090297.

[26] The Cancer Genome Atlas Program - National Cancer Institute n.d. https://www.cancer.gov/about-nci/organization/ccg/research/structural-genomics/tcga (accessed October 8, 2019).

[27] Zhou X-Y, Liu H, Ding Z-B, Xi H-P, Wang G-W. lncRNA SNHG16 Exerts Oncogenic Functions in Promoting Proliferation of Glioma Through Suppressing p21. Pathol Oncol Res 2019:1–8. doi:10.1007/s12253-019-00648-7.

[28] Xu H, Zong H, Ma C, Ming X, Shang M, Li K, et al. Epidermal growth factor receptor in glioblastoma. Oncol Lett 2017;14:512–6. doi:10.3892/ol.2017.6221.

[29] Colebatch AJ, Dobrovic A, Cooper WA. *TERT* gene: its function and dysregulation in cancer. J Clin Pathol 2019;72:281–4. doi:10.1136/jclinpath-2018-205653.

[30] Gong Y, Dong Y, Cui J, Sun Q, Zhen Z, Gao Y, et al. Receptor Tyrosine Kinase Interaction with the Tumor Microenvironment in Malignant Progression of Human Glioblastoma. Glioma - Contemp. Diagnostic Ther. Approaches, IntechOpen; 2019. doi:10.5772/intechopen.76873.

[31] Stupp R, Mason WP, van den Bent MJ, Weller M, Fisher B, Taphoorn

MJB, et al. Radiotherapy plus Concomitant and Adjuvant Temozolomide for Glioblastoma. N Engl J Med 2005;352:987–96. doi:10.1056/NEJMoa043330.

[32] Lanzetta G, Campanella C, Rozzi A, Nappa M, Costa A, Fedele F, et al. Temozolomide in radio-chemotherapy combined treatment for newly-diagnosed glioblastoma multiforme: phase II clinical trial. Anticancer Res n.d.;23:5159–64.

[33] Han X, Xue X, Zhou H, Zhang G, Han X, Xue X, et al. A molecular view of the radioresistance of gliomas. Oncotarget 2017;8:100931–41. doi:10.18632/oncotarget.21753.

[34] Strickland M, Stoll EA. Metabolic Reprogramming in Glioma. Front Cell Dev Biol 2017;5:43. doi:10.3389/fcell.2017.00043.

[35] Wanandi SI, Hardiany NS, Siregar NC, Sadikin M. SUPPRESSION OF MANGANESE SUPEROXIDE DISMUTASE ACTIVITY IN ROTENONE-TREATED HUMAN GLIOBLASTOMA T98G CELLS REDUCES CELL VIABILITY. Asian J Pharm Clin Res 2018;11:48. doi:10.22159/ajpcr.2018.v11i1.19777.

[36] Datta K, Babbar P, Srivastava T, Sinha S, Chattopadhyay P. p53 dependent apoptosis in glioma cell lines in response to hydrogen peroxide induced oxidative stress. Int J Biochem Cell Biol 2002;34:148–57. doi:10.1016/S1357-2725(01)00106-6.

[37] Nita M, Grzybowski A. The Role of the Reactive Oxygen Species and Oxidative Stress in the Pathomechanism of the Age-Related Ocular Diseases and Other Pathologies of the Anterior and Posterior Eye Segments in Adults. Oxid Med Cell Longev 2016;2016:1–23. doi:10.1155/2016/3164734.

[38] Groussard C, Morel I, Chevanne M, Monnier M, Cillard J, Delamarche A. Free radical scavenging and antioxidant effects of lactate ion: an in vitro study. Https://DoiOrg/101152/Jappl2000891169 2000. doi:10.1152/JAPPL.2000.89.1.169.

[39] Frontiñán-Rubio J, Santiago-Mora RM, Nieva-Velasco CM, Ferrín G, Martínez-González A, Gómez MV, et al. Regulation of the oxidative balance with coenzyme Q10 sensitizes human glioblastoma cells to radiation and temozolomide. Radiother Oncol 2018;128:236–44. doi:10.1016/j.radonc.2018.04.033.

[40] Schulz A, Meyer F, Dubrovska A, Borgmann K. Cancer Stem Cells and Radioresistance: DNA Repair and Beyond. Cancers (Basel)

2019;11:862. doi:10.3390/cancers11060862.

[41] Wang J, Wang H, Qian H. Biological effects of radiation on cancer cells. Mil Med Res 2018;5:20. doi:10.1186/s40779-018-0167-4.

[42] Mann J, Ramakrishna R, Magge R, Wernicke AG. Advances in Radiotherapy for Glioblastoma. Front Neurol 2018;8:748. doi:10.3389/fneur.2017.00748.

[43] Chang EL, Brown PD, Lo SS, Sahgal A, Suh JH, editors. Adult CNS Radiation Oncology. Cham: Springer International Publishing; 2018. doi:10.1007/978-3-319-42878-9.

[44] Pauwels EKJ, McCready VR, Stoot JHMB, van Deurzen DFP. The mechanism of accumulation of tumour-localising radiopharmaceuticals. Eur J Nucl Med Mol Imaging 1998;25:277–305. doi:10.1007/s002590050229.

[45] Stevens MF, Hickman JA, Langdon SP, Chubb D, Vickers L, Stone R, et al. Antitumor activity and pharmacokinetics in mice of 8-carbamoyl-3-methyl-imidazo[5,1-d]-1,2,3,5-tetrazin-4(3H)-one (CCRG 81045; M & B 39831), a novel drug with potential as an alternative to dacarbazine. Cancer Res 1987;47:5846–52.

[46] Zhu P, Du XL, Lu G, Zhu J-J. Survival benefit of glioblastoma patients after FDA approval of temozolomide concomitant with radiation and bevacizumab: A population-based study. Oncotarget 2017;8:44015–31. doi:10.18632/oncotarget.17054.

[47] Arora A, Somasundaram K. Glioblastoma vs temozolomide: can the red queen race be won? Cancer Biol Ther 2019;20:1083–90. doi:10.1080/15384047.2019.1599662.

[48] Lee SY. Temozolomide resistance in glioblastoma multiforme. Genes Dis 2016;3:198–210. doi:10.1016/J.GENDIS.2016.04.007.

[49] Akgül S, Patch AM, D'souza RCJ, Mukhopadhyay P, Nones K, Kempe S, et al. Intratumoural heterogeneity underlies distinct therapy responses and treatment resistance in glioblastoma. Cancers (Basel) 2019;11. doi:10.3390/cancers11020190.

[50] Köhler T, Schill C, Deininger M, Krahl R, Borchert S, Hasenclever D, et al. High Bad and Bax mRNA expression correlate with negative outcome in acute myeloid leukemia (AML). Leukemia 2002;16:22–9. doi:10.1038/sj.leu.2402340.

[51] Pattingre S, Tassa A, Qu X, Garuti R, Liang XH, Mizushima N, et al.

Bcl-2 Antiapoptotic Proteins Inhibit Beclin 1-Dependent Autophagy. Cell 2005;122:927–39. doi:10.1016/j.cell.2005.07.002.

[52] Yan Y, Xu Z, Dai S, Qian L, Sun L, Gong Z. Targeting autophagy to sensitive glioma to temozolomide treatment. J Exp Clin Cancer Res 2016;35:23. doi:10.1186/s13046-016-0303-5.

[53] Bahadur S, Sahu AK, Baghel P, Saha S. Current promising treatment strategy for glioblastoma multiform: A review. Oncol Rev 2019;13:417. doi:10.4081/oncol.2019.417.

[54] Kriel J, Müller-Nedebock K, Maarman G, Mbizana S, Ojuka E, Klumperman B, et al. Coordinated autophagy modulation overcomes glioblastoma chemoresistance through disruption of mitochondrial bioenergetics. Sci Rep 2018;8:10348. doi:10.1038/s41598-018-28590-9.

[55] Würstle S, Schneider F, Ringel F, Gempt J, Lämmer F, Delbridge C, et al. Temozolomide induces autophagy in primary and established glioblastoma cells in an EGFR independent manner. Oncol Lett 2017;14:322–8. doi:10.3892/ol.2017.6107.

[56] Zhang J, F.G. Stevens M, D. Bradshaw T. Temozolomide: Mechanisms of Action, Repair and Resistance n.d.

[57] Christmann M, Kaina B. MGMT—a critical DNA repair gene target for chemotherapy resistance. DNA Repair Cancer Ther 2016:55–82. doi:10.1016/B978-0-12-803582-5.00002-4.

[58] Kanazawa T, Minami Y, Jinzaki M, Toda M, Yoshida K, Sasaki H. Predictive markers for MGMT promoter methylation in glioblastomas. Neurosurg Rev 2019:1–10. doi:10.1007/s10143-018-01061-5.

[59] Fan C-H, Liu W-L, Cao H, Wen C, Chen L, Jiang G. O6-methylguanine DNA methyltransferase as a promising target for the treatment of temozolomide-resistant gliomas. Cell Death Dis 2013;4:e876–e876. doi:10.1038/cddis.2013.388.

[60] Shinsato Y, Furukawa T, Yunoue S, Yonezawa H, Minami K, Nishizawa Y, et al. Reduction of MLH1 and PMS2 confers temozolomide resistance and is associated with recurrence of glioblastoma. Oncotarget 2013;4:2261–70. doi:10.18632/oncotarget.1302.

[61] Xie C, Sheng H, Zhang N, Li S, Wei X, Zheng X. Association of MSH6 mutation with glioma susceptibility, drug resistance and progression. Mol Clin Oncol 2016;5:236–40. doi:10.3892/mco.2016.907.

[62] Agnihotri S, Gajadhar AS, Ternamian C, Gorlia T, Diefes KL, Mischel PS, et al. Alkylpurine-DNA-N-glycosylase confers resistance to temozolomide in xenograft models of glioblastoma multiforme and is associated with poor survival in patients. J Clin Invest 2012;122:253–66. doi:10.1172/JCI59334.

[63] Wenger A, Ferreyra Vega S, Kling T, Bontell TO, Jakola AS, Carén H. Intratumor DNA methylation heterogeneity in glioblastoma: implications for DNA methylation-based classification. Neuro Oncol 2019;21:616–27. doi:10.1093/neuonc/noz011.

[64] Hanif F, Muzaffar K, Perveen K, Malhi SM, Simjee SU. Glioblastoma Multiforme: A Review of its Epidemiology and Pathogenesis through Clinical Presentation and Treatment. Asian Pac J Cancer Prev 2017;18:3–9. doi:10.22034/APJCP.2017.18.1.3.

[65] Ge X, Pan MH, Wang L, Li W, Jiang C, He J, et al. Hypoxia-mediated mitochondria apoptosis inhibition induces temozolomide treatment resistance through miR-26a/Bad/Bax axis. Cell Death Dis 2018;9. doi:10.1038/s41419-018-1176-7.

[66] Marampon F, Gravina GL, Zani BM, Popov VM, Fratticci A, Cerasani M, et al. Hypoxia sustains glioblastoma radioresistance through ERKs/DNA-PKcs/HIF- 1α functional interplay. Int J Oncol 2014;45:2121–31. doi:10.3892/ijo.2014.2358.

[67] Vaupel P, Harrison L. Tumor Hypoxia: Causative Factors, Compensatory Mechanisms, and Cellular Response. Oncologist 2004;9:4–9. doi:10.1634/theoncologist.9-90005-4.

[68] Monteiro A, Hill R, Pilkington G, Madureira P. The Role of Hypoxia in Glioblastoma Invasion. Cells 2017;6:45. doi:10.3390/cells6040045.

[69] Chipurupalli S, Kannan E, Tergaonkar V, D'Andrea R, Robinson N, Chipurupalli S, et al. Hypoxia Induced ER Stress Response as an Adaptive Mechanism in Cancer. Int J Mol Sci 2019;20:749. doi:10.3390/ijms20030749.

[70] Liu Z, Semenza GL, Zhang H. Hypoxia-inducible factor 1 and breast cancer metastasis. J Zhejiang Univ B 2015;16:32–43. doi:10.1631/jzus.B1400221.

[71] Iommarini L, Porcelli AM, Gasparre G, Kurelac I. Non-Canonical Mechanisms Regulating Hypoxia-Inducible Factor 1 Alpha in Cancer. Front Oncol 2017;7:286. doi:10.3389/fonc.2017.00286.

[72] Zhang W, Shi X, Peng Y, Wu M, Zhang P, Xie R, et al. HIF-1α

Promotes Epithelial-Mesenchymal Transition and Metastasis through Direct Regulation of ZEB1 in Colorectal Cancer. PLoS One 2015;10:e0129603. doi:10.1371/journal.pone.0129603.

[73] Huang C-H, Yang W-H, Chang S-Y, Tai S-K, Tzeng C-H, Kao J-Y, et al. Regulation of Membrane-Type 4 Matrix Metalloproteinase by SLUG Contributes to Hypoxia-Mediated Metastasis. Neoplasia 2009;11:1371-IN14. doi:10.1593/neo.91326.

[74] IWADATE Y. Epithelial-mesenchymal transition in glioblastoma progression. Oncol Lett 2016;11:1615–20. doi:10.3892/ol.2016.4113.

[75] Nakada M, Nakada S, Demuth T, Tran NL, Hoelzinger DB, Berens ME. Molecular targets of glioma invasion. Cell Mol Life Sci 2007;64:458–78. doi:10.1007/s00018-007-6342-5.

[76] Lo Dico A, Martelli C, Valtorta S, Raccagni I, Diceglie C, Belloli S, et al. Identification of imaging biomarkers for the assessment of tumour response to different treatments in a preclinical glioma model. Eur J Nucl Med Mol Imaging 2015;42:1093–105. doi:10.1007/s00259-015-3040-7.

[77] Belozerov VE, Van Meir EG. Hypoxia inducible factor-1: a novel target for cancer therapy. Anticancer Drugs 2005;16:901–9. doi:10.1097/01.cad.0000180116.85912.69.

[78] Tibes R, Falchook GS, Von Hoff DD, Weiss GJ, Iyengar T, Kurzrock R, et al. Results from a phase I, dose-escalation study of PX-478, an orally available inhibitor of HIF-1α. J Clin Oncol 2010;28:3076–3076. doi:10.1200/jco.2010.28.15_suppl.3076.

[79] Lee K, Kim HM. A novel approach to cancer therapy using PX-478 as a HIF-1α inhibitor. Arch Pharm Res 2011;34:1583–5. doi:10.1007/s12272-011-1021-3.

[80] Bejarano E, Cuervo AM. Chaperone-Mediated Autophagy. Proc Am Thorac Soc 2010;7:29–39. doi:10.1513/pats.200909-102JS.

[81] Parzych KR, Klionsky DJ. An overview of autophagy: morphology, mechanism, and regulation. Antioxid Redox Signal 2014;20:460–73. doi:10.1089/ars.2013.5371.

[82] Antunes F, Erustes A, Costa A, Nascimento A, Bincoletto C, Ureshino R, et al. Autophagy and intermittent fasting: the connection for cancer therapy? Clinics 2018;73:e814s. doi:10.6061/clinics/2018/e814s.

[83] Kiffin R, Christian C, Knecht E, Cuervo AM. Activation of Chaperone-

mediated Autophagy during Oxidative Stress. Mol Biol Cell 2004;15:4829–40. doi:10.1091/mbc.e04-06-0477.

[84] Dewaele M, Maes H, Agostinis P. ROS-mediated mechanisms of autophagy stimulation and their relevance in cancer therapy. Autophagy 2010;6:838–54. doi:10.4161/auto.6.7.12113.

[85] Wu H, Chen S, Ammar A-B, Xu J, Wu Q, Pan K, et al. Crosstalk Between Macroautophagy and Chaperone-Mediated Autophagy: Implications for the Treatment of Neurological Diseases. Mol Neurobiol 2015;52:1284–96. doi:10.1007/s12035-014-8933-0.

[86] Hubbi ME, Hu H, Kshitiz, Ahmed I, Levchenko A, Semenza GL. Chaperone-mediated autophagy targets hypoxia-inducible factor-1α (HIF-1α) for lysosomal degradation. J Biol Chem 2013;288:10703–14. doi:10.1074/jbc.M112.414771.

[87] Vasco Ferreira J, Rosa Soares A, Silva Ramalho J, Pereira P, Girao H. K63 linked ubiquitin chain formation is a signal for HIF1A degradation by Chaperone-Mediated Autophagy. Sci Rep 2015;5:10210. doi:10.1038/srep10210.

[88] Peng M, Wang J, Tian Z, Zhang D, Jin H, Liu C, et al. Autophagy-mediated *Mir6981* degradation exhibits *CDKN1B* promotion of PHLPP1 protein translation. Autophagy 2019;15:1523–38. doi:10.1080/15548627.2019.1586254.

[89] Arias E, Koga H, Diaz A, Mocholi E, Patel B, Cuervo AM. Lysosomal mTORC2/PHLPP1/Akt Regulate Chaperone-Mediated Autophagy. Mol Cell 2015;59:270–84. doi:10.1016/J.MOLCEL.2015.05.030.

[90] Lin C-J, Lee C-C, Shih Y-L, Lin T-Y, Wang S-H, Lin Y-F, et al. Resveratrol enhances the therapeutic effect of temozolomide against malignant glioma in vitro and in vivo by inhibiting autophagy. Free Radic Biol Med 2012;52:377–91. doi:10.1016/j.freeradbiomed.2011.10.487.

[91] He Y, Su J, Lan B, Gao Y, Zhao J. Targeting off-target effects: endoplasmic reticulum stress and autophagy as effective strategies to enhance temozolomide treatment. Onco Targets Ther 2019;Volume 12:1857–65. doi:10.2147/OTT.S194770.

[92] Salazar-Ramiro A, Ramírez-Ortega D, Pérez de la Cruz V, Hérnandez-Pedro NY, González-Esquivel DF, Sotelo J, et al. Role of Redox Status in Development of Glioblastoma. Front Immunol 2016;7:156. doi:10.3389/fimmu.2016.00156.

[93] Burić SS, Podolski-Renić A, Dinić J, Stanković T, Jovanović M, Hadžić S, et al. Modulation of Antioxidant Potential with Coenzyme Q10 Suppressed Invasion of Temozolomide-Resistant Rat Glioma *In Vitro* and *In Vivo*. Oxid Med Cell Longev 2019;2019:1–14. doi:10.1155/2019/3061607.

[94] Ding W, Liu T, Bi X, Zhang Z. Mitochondria-Targeted Antioxidant Mito-Tempo Protects Against Aldosterone-Induced Renal Injury <i>In Vivo</i> Cell Physiol Biochem 2017;44:741–50. doi:10.1159/000485287.

[95] Redza-Dutordoir M, Averill-Bates DA. Activation of apoptosis signalling pathways by reactive oxygen species. Biochim Biophys Acta 2016;1863:2977–92. doi:10.1016/j.bbamcr.2016.09.012.

[96] Aoyama K, Nakaki T. Inhibition of GTRAP3-18 May Increase Neuroprotective Glutathione (GSH) Synthesis. Int J Mol Sci 2012;13:12017–35. doi:10.3390/ijms130912017.

[97] Barbusiński K. Fenton reaction - controversy concerning the chemistry 2009.

[98] Qutub AA, Popel AS. Reactive oxygen species regulate hypoxia-inducible factor 1alpha differentially in cancer and ischemia. Mol Cell Biol 2008;28:5106–19. doi:10.1128/MCB.00060-08.

[99] Kohsaka S, Takahashi K, Wang L, Tanino M, Kimura T, Nishihara H, et al. Inhibition of GSH synthesis potentiates temozolomide-induced bystander effect in glioblastoma. Cancer Lett 2013;331:68–75. doi:10.1016/j.canlet.2012.12.005.

[100] Rocha CRR, Garcia CCM, Vieira DB, Quinet A, de Andrade-Lima LC, Munford V, et al. Glutathione depletion sensitizes cisplatin- and temozolomide-resistant glioma cells in vitro and in vivo. Cell Death Dis 2014;5:e1505–e1505. doi:10.1038/cddis.2014.465.

[101] Payen VL, Zampieri LX, Porporato PE, Sonveaux P. Pro- and antitumor effects of mitochondrial reactive oxygen species. Cancer Metastasis Rev 2019;38:189–203. doi:10.1007/s10555-019-09789-2.

[102] Zhu Z, Du S, Du Y, Ren J, Ying G, Yan Z. Glutathione reductase mediates drug resistance in glioblastoma cells by regulating redox homeostasis. J Neurochem 2018;144:93–104. doi:10.1111/jnc.14250.

[103] Rocha CRR, Kajitani GS, Quinet A, Fortunato RS, Menck CFM, Ribeiro Reily Rocha C, et al. NRF2 and glutathione are key resistance mediators to temozolomide in glioma and melanoma cells. Oncotarget

2016;7:48081–92. doi:10.18632/oncotarget.10129.

[104] Kumar DM, Patil V, Ramachandran B, Nila M V., Dharmalingam K, Somasundaram K. Temozolomide-modulated glioma proteome: Role of interleukin-1 receptor-associated kinase-4 (IRAK4) in chemosensitivity. Proteomics 2013;13:2113–24. doi:10.1002/pmic.201200261.

[105] ATCC: The Global Bioresource Center n.d. https://www.lgcstandards-atcc.org/?geo_country=it (accessed October 8, 2019).

[106] Zhang S, Xie R, Wan F, Ye F, Guo D, Lei T. Identification of U251 glioma stem cells and their heterogeneous stem-like phenotypes. Oncol Lett 2013;6:1649–55. doi:10.3892/ol.2013.1623.

[107] Cakar B, Muslu U, Bozkurt E, Atmaca H, Karaca B, Karabulut B, et al. Angiogenesis inhibition on glioblastoma multiforme cell lines (U-87 MG and T98G) by AT-101. J Oncol Sci 2018;4:65–9. doi:10.1016/J.JONS.2018.06.002.

[108] Oraiopoulou M-E, Tampakaki M, Tzamali E, Tamiolakis T, Makatounakis V, Vakis AF, et al. A 3D tumor spheroid model for the T98G Glioblastoma cell line phenotypic characterization. Tissue Cell 2019;59:39–43. doi:10.1016/J.TICE.2019.05.007.

[109] Kanamori M, Higa T, Sonoda Y, Murakami S, Dodo M, Kitamura H, et al. Activation of the NRF2 pathway and its impact on the prognosis of anaplastic glioma patients. Neuro Oncol 2015;17:555–65. doi:10.1093/neuonc/nou282.

[110] Godoy PRDV, Mello SS, Magalhães DAR, Donaires FS, Nicolucci P, Donadi EA, et al. Ionizing radiation-induced gene expression changes in TP53 proficient and deficient glioblastoma cell lines. Mutat Res Toxicol Environ Mutagen 2013;756:46–55. doi:10.1016/J.MRGENTOX.2013.06.010.

[111] Weller M, Cloughesy T, Perry JR, Wick W. Standards of care for treatment of recurrent glioblastoma—are we there yet? Neuro Oncol 2013;15:4–27. doi:10.1093/neuonc/nos273.

[112] Binello E, Qadeer ZA, Kothari HP, Emdad L, Germano IM. Stemness of the CT-2A Immunocompetent Mouse Brain Tumor Model: Characterization *In Vitro*. J Cancer 2012;3:166–74. doi:10.7150/jca.4149.

[113] Nakashima H, Alayo QA, Penaloza-Macmaster P, Freeman GJ, Kuchroo VK, Reardon DA, et al. Modeling tumor immunity of mouse

glioblastoma by exhausted CD8 + T cells n.d. doi:10.1038/s41598-017-18540-2.

[114] Singh M, Murriel CL, Johnson L. Genetically Engineered Mouse Models: Closing the Gap between Preclinical Data and Trial Outcomes. Cancer Res 2012;72:2695–700. doi:10.1158/0008-5472.CAN-11-2786.

[115] Stylli SS, Luwor RB, Ware TMB, Tan F, Kaye AH. Mouse models of glioma. J Clin Neurosci 2015;22:619–26. doi:10.1016/J.JOCN.2014.10.013.

[116] KIJIMA N, KANEMURA Y. Mouse Models of Glioblastoma. Glioblastoma, Codon Publications; 2017, p. 131–9. doi:10.15586/codon.glioblastoma.2017.ch7.

[117] Li G. Patient-derived xenograft models for oncology drug discovery. J Cancer Metastasis Treat 2015;0:0. doi:10.4103/2394-4722.152769.

[118] Patrizii M, Bartucci M, Pine SR, Sabaawy HE. Utility of glioblastoma patient-derived orthotopic xenografts in drug discovery and personalized therapy. Front Oncol 2018;8. doi:10.3389/fonc.2018.00023.

[119] Johannessen T, Hasan-Olive MM, Zhu H, Denisova O, Grudic A, Latif MA, et al. Thioridazine inhibits autophagy and sensitizes glioblastoma cells to temozolomide. Int J Cancer 2019;144:1735–45. doi:10.1002/ijc.31912.

[120] Lo Dico A, Valtorta S, Ottobrini L, Moresco RM. Role of metformin and AKT axis modulation in the reversion of hypoxia induced TMZ-resistance in glioma cells. Front Oncol 2019;9. doi:10.3389/fonc.2019.00463.

[121] da Hora CC, Schweiger MW, Wurdinger T, Tannous BA. Patient-Derived Glioma Models: From Patients to Dish to Animals. Cells 2019;8:1177. doi:10.3390/cells8101177.

[122] Hambardzumyan D, Parada LF, Holland EC, Charest A. Genetic modeling of gliomas in mice: New tools to tackle old problems. Glia 2011;59:1155–68. doi:10.1002/glia.21142.

[123] Zhao SG, Yu M, Spratt DE, Chang SL, Feng FY, Kim MM, et al. Xenograft-based, platform-independent gene signatures to predict response to alkylating chemotherapy, radiation, and combination therapy for glioblastoma. Neuro Oncol 2019;21:1141–9. doi:10.1093/neuonc/noz090.

[124] Linkous A, Balamatsias D, Snuderl M, Edwards L, Miyaguchi K, Milner T, et al. Modeling Patient-Derived Glioblastoma with Cerebral Organoids. Cell Rep 2019;26:3203-3211.e5. doi:10.1016/j.celrep.2019.02.063.

[125] Pompili L, Porru M, Caruso C, Biroccio A, Leonetti C. Patient-derived xenografts: A relevant preclinical model for drug development. J Exp Clin Cancer Res 2016;35. doi:10.1186/s13046-016-0462-4.

[126] Daniel VC, Marchionni L, Hierman JS, Rhodes JT, Devereux WL, Rudin CM, et al. A primary xenograft model of small-cell lung cancer reveals irreversible changes in gene expression imposed by culture in vitro. Cancer Res 2009;69:3364–73. doi:10.1158/0008-5472.CAN-08-4210.

[127] Miyai M, Tomita H, Soeda A, Yano H, Iwama T, Hara A. Current trends in mouse models of glioblastoma. J Neurooncol 2017;135:423–32. doi:10.1007/s11060-017-2626-2.

[128] Huse JT, Holland EC. Genetically engineered mouse models of brain cancer and the promise of preclinical testing. Brain Pathol., vol. 19, 2009, p. 132–43. doi:10.1111/j.1750-3639.2008.00234.x.

[129] Simeonova I, Huillard E. In vivo models of brain tumors: roles of genetically engineered mouse models in understanding tumor biology and use in preclinical studies. Cell Mol Life Sci 2014;71:4007–26. doi:10.1007/s00018-014-1675-3.

[130] Del Vecchio C, Calistri A, Parolin C, Mucignat-Caretta C. Lentiviral vectors as tools for the study and treatment of glioblastoma. Cancers (Basel) 2019;11. doi:10.3390/cancers11030417.

[131] Oh T, Fakurnejad S, Sayegh ET, Clark AJ, Ivan ME, Sun MZ, et al. Immunocompetent murine models for the study of glioblastoma immunotherapy. J Transl Med 2014;12. doi:10.1186/1479-5876-12-107.

[132] Kim S, Harford JB, Moghe M, Slaughter T, Doherty C, Chang EH. A tumor-targeting nanomedicine carrying the p53 gene crosses the blood–brain barrier and enhances anti-PD-1 immunotherapy in mouse models of glioblastoma. Int J Cancer 2019;145:2535–46. doi:10.1002/ijc.32531.

[133] Yu K, Youshani AS, Wilkinson FL, O'Leary C, Cook P, Laaniste L, et al. A nonmyeloablative chimeric mouse model accurately defines microglia and macrophage contribution in glioma. Neuropathol Appl

Neurobiol 2019;45:119–40. doi:10.1111/nan.12489.

[134] Jacobs VL, Valdes PA, Hickey WF, De Leo JA. Current Review of *in Vivo* GBM Rodent Models: Emphasis on the CNS-1 Tumour Model. ASN Neuro 2011;3:AN20110014. doi:10.1042/AN20110014.

[135] Candolfi M, Curtin JF, Nichols WS, Muhammad AG, King GD, Pluhar GE, et al. Intracranial glioblastoma models in preclinical neuro-oncology: neuropathological characterization and tumor progression. J Neurooncol 2007;85:133–48. doi:10.1007/s11060-007-9400-9.

[136] Massoud TF, Gambhir SS. Molecular imaging in living subjects: seeing fundamental biological processes in a new light. Genes Dev 2003;17:545–80. doi:10.1101/gad.1047403.

[137] Bulte JWM, Kraitchman DL. Iron oxide MR contrast agents for molecular and cellular imaging. NMR Biomed 2004;17:484–99. doi:10.1002/nbm.924.

[138] Lewis JS, Achilefu S, Garbow JR, Laforest R, Welch MJ. Small animal imaging. current technology and perspectives for oncological imaging. Eur J Cancer 2002;38:2173–88. doi:10.1016/s0959-8049(02)00394-5.

[139] Ando Y, Sakurai T, Koida K, Tei H, Hida A, Nakao K, et al. In vivo bioluminescence and reflectance imaging of multiple organs in bioluminescence reporter mice by bundled-fiber-coupled microscopy. Biomed Opt Express 2016;7:963. doi:10.1364/BOE.7.000963.

[140] van Willigen DM, van den Berg NS, Buckle T, KleinJan GH, Hardwick JC, van der Poel HG, et al. Multispectral fluorescence guided surgery; a feasibility study in a phantom using a clinical-grade laparoscopic camera system. Am J Nucl Med Mol Imaging 2017;7:138–47.

[141] Ottobrini L, Ciana P, Biserni A, Lucignani G, Maggi A. Molecular imaging: A new way to study molecular processes in vivo. Mol Cell Endocrinol 2006;246:69–75. doi:10.1016/j.mce.2005.11.013.

[142] Glunde K, Pathak AP, Bhujwalla ZM. Molecular-functional imaging of cancer: to image and imagine. Trends Mol Med 2007;13:287–97. doi:10.1016/j.molmed.2007.05.002.

[143] Lucignani G, Ottobrini L, Martelli C, Rescigno M, Clerici M. Molecular imaging of cell-mediated cancer immunotherapy. Trends Biotechnol 2006;24:410–8. doi:10.1016/j.tibtech.2006.07.003.

[144] Massoud TF, Gambhir SS. Integrating noninvasive molecular imaging

into molecular medicine: an evolving paradigm. Trends Mol Med 2007;13:183–91. doi:10.1016/j.molmed.2007.03.003.

[145] De A, Lewis XZ, Gambhir SS. Noninvasive imaging of lentiviral-mediated reporter gene expression in living mice. Mol Ther 2003;7:681–91. doi:10.1016/S1525-0016(03)00070-4.

[146] Gambhir SS, Herschman HR, Cherry SR, Barrio JR, Satyamurthy N, Toyokuni T, et al. Imaging transgene expression with radionuclide imaging technologies. Neoplasia 2000;2:118–38. doi:10.1038/sj.neo.7900083.

[147] Bolon B, Galbreath E. Use of Genetically Engineered Mice in Drug Discovery and Development: Wielding Occam's Razor to Prune the Product Portfolio. Int J Toxicol 2002;21:55–64. doi:10.1080/10915810252826019.

[148] Thyagarajan T, Totey S, Danton MJS, Kulkarni AB. Genetically altered mouse models: the good, the bad, and the ugly. Crit Rev Oral Biol Med 2003;14:154–74.

[149] Törnqvist E, Annas A, Granath B, Jalkesten E, Cotgreave I, Öberg M. Strategic Focus on 3R Principles Reveals Major Reductions in the Use of Animals in Pharmaceutical Toxicity Testing. PLoS One 2014;9:e101638. doi:10.1371/journal.pone.0101638.

[150] Barisano G, Sepehrband F, Ma S, Jann K, Cabeen R, Wang DJ, et al. Clinical 7 T MRI: Are we there yet? A review about magnetic resonance imaging at ultra-high field. Br J Radiol 2019;92:20180492. doi:10.1259/bjr.20180492.

[151] Grover VPB, Tognarelli JM, Crossey MME, Cox IJ, Taylor-Robinson SD, McPhail MJW. Magnetic Resonance Imaging: Principles and Techniques: Lessons for Clinicians. J Clin Exp Hepatol 2015;5:246–55. doi:10.1016/j.jceh.2015.08.001.

[152] El-Dahshan E-SA, Mohsen HM, Revett K, Salem A-BM. Computer-aided diagnosis of human brain tumor through MRI: A survey and a new algorithm. Expert Syst Appl 2014;41:5526–45. doi:10.1016/J.ESWA.2014.01.021.

[153] Hasse A, Dapash M, Jeong Y, Ansari SA, Carroll TJ, Lesniak M, et al. Correlation of post-contrast T1-weighted MRI surface regularity, tumor bulk, and necrotic volume with Ki67 and p53 in glioblastomas. Neuroradiology 2019;61:861–7. doi:10.1007/s00234-019-02204-1.

[154] Guo BJ, Yang ZL, Zhang LJ. Gadolinium Deposition in Brain: Current

Scientific Evidence and Future Perspectives. Front Mol Neurosci 2018;11:335. doi:10.3389/fnmol.2018.00335.

[155] Salama GR, Heier LA, Patel P, Ramakrishna R, Magge R, Tsiouris AJ. Diffusion Weighted/Tensor Imaging, Functional MRI and Perfusion Weighted Imaging in Glioblastoma—Foundations and Future. Front Neurol 2018;8:660. doi:10.3389/fneur.2017.00660.

[156] Alvarez-Linera J. 3T MRI: Advances in brain imaging. Eur J Radiol 2008;67:415–26. doi:10.1016/j.ejrad.2008.02.045.

[157] Macdonald DR, Cascino TL, Schold SC, Cairncross JG. Response criteria for phase II studies of supratentorial malignant glioma. J Clin Oncol 1990;8:1277–80. doi:10.1200/JCO.1990.8.7.1277.

[158] Wen PY, Macdonald DR, Reardon DA, Cloughesy TF, Sorensen AG, Galanis E, et al. Updated Response Assessment Criteria for High-Grade Gliomas: Response Assessment in Neuro-Oncology Working Group. J Clin Oncol 2010;28:1963–72. doi:10.1200/JCO.2009.26.3541.

[159] Almansory KO, Fraioli F. Combined PET/MRI in brain glioma imaging. Br J Hosp Med 2019;80:380–6. doi:10.12968/hmed.2019.80.7.380.

[160] Shukla AK, Kumar U. Positron emission tomography: An overview. J Med Phys 2006;31:13–21. doi:10.4103/0971-6203.25665.

[161] Davidson CQ, Phenix CP, Tai T, Khaper N, Lees SJ. Searching for novel PET radiotracers: imaging cardiac perfusion, metabolism and inflammation. Am J Nucl Med Mol Imaging 2018;8:200.

[162] Fong Y, Giulianotti PC, Lewis J, Koerkamp BG, Reiner T. Imaging and visualization in the modern operating room : a comprehensive guide for physicians. n.d.

[163] Thompson C, Goertzen A, Thiessen J, Bishop D, Stortz G, Kozlowski P, et al. Development of a PET Scanner for Simultaneously Imaging Small Animals with MRI and PET. Sensors 2014;14:14654–71. doi:10.3390/s140814654.

[164] Hutton BF, Erlandsson K, Thielemans K. Advances in clinical molecular imaging instrumentation. Clin Transl Imaging 2018;6:31–45. doi:10.1007/s40336-018-0264-0.

[165] Ancey P, Contat C, Meylan E. Glucose transporters in cancer – from tumor cells to the tumor microenvironment. FEBS J 2018;285:2926–43. doi:10.1111/febs.14577.

[166] Ahmad Sarji S. Physiological uptake in FDG PET simulating disease. Biomed Imaging Interv J 2006;2:e59. doi:10.2349/biij.2.4.e59.

[167] Hadziahmetovic M, Shirai K, Chakravarti A. Recent advancements in multimodality treatment of gliomas. Future Oncol 2011;7:1169–83. doi:10.2217/fon.11.102.

[168] Srivastava A, Creek DJ. Discovery and Validation of Clinical Biomarkers of Cancer: A Review Combining Metabolomics and Proteomics. Proteomics 2019;19:1700448. doi:10.1002/pmic.201700448.

[169] Verger A, Langen K-J. PET Imaging in Glioblastoma: Use in Clinical Practice. Codon Publications; 2017. doi:10.15586/CODON.GLIOBLASTOMA.2017.CH9.

[170] Lopci E, Grassi I, Chiti A, Nanni C, Cicoria G, Toschi L, et al. PET radiopharmaceuticals for imaging of tumor hypoxia: a review of the evidence. Am J Nucl Med Mol Imaging 2014;4:365–84.

[171] Unterrainer M, Fleischmann DF, Vettermann F, Ruf V, Kaiser L, Nelwan D, et al. TSPO PET, tumour grading and molecular genetics in histologically verified glioma: a correlative 18F-GE-180 PET study. Eur J Nucl Med Mol Imaging 2019:1–13. doi:10.1007/s00259-019-04491-5.

[172] Marciscano AE, Thorek DLJ. Role of noninvasive molecular imaging in determining response. Adv Radiat Oncol 2018;3:534–47. doi:10.1016/j.adro.2018.07.006.

[173] Lukas R V., Juhász C, Wainwright DA, James CD, Kennedy E, Stupp R, et al. Imaging tryptophan uptake with positron emission tomography in glioblastoma patients treated with indoximod. J Neurooncol 2018:1–10. doi:10.1007/s11060-018-03013-x.

[174] Schuster DM, Nanni C, Fanti S. PET Tracers Beyond FDG in Prostate Cancer. Semin Nucl Med 2016;46:507–21. doi:10.1053/j.semnuclmed.2016.07.005.

[175] Nye JA, Schuster DM, Yu W, Camp VM, Goodman MM, Votaw JR. Biodistribution and radiation dosimetry of the synthetic nonmetabolized amino acid analogue anti-18F-FACBC in humans. J Nucl Med 2007;48:1017–20. doi:10.2967/jnumed.107.040097.

[176] Kondo A, Ishii H, Aoki S, Suzuki M, Nagasawa H, Kubota K, et al. Phase IIa clinical study of [18F]fluciclovine: efficacy and safety of a new PET tracer for brain tumors. Ann Nucl Med 2016;30:608–18.

doi:10.1007/s12149-016-1102-y.

[177] Oka S, Okudaira H, Yoshida Y, Schuster DM, Goodman MM, Shirakami Y. Transport mechanisms of trans-1-amino-3-fluoro[1-14C]cyclobutanecarboxylic acid in prostate cancer cells. Nucl Med Biol 2012;39:109–19. doi:10.1016/J.NUCMEDBIO.2011.06.008.

[178] Scalise M, Pochini L, Console L, Losso MA, Indiveri C. The Human SLC1A5 (ASCT2) Amino Acid Transporter: From Function to Structure and Role in Cell Biology. Front Cell Dev Biol 2018;6:96. doi:10.3389/fcell.2018.00096.

[179] Dickens D, Chiduza GN, Wright GSA, Pirmohamed M, Antonyuk S V., Hasnain SS. Modulation of LAT1 (SLC7A5) transporter activity and stability by membrane cholesterol. Sci Rep 2017;7:43580. doi:10.1038/srep43580.

[180] Blue Earth Diagnostics | Amino Acid - Blue Earth Diagnostics n.d. http://www.blueearthdiagnostics.com/technology/amino-acid/ (accessed October 7, 2019).

[181] Fuchs BC, Bode BP. Amino acid transporters ASCT2 and LAT1 in cancer: Partners in crime? Semin Cancer Biol 2005;15:254–66. doi:10.1016/j.semcancer.2005.04.005.

[182] Parent EE, Benayoun M, Ibeanu I, Olson JJ, Hadjipanayis CG, Brat DJ, et al. [18F]Fluciclovine PET discrimination between high- and low-grade gliomas. EJNMMI Res 2018;8:67. doi:10.1186/s13550-018-0415-3.

[183] Savir-Baruch B, Zanoni L, Schuster DM. Imaging of Prostate Cancer Using Fluciclovine. PET Clin 2017;12:145–57. doi:10.1016/j.cpet.2016.11.005.

[184] ImageJ n.d. https://imagej.nih.gov/ij/index.html (accessed October 7, 2019).

[185] Monzio Compagnoni G, Kleiner G, Bordoni A, Fortunato F, Ronchi D, Salani S, et al. Mitochondrial dysfunction in fibroblasts of Multiple System Atrophy. Biochim Biophys Acta - Mol Basis Dis 2018;1864:3588–97. doi:10.1016/j.bbadis.2018.09.018.

[186] 000664 - C57BL/6J n.d. https://www.jax.org/strain/000664 (accessed October 7, 2019).

[187] VivoQuant - Pre-clinical image post-processing n.d. http://www.vivoquant.com/ (accessed October 7, 2019).

[188] SARRP | Xstrahl Medical & Life Sciences n.d. https://xstrahl.com/life-science-systems/small-animal-radiation-research-platform/ (accessed October 8, 2019).

[189] Zhang W, Wang Z, Shu F, Jin Y, Liu H, Wang Q, et al. Activation of AMP-activated Protein Kinase by Temozolomide Contributes to Apoptosis in Glioblastoma Cells via p53 Activation and mTORC1 Inhibition. J Biol Chem 2010;285:40461–71. doi:10.1074/jbc.M110.164046.

[190] Coluzzi E, Leone S, Sgura A. Oxidative Stress Induces Telomere Dysfunction and Senescence by Replication Fork Arrest. Cells 2019;8:19. doi:10.3390/cells8010019.

[191] Oraki Kohshour M, Najafi L, Heidari M, Ghaffari Sharaf M. Antiproliferative effect of H2O2 against human acute myelogenous leukemia KG1 cell line. JAMS J Acupunct Meridian Stud 2013;6:134–41. doi:10.1016/j.jams.2012.08.004.

[192] Chetsawang B, Chetsawang J, Govitrapong P. Hydrogen peroxide toxicity induces Ras signaling in human neuroblastoma SH-SY5Y cultured cells. J Biomed Biotechnol 2010;2010. doi:10.1155/2010/803815.

[193] Cote GJ, Zhu W, Thomas A, Martin E, Murad F, Sharina IG. Hydrogen Peroxide Alters Splicing of Soluble Guanylyl Cyclase and Selectively Modulates Expression of Splicing Regulators in Human Cancer Cells. PLoS One 2012;7:e41099. doi:10.1371/journal.pone.0041099.

[194] Zhang M, Herion TW, Timke C, Han N, Hauser K, Weber KJ, et al. Trimodal glioblastoma treatment consisting of concurrent radiotherapy, temozolomide, and the novel TGF-β receptor I kinase inhibitor LY2109761. Neoplasia 2011;13:537–49. doi:10.1593/neo.11258.

[195] Ryu CH, Yoon WS, Park KY, Kim SM, Lim JY, Woo JS, et al. Valproic Acid Downregulates the Expression of MGMT and Sensitizes Temozolomide-Resistant Glioma Cells. J Biomed Biotechnol 2012;2012:1–9. doi:10.1155/2012/987495.

[196] Rubenstein M, Shaw M, Mirochnik Y, Slobodskoy L, Glick R, Lichtor T, et al. In vivo establishment of T98G human glioblastoma. Methods Find Exp Clin Pharmacol n.d.;21:391–3.

[197] Yi G-Z, Huang G, Guo M, Zhang X, Wang H, Deng S, et al. Acquired temozolomide resistance in MGMT-deficient glioblastoma cells is

associated with regulation of DNA repair by DHC2. Brain 2019;142:2352–66. doi:10.1093/brain/awz202.

[198] Sarkaria JN, Kitange GJ, James CD, Plummer R, Calvert H, Weller M, et al. Mechanisms of chemoresistance to alkylating agents in malignant glioma. Clin Cancer Res 2008;14:2900–8. doi:10.1158/1078-0432.CCR-07-1719.

[199] Lo Dico A, Martelli C, Diceglie C, Lucignani G, Ottobrini L. Hypoxia-Inducible Factor-1α Activity as a Switch for Glioblastoma Responsiveness to Temozolomide. Front Oncol 2018;8:249. doi:10.3389/fonc.2018.00249.

[200] Wen Y-A, Stevens PD, Gasser ML, Andrei R, Gao T. Downregulation of PHLPP expression contributes to hypoxia-induced resistance to chemotherapy in colon cancer cells. Mol Cell Biol 2013;33:4594–605. doi:10.1128/MCB.00695-13.

[201] Kaushik S, Cuervo AM. The coming of age of chaperone-mediated autophagy. Nat Rev Mol Cell Biol 2018;19:365. doi:10.1038/S41580-018-0001-6.

[202] Ježek J, Cooper KF, Strich R. Reactive Oxygen Species and Mitochondrial Dynamics: The Yin and Yang of Mitochondrial Dysfunction and Cancer Progression. Antioxidants 2018;7. doi:10.3390/ANTIOX7010013.

[203] Tan SK, Jermakowicz A, Mookhtiar AK, Nemeroff CB, Schürer SC, Ayad NG. Drug Repositioning in Glioblastoma: A Pathway Perspective. Front Pharmacol 2018;9:218. doi:10.3389/fphar.2018.00218.

[204] Jung Y, Ahn SH, Park SH, Choi YH. Effect of glucose level on chemical hypoxia- and hydrogen peroxide-induced chemokine expression in human glioblastoma cell lines. Korean J Physiol Pharmacol 2017;21:509–18. doi:10.4196/kjpp.2017.21.5.509.

[205] Xu Y, Kang J, Yuan Z, Li H, Su J, Li Y, et al. Suppression of CLIC4/mtCLIC enhances hydrogen peroxide-induced apoptosis in C6 glioma cells. Oncol Rep 2013;29:1483–91. doi:10.3892/or.2013.2265.

[206] Gülden M, Jess A, Kammann J, Maser E, Seibert H. Cytotoxic potency of H2O2 in cell cultures: Impact of cell concentration and exposure time. Free Radic Biol Med 2010;49:1298–305. doi:10.1016/j.freeradbiomed.2010.07.015.

[207] Kim SH, Kim KH, Yoo BC, Ku JL. Induction of LGR5 by H 2O 2

treatment is associated with cell proliferation via the JNK signaling pathway in colon cancer cells. Int J Oncol 2012;41:1744–50. doi:10.3892/ijo.2012.1596.

[208] Zhang H, Kong X, Kang J, Su J, Li Y, Zhong J, et al. Oxidative Stress Induces Parallel Autophagy and Mitochondria Dysfunction in Human Glioma U251 Cells. Toxicol Sci 2009;110:376–88. doi:10.1093/toxsci/kfp101.

[209] Martínez-Murillo R, Martínez A. Standardization of an orthotopic mouse brain tumor model following transplantation of CT-2A astrocytoma cells. Histol Histopathol 2007;22:1309–26. doi:10.14670/HH-22.1309.

[210] Cormerais Y, Massard PA, Vucetic M, Giuliano S, Tambutté E, Durivault J, et al. The glutamine transporter ASCT2 (SLC1A5) promotes tumor growth independently of the amino acid transporter LAT1 (SLC7A5). J Biol Chem 2018;293:2877–87. doi:10.1074/jbc.RA117.001342.

[211] Beaumatin F, O'Prey J, Barthet VJA, Zunino B, Parvy J-P, Bachmann AM, et al. mTORC1 Activation Requires DRAM-1 by Facilitating Lysosomal Amino Acid Efflux. Mol Cell 2019;76:163-176.e8. doi:10.1016/J.MOLCEL.2019.07.021.

[212] Lo Dico A, Costa V, Martelli C, Diceglie C, Rajata F, Rizzo A, et al. MiR675-5p Acts on HIF-1α to Sustain Hypoxic Responses: A New Therapeutic Strategy for Glioma. Theranostics 2016;6:1105–18. doi:10.7150/thno.14700.

SCIENTIFIC PRODUCTS

Publications:

- **"PET BIOMARKERS AND PROBES FOR TREATMENT RESPONSE ASSESSMENT IN GLIOBLASTOMA: A WORK IN PROGRESS"**
  Salvatore D., Lo Dico A., Martelli C., Diceglie C., Ottobrini L.
  Clinical and Translational Imaging (2019) 7: 285. https://doi.org/10.1007/s40336-019-00329-0

- **"INTRACELLULAR REDOX-BALANCE INVOLVEMENT IN TMZ RESISTANCE-RELATED MOLECULAR MECHANISMS IN GLIOBLASTOMA"**
  Lo Dico A., **Salvatore D.**, Martelli C., Ronchi D., Diceglie C., Lucignani G., Ottobrini L.
  Cells (2019) 24; 8(11). pii: E1315.
  doi: 10.3390/cells8111315

Abstracts:

- **"HIF-1α ACTIVITY AS A MOLECULAR AND OPTICAL IMAGING BIOMARKER OF GBM RESPONSIVENESS TO TMZ"**
  Lo Dico A., **Salvatore D.**, Martelli C., Diceglie C., Lucignani G., Ottobrini L.

  60th Annual Meeting of the Italian Cancer Society (SIC), Milan 2018

- **"RADIOTHERAPY COMBINED WITH A MULTIMODAL IMAGING APPROACH IN A GLIOBLASTOMA PRECLINICAL MODEL"**
  Salvatore D., Shaw G., Wright J., The I., Koch-Paszkowski J., Murray L., Scarsbrook A., Schneider J., Ottobrini L., Short S.

Neuro-Oncology (2019) 21 (Suppl3): iii45. https://doi.org/10.1093/neuonc/noz126.159

- **"Chaperon mediated autophagy in placentas of obese women: a pilot study"**
  Mando C., Martelli C., Anelli G.M., **Salvatore D.**, Novielli C., Lisso F., Serati A., Cetin I., Ottobrini L.

  67th Annual Scientific Meeting of Society for Reproductive Investigation, Vancouver, BC, Canada 2020

Poster:

- **"RADIOTHERAPY COMBINED WITH A MULTIMODAL IMAGING APPROACH IN A GLIOBLASTOMA PRECLINICAL MODEL"**
  Salvatore D., Shaw G., Wright J., The I., Koch-Paszkowski J., Murray L., Scarsbrook A., Schneider J., Ottobrini L., Short S.

  14th Annual Meeting of European Association of Neuro-Oncology (EANO), Lyon 2019

GRANTS

This work has been supported in part by fundings made available for each PhD student from Doctoral School in Molecular and Translational Medicine of University of Milan.

This study was supported in part by the FP7-funded INSERT project (HEALTH-2012- INNOVATION-1, GA305311).

AKNOWLEDGEMENTS

I thank my tutor, Dr. Luisa Ottobrini, my co-tutor, Dr. Alessia Lo Dico, and the other colleagues of laboratory team, Dr. Cristina Martelli and Dr. Cecilia Diceglie, for having constantly supported me along these three years of PhD. Thank you so much for having allowed me to make my science passion grow and for having always encouraged me during this important route.

I thank the collaborators of the Policlinico of Milan, Prof.ssa Monica Miozzo and Dr. Dario Ronchi, for their precious availability in experimental support and their experimental contribution itself.

Moreover, I thank Prof. Susan Short for having hosted me in her laboratory in St James's University Hospital of Leeds during my stage period abroad in Leeds; I thank her, Prof. Jurgen Schneider and their respective laboratories for their pivotal support and collaboration. I thank all the other people which have contributed to the project in which I have been involved during my stage period abroad.

DISCLOSURE INFORMATION

Radiotracer availability has been possible through an agreement between the University of Leeds and the company which has furnished the radiotracer, the Blue Earth Diagnostics (Principal Investigator: Prof. Andrew Scarsbook, Leeds Teaching Hospitals NHS Trust, Leeds, UK).

PhD THESIS EVALUATION

This thesis was evaluated by 3 independent reviewers:

- Dr. Gloria Rita Bertoli, Institute Of Bioimaging and Molecular Physiology (IBFM) of the National Research Council (CNR), Milan

- Prof. Rosa Maria Moresco, Department of Medicine and Surgery, University of Milan Bicocca, Milan

- Prof. Susan Short, Leeds Institute of Medical Research at St James's, Faculty of Medicine and Health, University of Leeds, UK.